

REVIEW ARTICLE

Magnetars: the physics behind observations

R Turolla^{1,2}, S Zane², A L Watts³

¹ Department of Physics and Astronomy, University of Padova, via Marzolo 8, 35131 Padova, Italy

² Mullard Space Science Laboratory, University College London, Holbury St. Mary, Surrey, RH5 6NT, UK

³ Anton Pannekoek Institute for Astronomy, University of Amsterdam, Postbus 94249, 1090 GE Amsterdam, The Netherlands

E-mail: turolla@pd.infn.it

Abstract. Magnetars are the strongest magnets in the present universe and the combination of extreme magnetic field, gravity and density makes them unique laboratories to probe current physical theories (from quantum electrodynamics to general relativity) in the strong field limit. Magnetars are observed as peculiar, burst-active X-ray pulsars, the Anomalous X-ray Pulsars (AXPs) and the Soft Gamma Repeaters (SGRs); the latter emitted also three “giant flares”, extremely powerful events during which luminosities can reach up to 10^{47} erg/s for about one second. The last five years have witnessed an explosion in magnetar research which has led, among other things, to the discovery of transient, or “outbursting”, and “low-field” magnetars. Substantial progress has been made also on the theoretical side. Quite detailed models for explaining the magnetars’ persistent X-ray emission, the properties of the bursts, the flux evolution in transient sources have been developed and confronted with observations. New insight on neutron star asteroseismology has been gained through improved models of magnetar oscillations. The long-debated issue of magnetic field decay in neutron stars has been addressed, and its importance recognized in relation to the evolution of magnetars and to the links among magnetars and other families of isolated neutron stars. The aim of this paper is to present a comprehensive overview in which the observational results are discussed in the light of the most up-to-date theoretical models and their implications. This addresses not only the particular case of magnetar sources, but the more fundamental issue of how physics in strong magnetic fields can be constrained by the observations of these unique sources.

1. Introduction

Neutron stars (NSs), the endpoint of the evolution of massive stars with $10 \lesssim M/M_{\odot} \lesssim 25$, are extremely compact remnants endowed with strong magnetic fields. Isolated (i.e. not belonging to a binary system) neutron stars were for a long time identified with radio-pulsars, and only in the last two decades, mainly thanks to high-energy observations, was the existence of other manifestations of isolated neutron stars recognized. Among them, there are two groups of X-ray pulsars with remarkably peculiar properties, the Soft Gamma Repeaters (SGRs) and the Anomalous X-ray Pulsars (AXPs, see e.g. Mereghetti, 2008, for a review). The separation into two classes reflects the way in which these sources were originally discovered. SGRs were revealed through the detection of short, intense bursts in the hard X-/soft gamma-ray range (Mazets et al., 1979b,a), and because of this were initially associated with gamma ray bursts (GRBs); however, burst emission from SGRs was soon recognized to repeat, at variance to what was observed in GRBs, setting the two phenomena apart. On the other hand, AXPs were identified as X-ray pulsar in the soft X-ray range (< 10 keV, Mereghetti & Stella, 1995). They were dubbed “anomalous” because their high X-ray luminosity ($\sim 10^{34} - 10^{36}$ erg/s) cannot be easily explained in terms of the conventional processes which apply to other classes of pulsars, i.e. accretion from a binary companion or injection of rotational energy in the pulsar wind/magnetosphere. Over the last few years, observations have revealed many similarities between these two classes of objects (see e.g. Woods & Thompson, 2006), including the discovery that AXPs too emit short, SGR-like bursts (Kaspi, 2000, 2003) and nowadays the idea that SGRs and AXPs belong to a single, unified class is widely accepted.

The main observational characteristics of SGRs and AXPs are: a) lack of evidence of binary companions; b) persistent (i.e. non-bursting), often variable X-ray luminosity in the range $\sim 10^{33} - 10^{36}$ erg/s, emitted in the soft (0.5–10 keV) and hard (20–100 keV) X-ray range; c) pulsations at relatively long spin periods, clustered in the range $\sim 2 - 12$ s; d) large secular spin-down rate, $\dot{P} \sim 10^{-13} - 10^{-11}$ s/s, which, if interpreted in terms of electromagnetic losses from a rotating dipole in vacuo, leads to huge magnetic fields, $\sim 10^{14} - 10^{15}$ G. SGRs (and AXPs, to a somewhat lesser extent) exhibit spectacular and frequent bursting activity, which is observed in the X-/gamma-rays on several timescales, ranging from sub-s to several tens of seconds. In particular, three different kinds of bursting events have been observed (see Sec. 5):

- short bursts: these are the most common, with typical duration of $\sim 0.1 - 1$ s, peak luminosity of $\sim 10^{39} - 10^{41}$ erg/s, and soft (~ 10 keV), thermal spectra; they are detected from both SGRs and AXPs;
- intermediate bursts, which last $\sim 1 - 40$ s and have a peak luminosity of $\sim 10^{41} - 10^{43}$ erg/s. These are characterized by an abrupt onset and usually also show thermal spectra; again, they were seen in both SGRs and AXPs;
- giant flares. These are exceptional, rare events, with an energy output of $\sim 10^{44} - 10^{47}$ erg/s, only exceeded by blazars and GRBs. They have been observed

only in SGRs and only three times since SGRs were discovered: from SGR 0526-66 in 1979 (Mazets et al., 1979a), from SGR 1900+14 in 1998 (Hurley et al., 1999), and from SGR 1806-20 in 2004 (e.g. Hurley et al., 2005; Palmer et al., 2005). All three events started with an initial spike of ~ 0.1 – 0.2 s duration, followed by a long pulsating tail (lasting a few hundred seconds) modulated at the neutron star spin period.

All together, these properties find an explanation in the so-called “magnetar” scenario (Duncan & Thompson, 1992; Thompson & Duncan, 1993, 1995), according to which the relatively high X-ray luminosity and the bursting/outbursting activity are powered by the dissipation and decay of a superstrong magnetic field, $\approx 10^{14}$ – 10^{15} G on the surface and possibly higher in the star’s interior. Despite no indisputable measure of an ultra-high magnetic field has been obtained as yet, a number of independent arguments strongly support the idea that SGRs/AXPs are indeed magnetically-powered, as first discussed by Thompson & Duncan (1995). A few of them are

- the rotational energy loss rate \dot{E} (which is believed to fuel standard pulsars) is well below the persistent X-ray luminosity, $\dot{E} \ll L_X$;
- long spin periods (≈ 10 s) can be attained in $\approx 10^3 - 10^4$ yrs (the source age as inferred from that of the associated SNR) via magneto-dipolar braking only for fields $\gtrsim 10^{14}$ G;
- huge spin-down rates have been indeed measured in these sources, implying dipole magnetic fields in the range $\approx 10^{14} - 10^{15}$ G;
- the decrease of the scattering opacity in a superstrong magnetic field ($B \gtrsim 10^{14}$ G) pushes upwards the Eddington limit and allows a much larger luminosity to escape from a (magnetically) confined plasma: this can explain the apparently super-Eddington luminosity of a number of bursts;
- no stellar companions have been discovered in SGRs/AXPs, ruling out accretion as a possible source of energy;
- if no more than a fraction of the magnetic energy was released in a giant flare, this requires $B \gtrsim 10^{14}$ G; in order to power ≈ 100 giant flares like that emitted in 2004 by SGR 1806-20 over the source lifetime an internal field $\approx 10^{16}$ G is needed (Stella et al., 2005).

Although alternative interpretations have been proposed (see e.g. Turolla & Esposito, 2013, for a review and references therein), the magnetar model more naturally explains the properties of SGRs and AXPs, including the bursting activity and the hyper-energetic giant flares, and will be the focus of this review.

Even the “persistent” emission of these sources is far from being steady. Magnetars’ spin-down is quite irregular, and often accompanied by glitches and timing noise. Long term variations in magnetars’ emission can occur either as gradual and moderate changes in the flux, accompanied by variations in the spectrum, pulse profile, and spin-down rate, or as sudden outbursts, i.e. events during which the flux raises up to a factor ~ 1000

and then decays back to a level compatible with the quiescent state over a time scale of months/years (see Sec. 4). Within the magnetar scenario, the first kind of variability is thought to be driven by plastic deformations in the crust which, in turn, induce changes in the magnetic current configurations. The more violent outbursts, as well as the glitches, the bursting activity and even the hyper-energetic giant flares could instead be due to sudden reconfigurations of the magnetosphere, when unstable conditions are reached. This may lead to crustal fractures (starquakes) and/or instabilities in the outer magnetosphere (possibly involving magnetic reconnection).

Although originally discovered in the X-/soft gamma-rays, magnetars have been detected at different wavelengths, revealing a rich phenomenology across the electromagnetic spectrum. AXPs and SGRs have been discovered to emit in the optical and/or near-infrared (NIR) bands (e.g. Hulleman et al., 2000; Israel et al., 2004; Durant & van Kerkwijk, 2006). The optical/NIR counterparts are faint ($K \sim 20$) and the flux is only a small fraction of the bolometric flux, but still its detection can place important constraints on models. Several AXPs have exhibited long-term variability both in their optical/infrared emission and in X-rays (Israel et al., 2002; Hulleman et al., 2004; Rea et al., 2005). Unavoidably this introduces additional uncertainties in the modelling of broad band spectra, based on observations at different wavelengths taken at different times.

Magnetars were traditionally considered to be radio-silent, but this picture was challenged by the (unexpected) discovery of a pulsed radio counterpart in some sources, a property that seems to be peculiar to transient magnetars (Gelfand & Gaensler, 2007, see also Sec. 4.3 and references therein). When detected, the radio emission of magnetars appears to be different from that of standard radio-pulsars: the spectrum is flatter and the flux and pulse profile show strong variations with time, indicating that the mechanisms causing the emission (or the topology of the emission region) may differ in the two kinds of sources.

Association with supernova remnants or, possibly, young stellar clusters has been proposed for a number of sources (see e.g. Table 1 in Mereghetti, 2008; Munro et al., 2006; Vrba et al., 2000; Eikenberry et al., 2001; Figer et al., 2005; Kloze et al., 2004), which, if confirmed, leads in some cases to a progenitor with high mass ($> 20 M_{\odot}$), high metallicity, and to a relatively young age $\sim 10^4$ yr for the neutron star (see Sec. 2.1).

The magnetar paradigm that bursting activity is necessarily associated with a high dipolar field has been revolutionized by the recent discovery of a few full-fledged magnetars (i.e. neutron stars that displayed bursting, SGR-like activity) with a dipolar magnetic field comparable with that of standard radio pulsars (see Sec. 4 and references therein). The properties of these sources are compatible with those expected from aged magnetars, which may still retain a large toroidal field in the interior, occasionally capable of cracking the star's crust. This discovery suggests that magnetars could be far more numerous than previously expected (Rea et al., 2010; Tiengo et al., 2013), and has had a number of profound implications, e.g. for star formation, supernovae, gamma ray bursts (see Rea, 2014b, for a complete discussion).

Despite the wide interest in the astrophysical community, review papers on magnetars were comparatively few, and mainly devoted to the diverse aspects of their phenomenology. Theoretical results are often scattered across many specialized papers, the comparison and interpretation of which are quite a challenge even for an informed reader. It is outside the scope of this paper to provide a detailed summary of magnetars' observational properties, about which excellent review papers have been already published (Woods & Thompson, 2006; Kaspi, 2007; Mereghetti, 2008; Hurley, 2011b; Rea & Esposito, 2011); an updated list of sources, containing all the essential data, is available in the online McGill magnetar catalogue‡ (Olausen & Kaspi, 2014), and while preparing this review we also created a Magnetar Burst Library which is now maintained by the Univ. of Amsterdam §. Here we will focus on the theoretical interpretation of the emission properties of magnetars and on a cross comparison of the models presented so far to describe them. A brief summary of the observational properties, which is not necessarily complete but sets the context for the subsequent discussion, is placed at the beginning of each section, when needed. Our main aims are to review the state of the art in the theoretical modelling, to outline which observational facts are robustly explained by current models and to discuss the open issues which still remain to be addressed.

The paper is organized as follows. We begin with a summary of the mechanisms that can lead to the birth of a highly magnetized neutron star, discuss how magnetars evolve and briefly touch the link between magnetars and other classes of Galactic, isolated neutron stars (Sec. 2). Sec. 3 is dedicated to the twisted magnetosphere model and its ability to explain the observed persistent emission in different wavebands. Transient magnetars and their observations in the radio band are reviewed in Sec. 4, while Sec. 5 contains a thorough discussion of burst emission and magnetar seismology. Conclusions follow.

2. Birth and evolution of a magnetar

2.1. Magnetars formation

According to the original picture by Duncan and Thompson (Duncan & Thompson, 1992; Thompson & Duncan, 1993), ultra-magnetized neutron stars form through magnetic field amplification by a vigorous dynamo action in the early, highly convective stages. Rotation and convection produce two types of dynamo effects in an astrophysical plasma: the α dynamo, arising from the coupling of convective motions and rotation, and the ω dynamo, driven by differential rotation. In proto NSs both effects are present and since the α - ω dynamo operates at low Rossby numbers, the initial spin period must be short, $\lesssim 3$ ms, to ensure efficient convective mixing (Duncan & Thompson, 1992). Magnetars would be, then, the endpoint of the evolution of massive stars

‡ The on line McGill catalogue can be found at <http://www.physics.mcgill.ca/~pulsar/magnetar/main.html>.

§ See the Amsterdam Magnetar Burst Library, <http://staff.fnwi.uva.nl/a.l.watts/magnetar/mb.html>

with rapidly rotating cores. Rapidly spinning, collapsing stellar cores are expected to produce highly energetic supernovae (Duncan & Thompson, 1992; Thompson et al., 2004; Bucciantini et al., 2007), because a significant fraction of the rotational energy, $E_{rot} \sim 3 \times 10^{52} (P/1 \text{ ms})^{-2}$ erg, is transferred to the ejecta via the strong magnetic coupling with the proto-neutron star. Any observational signatures that magnetars were born in (above-average) energetic events were searched for in a number of supernova remnants positively associated with SGRs/AXPs, but no evidence has yet been found (Vink & Kuiper, 2006; Vink, 2008). If the internal magnetic field is $\sim 10^{16}$ G, however, rotational energy can be efficiently carried away by gravitational waves, which do not interact with the ejecta (Dall’Osso, Shore & Stella, 2009).

Alternatively, it has been suggested that ultra-strong fields in neutron stars result from magnetic flux conservation (the fossil field scenario; Ferrario & Wickramasinghe, 2006, 2008). Ferrario & Wickramasinghe (2006), starting from a parameterized model of the distribution of magnetic flux on the main sequence and of the spin period of neutron stars at birth, derived the expected properties of isolated radio pulsars in the Galaxy, given the spatial distribution of the initial mass function and star formation rate. Comparison with the data in the 1374-MHz Parkes Multi-Beam Survey was then used to constrain the model parameters. They find that the distribution of the magnetic field in the core of the OB progenitors comprises $\sim 8\%$ of stars with a magnetic field in excess of ~ 1000 G. The core-collapse supernovae of these high-field stars can produce ~ 25 magnetars with properties (surface magnetic field, spin period, age) in agreement with those observed in SGRs/AXPs. As first noted by Spruit (2008), the number of Galactic magnetars predicted by the fossil field model may be too low, and this is a more and more serious issue, given the steady increase of the magnetar population and the possibility that many “dormant” SGRs/AXPs lurk among “standard” radio pulsar (see Sec. 4). A possibility is that magnetars are formed through different channels: for instance it has been suggested that at least part of the magnetars may be born as rapidly rotating neutron stars in systems in which the core of the collapsing star was accelerated by tidal synchronization in a very close binary (Popov & Prokhorov, 2006; Bogomazov & Popov, 2009).

Interestingly, the high-field progenitors of magnetars should be in the far end of the mass distribution of OB stars, with masses $\sim 20\text{--}45M_{\odot}$, which, in standard evolutionary models, should mostly have given rise to black holes (Ferrario & Wickramasinghe, 2008, see also Clark et al. 2005). The notion that magnetars descend from massive stars (typically above the canonical neutron star-black hole divide) received further support from the observational evidence that (some) SGRs/AXPs are associated with young clusters of massive stars. The progenitor mass of SGR 1806-20 and the AXP 1E 1048.1-5937 has been estimated to be in excess of $\sim 30M_{\odot}$ (Bibby et al., 2008; Gaensler et al., 2005a); the progenitor mass of SGR 1900+14 appears, however, to be $\sim 17M_{\odot}$ (Clark et al., 2008; Davies et al., 2009). One of the strongest evidence in favour of high-mass progenitors of SGRs/AXPs came from the robust association of the AXP CXO J164710.2-455216 with the young cluster Westerlund 1 (Muno et al., 2006). Since

the cluster is ~ 4 Myr old (Clark et al., 2005), the minimum mass of a star that could have reached the supernova stage is $\sim 40M_{\odot}$. Hence the claim that CXO J164710.2-455216 originated from a star with $M \gtrsim 40M_{\odot}$. Very recently Clark et al. (2014) proposed that CXO J164710.2-455216 was born in a massive binary and found evidence for the former companion, the runaway star Wd1-5, ejected from the system when the magnetar progenitor exploded. If Wd1-5 and CXO J164710.2-455216 were indeed related, evolution in the binary would lead to a decrease of the progenitor mass through strong mass loss when it entered a Wolf-Rayet phase, and common envelope evolution would prevent spin-down of its core. Magnetar birth in a binary may then be a key ingredient to bring the progenitor mass within the neutron star formation range, and to provide the high core rotational speed required for the onset of the convective dynamo.

Magnetars are also increasingly popular as the central engine powering GRBs, following the original suggestion by Usov (1992, see also Zhang & Mészáros 2001; Metzger et al. 2011). Ultra-magnetized neutron stars have been invoked to explain the properties of both short and long GRBs. The proto-magnetar would result from coalescence in a double-degenerate binary (or accretion-induced collapse of a white dwarf) in this first case and in a core-collapse supernova in the second (e.g. Paczyński, 1986; Rosswog, Ramirez-Ruiz & Davies, 2003; Giacomazzo & Perna, 2013; Metzger, Quataert & Thompson, 2008; Woosley, 1993; MacFayden & Woosley, 1999). Indeed, a significant fraction of the *Swift* long GRBs exhibit late flares and plateau phases in the lightcurve that provide evidence for longevity and on-going activity of the central engine (see e.g. Curran et al., 2008; Margutti et al., 2010; Bernardini, et al., 2011b; Nousek et al., 2006; Zhang et al., 2006). The plateau, which occurs around $10^2 - 10^4$ s after the trigger, has a fluence that can be as high as the fluence of the prompt emission. According to the magnetar model the plateau phase is powered by the initial spin-down of a newly born magnetar, powering a relativistic wind (Fan et al., 2006; Troja et al., 2007; Lyons et al., 2010; Dall’Osso et al., 2011; Bernardini et al., 2012; Metzger et al., 2011). Moreover, Rowlinson et al. (2013) have recently shown that 18 of the *Swift* short GRBs (i.e. 64% of the entire sample) can be clearly fitted with a magnetar plateau phase, while for the rest the quality of the data is insufficient to prove or exclude the presence of the plateau. Out of 18 robust candidates, 10 are thought to collapse later to a black hole, while the others may have left behind a rapidly rotating new magnetar. Although these studies are not a direct, conclusive proof of the magnetar paradigm, they certainly indicate the frequent occurrence of late central activity, which has crucial implications for the origin of the central engine. A smoking gun that may allow to differentiate between models would be the detection of gravitational waves associated to the event (Rowlinson et al., 2013, and references therein).

Another link between magnetars and GRBs has been proposed following the observations of giant flares. Since all these events started with an initial, very energetic sub-s spike, it has been proposed that giant flares, if emitted by extragalactic SGRs, may appear at Earth as short gamma-ray bursts (Palmer et al., 2005; Hurley et al., 2005; Hurley, 2011a). The main causes of uncertainty for proving this idea are in maximum

energy released in the flare and in the spectral properties of the narrow peak. By considering the flare emitted by SGR 1806-20 and by varying the assumptions about the peak spectral shape, Popov & Stern (2006) computed the possibility of detection by BATSE of giant flares with an energy of 10^{44} or 10^{46} erg, as a function of the distance. They found that the first kind of event can be seen up to a few Mpc (therefore in M82, M83, NGC253 and NGC4945), while the second can in principle be visible up to the Virgo cluster. However, as already noted by Popov & Stern (2006), this prediction may be too optimistic, since no evidence has been found for an excess of BATSE short GRBs from the direction of M82, M83, NGC253 and NGC4945, nor from the Virgo cluster (Palmer et al., 2005). Similarly, negative results have been reported by Lazzati et al. (2005); Tanvir et al. (2005), and overall these studies suggest that no more than a few percent, maybe up to $\sim 8\%$ of the short GRBs seen by BATSE could be giant flares from extragalactic SGRs (see also Hurley et al., 2005; Crowther et al., 2011; Svinikin et al., 2015, the latter for a recent update on the detection upper limits).

2.2. Magneto-thermal evolution

A major issue in establishing the magnetic evolution of NSs (and of magnetars in particular) is that observations place very little, if any, constraint on the structure and strength of the internal magnetic field. Clearly, in a magnetar the internal field must be strong enough to sustain the source activity and its geometry must allow magnetic energy to be released. While there are several indications that the large-scale, external field can be reasonably assumed to be (nearly) dipolar, the internal field most likely contains both toroidal and poloidal components (e.g. Geppert, Küker & Page, 2004, 2006, and Sec. 3.1). A further complication comes from the at present poor knowledge of where the internal field resides. The field can either permeate the entire star (“core” fields), or be mostly confined in the crust (“crustal” fields), depending on where its supporting (super)currents are located.

The more general configuration for the internal field in a NS will be, then, that produced by the superposition of current systems in the core and the crust. As stressed by Pons & Geppert (2007), the relative contribution of the core/crustal fields is likely different in different types of NSs. In old isolated radio pulsars, where no field decay is observed, the long-lived core component may dominate, while a sizeable, more volatile crustal field is probably present in magnetars, for which substantial field decay over a timescale $\approx 10^3$ – 10^5 yr is expected (e.g. Goldreich & Reisenegger, 1992). As pointed out by Glampedakis, Jones & Samuelsson (2011) ambipolar diffusion plays little role in magnetar cores during their active lifetime (after crystallization, the absence of convective motions already quenches ambipolar diffusion in the crust). Therefore, if the decay/evolution of the magnetic field is indeed the cause of magnetar activity, it is likely to take place outside the core and be governed by Hall/Ohmic diffusion in the stellar crust. Other mechanisms, e.g. flux expulsion from the superconducting core, due to the interaction between neutron vortices and magnetic flux tubes, are highly

uncertain and very difficult to model. For these reasons, recent investigations of the magnetic field evolution in magnetars has focused only on the crustal component of the field.

The relative importance of the Ohmic decay and Hall drift is strongly density- and temperature-dependent. Thus, any self-consistent study of the magnetic field evolution must be coupled to a detailed modelling of the neutron star thermal evolution, and vice versa. This basically means that the induction equation for \vec{B} must be solved together with the cooling, a quite challenging numerical task. Early efforts in this direction used a split approach. Pons & Geppert (2007) studied the evolution of the field by solving the complete induction equation in an isothermal crust, but assuming a prescribed time dependence for the temperature. They found that crustal magnetic fields in NSs suffer significant decay during the first $\approx 10^6$ yr and that the Hall drift, although inherently conservative (i.e. alone it cannot dissipate magnetic energy), plays an important role since it may reorganize the field from the larger to the smaller (spatial) scales where Ohmic dissipation proceeds faster.

The cooling of magnetized NSs with field decay was investigated by Aguilera et al. (2008, see also Aguilera et al. 2009; Kaminker et al. 2006, 2007, 2009) by adopting a simple, analytical law for the time variation of the field which incorporates the main features of the Ohmic and Hall processes. The fully coupled magneto-thermal evolution of a NS was addressed by Pons et al. (2009), including all realistic microphysics. However, owing to numerical difficulties in treating the Hall term, their models account only for Ohmic diffusion. A complete treatment of magneto-thermal evolution, properly including the Hall term, was recently presented by Viganò et al. (2013, see also Viganò, Pons & Miralles 2011b). Their calculations confirm the basic picture outlined in Pons et al. (2009), although the presence of the Hall drift introduces some remarkable differences. Contrary to the purely dissipative case, evolution is not very sensitive to the initial relative strength of the toroidal component with respect to the poloidal one, unless the former is much higher than the latter. This is because a toroidal component builds up anyway due to the Hall term, even starting with a purely poloidal field configuration. Models are not strongly dependent on other parameters (notably the star mass) either, so that the evolution is mostly controlled by the initial value of the dipolar field. Fig. 1 shows the evolution of the dipolar field and of the thermal luminosity for different initial magnetic geometries: core field (model B14), core+crustal field (C14) and purely crustal field (A14, AT14). The different decay pattern of crustal vs. core fields is evident.

2.3. Magnetars and other neutron star classes

Over the last two decades our picture of the Galactic neutron star population has changed drastically, mainly thanks to high-energy observations. Besides SGRs/AXPs, the existence of several new classes of isolated neutron stars (INSs), with properties quite at variance with those of ordinary radio-pulsars (PSRs), has emerged: the central compact objects in supernova remnants (CCOs in SNRs), the rotating radio transients

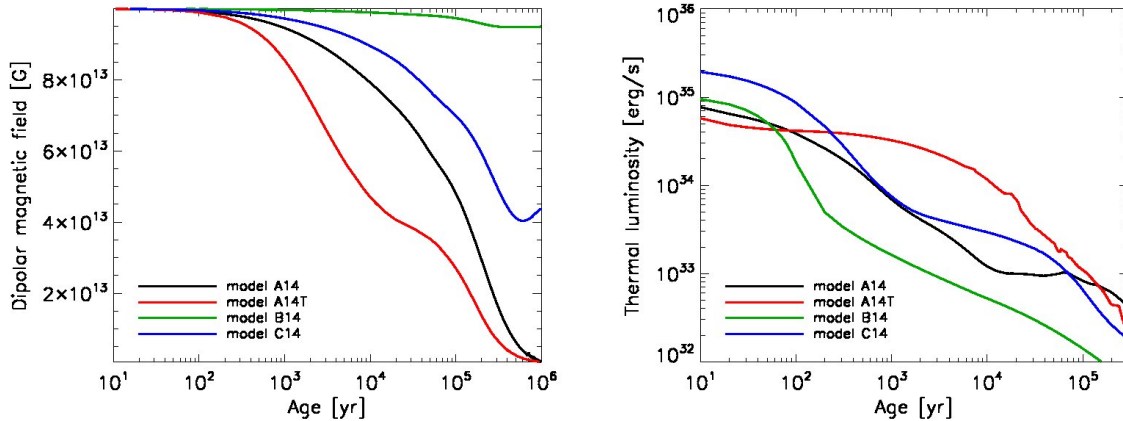


Figure 1 Left panel: evolution of the dipole field polar strength. Right panel: same for the thermal luminosity. In all models the initial poloidal field is 10^{14} G; the initial toroidal field is zero apart from model A14T, where it is 5×10^{15} G. The star mass is $1.4M_{\odot}$ (from Viganò et al., 2013, with OUP permission).

(RRaTs) and the X-ray dim INSs (XDINSs or M7) (see e.g. Kaspi, 2010; Harding, 2013; De Luca, 2008; Ho, 2012; Burke-Spolaor, 2012; Turolla, 2009, for reviews). All these sources are radio-silent or, in the case of RRaTs (and SGRs/AXPs), show only sporadic (transient) radio emission (see Sec. 4.3). They were discovered as X-ray pulsators, with the exception of the RRaTs (only one is currently known as an X-ray source, McLaughlin et al., 2007), and their spectrum is mostly thermal. While the periods are quite long (from ≈ 0.1 – 0.4 s for the CCOs to ≈ 1 – 10 s for the XDINSs and RRaTs), their period derivatives span a large interval, with implied magnetic fields ranging from as low as $\sim 3 \times 10^{10}$ G in some of the CCOs (which are sometimes referred to as the “anti-magnetars”), to $\sim 10^{12}$ – 10^{13} G in RRaTs and XDINSs (see Keane et al., 2011; Turolla, 2009). Ages are also very different, CCOs being quite young (the associated SNR age is $\lesssim 10^4$ yr) and XDINSs much older (the estimated dynamical ages are $\approx 10^5$ yr, e.g. Mignani et al., 2013, and references therein); in both cases the “true” ages turn out to be shorter than the spin-down ages. Like PSRs, RRaTs appear to be rotationally-powered, while the (thermal) X-ray emission from XDINSs and CCOs is powered by the release of residual heat. The position of the various sources in the P – \dot{P} diagram is shown in Fig. 2.

Although the number of detected sources in each class is fairly limited in comparison to that of PSRs (7 XDINSs, $\gtrsim 70$ RRaTs, 8 CCOs, about 20 SGRs/AXPs, and few candidates in each class, vs. > 2000 PSRs||), the estimated birthrate of XDINSs and RRaTs is comparable to and possibly higher than that of PSRs, $\beta_{\text{PSR}} \sim 0.015$ – 0.03 yr $^{-1}$ (Popov, Turolla, & Possenti, 2006; Keane & Kramer, 2008, and references therein). The magnetar birthrate is lower than those of other classes, $\beta_{\text{mag}} \sim 0.003$ yr $^{-1}$, although this

|| ATNF pulsar catalogue, <http://www.atnf.csiro.au/research/pulsar/psrcat/>

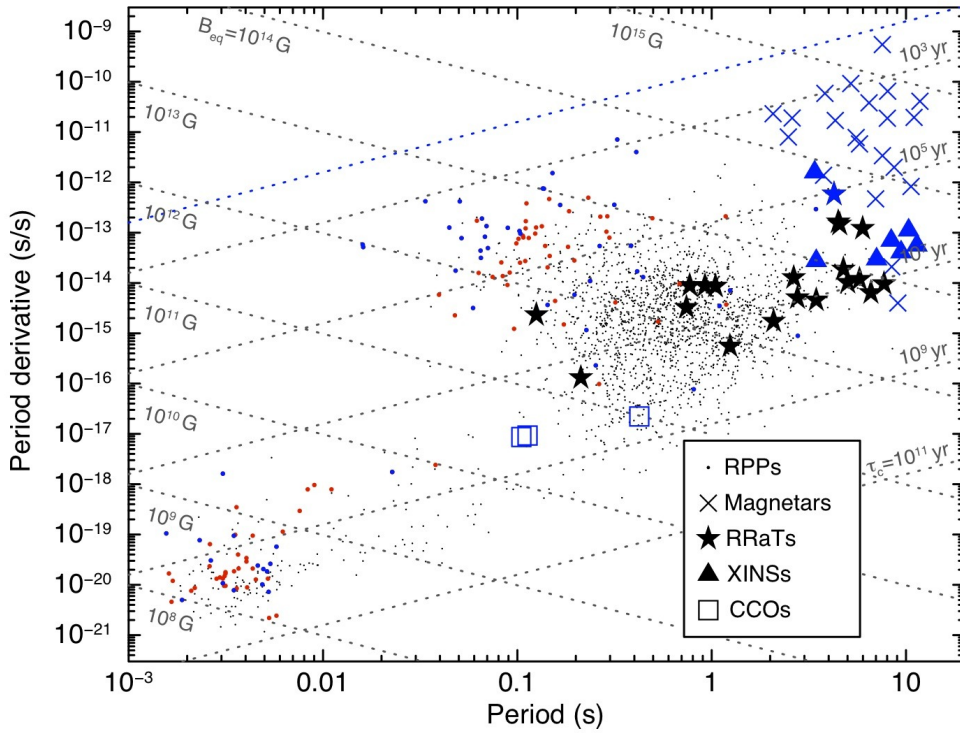


Figure 2 The $P-\dot{P}$ diagram illustrating the placement of the different isolated neutron star classes. The blue dots mark pulsars detected both in the radio and X-ray bands, the red ones those observed only at X-ray energies. The lines of constant age and magnetic field are also shown (courtesy R.P. Mignani).

is likely a lower limit given the increasing number of SGRs/AXPs discovered recently.

This clearly is an issue, since the sum of the birthrates of the various INS types cannot exceed the core-collapse supernova rate in the Galaxy, $\beta_{\text{SN}} \sim 0.02 \pm 0.01 \text{ yr}^{-1}$. Unless the current figures for the INS birthrates are grossly overestimated (and/or INSs can form through other channels), this implies that some evolutionary links exist among the different classes (Keane & Kramer, 2008). That XDINSs might be aged, worn-out magnetars has been suggested repeatedly, on the basis of the similarity of the periods and the (relatively) high magnetic fields of the former (e.g. Turolla, 2009). Besides the need to find evolutionary links among the groups, the variety of INS manifestations brings in an even more fundamental question: which initial parameters determine whether a proto NS will become, say, a magnetar or a PSR? The idea that the properties (and the evolution) of an INS are governed by a limited number of macrophysical quantities at birth (e.g. mass, magnetic field, period) may indeed open the way to what has been called the “grand unification of neutron stars”, or GUNS for short (e.g. Kaspi, 2010;

Igoshev, Popov & Turolla, 2014).

Magnetic field decay is bound to play a central role in any attempt to build a GUNS. Popov et al. (2010) were the first to perform INS population synthesis calculations including magneto-thermal evolution, adopting the treatment of Pons et al. (2009). Their model satisfactorily reproduces all INS populations if the initial magnetic field follows a log-normal distribution with a mean value $B_0 = 1.8 \times 10^{13}$ G. Their picture confirms that the magnetic field decays substantially (by a factor $\gtrsim 10$) in the most magnetic stars, but provides no clear indications for evolutionary links among the different INS groups. New population synthesis calculations, including more updated magneto-thermal evolutionary models, have been recently presented by Gullón et al. (2014). A more decisive indication that such links indeed exist comes from the tracks computed by Viganò et al. (2013) by coupling the magnetic field and period evolution (see Fig. 3). The main effect of magnetic field decay is to produce a sharp bending of the track downwards after a time $\approx 10^5$ yr for strong initial fields. This implies that the star’s period does not increase indefinitely but freezes at an asymptotic value which depends on the initial magnetic field, the mass of the star and the crust resistivity (see also Dall’Osso, Granot & Piran, 2012). A comparison between the theoretical tracks and the positions in the $P-\dot{P}$ plane of INSs of different types (see again Fig. 3) suggests that “moderate” magnetars ($B_0 = \text{a few} \times 10^{14}$ G) evolve into XDINSs.

3. Persistent emission

3.1. Magnetospheric twist

The current picture of a magnetar magnetosphere relies on the notion that the star’s external magnetic field differs from a simple, potential dipole, which is usually assumed to be the case for “standard” neutron stars. The reason for which the external field is not dipolar is to be sought in the structure of the internal magnetic field. Over the last decade, analytical and numerical investigations have shown that any stable configuration for the internal magnetic field of a star has necessarily to contain both a poloidal and a toroidal component (e.g. Tayler, 1973; Flowers & Ruderman, 1977; Braithwaite & Spruit, 2006; Braithwaite & Nordlund, 2006; Braithwaite, 2008, 2009). In particular, Braithwaite (2009) investigated stable, axisymmetric magnetic equilibria and found that the ratio of the two components must be such that $aE/U \lesssim E_p/E \lesssim 0.8$, where E and U are the total magnetic and gravitational energies, E_p is the energy associated with the poloidal component and a is a numerical factor. Given that $E/U \lesssim 10^{-23}$ and $a \approx 10^3$ for a neutron star, its internal magnetic field likely comprises a toroidal component at least of the same order as, and possibly much stronger than, the poloidal one. The instability of purely poloidal or toroidal magnetic configurations was proven also by Newtonian (e.g. Lander & Jones, 2011a,b) and general-relativistic (e.g. Ciolfi et al., 2011; Ciolfi & Rezzolla, 2012) numerical simulations (see also Ciolfi, 2014, for a recent overview). Although, earlier attempts with the twisted-torus model (a likely configuration for the

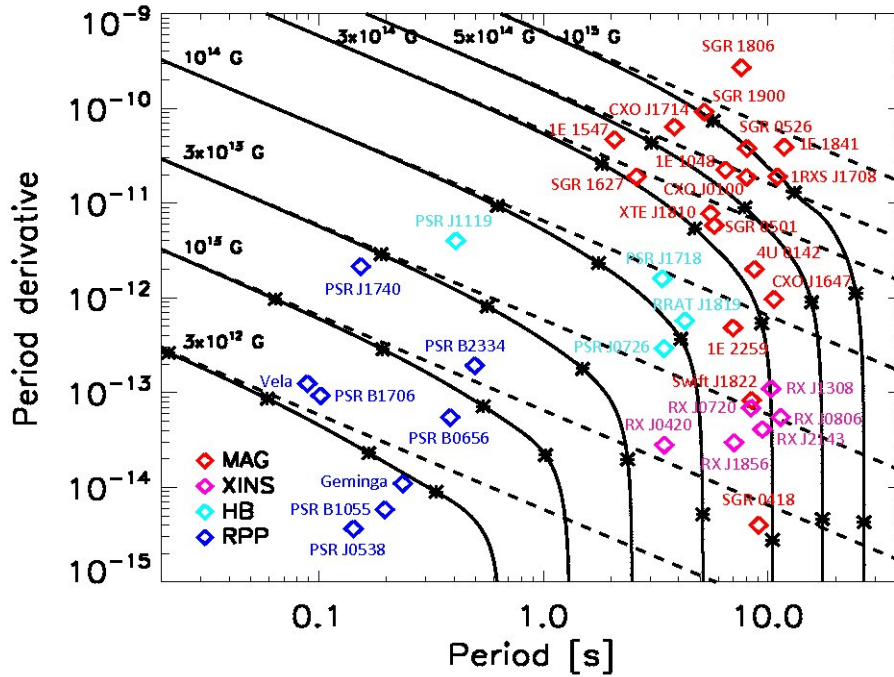


Figure 3 Evolutionary tracks in the $P-\dot{P}$ plane of INSs with different initial magnetic fields. Asterisks mark the real age of the source along the track (10^3 , 10^4 , 10^5 , 5×10^5 yr) and the dashed lines give the tracks with constant B . MAG = SGRs/AXPs, XIN = XDINSs, HB = high-B PSRs, RPP = PSRs (from Viganò et al., 2013, with OUP permission).

internal stellar field, e.g. Braithwaite & Nordlund, 2006) pointed towards poloidal-dominated geometries, which are themselves unstable (Ciolfi, 2014, and references therein), more recent calculations indicate that large toroidal fields (comprising up to 90% of the total magnetic energy) can indeed be achieved in this framework (Ciolfi & Rezzolla, 2013, see also Akgün et al., 2013 for magnetic configurations with $B_{tor} \gg B_{pol}$). Due to the complexity of the problem, most of those studies considered either the internal field structure (given an assumption for the magnetosphere) or the external magnetosphere (assuming an internal current distribution). The first global models, recently presented by Ruiz et al. (2014); Glampedakis et al. (2014), and Pili et al. (2015) in both Newtonian gravity and GR, appear promising, although a proper analysis of their stability has not been carried out yet.

In a magnetar, where the internal field can exceed 10^{15} G, magnetic stresses can overcome the crustal tensile strength (Thompson & Duncan, 1995). The easiest way in which the crust reacts to the applied forces is through horizontal displacements, parallel to the magnetic equipotential surfaces, i.e. a magnetically-stressed crustal patch tends to rotate by an angle $\Delta\phi$ (Thompson et al., 2000). This can be understood by considering a flux tube in which the toroidal component is non-zero in the crust and vanishes outside

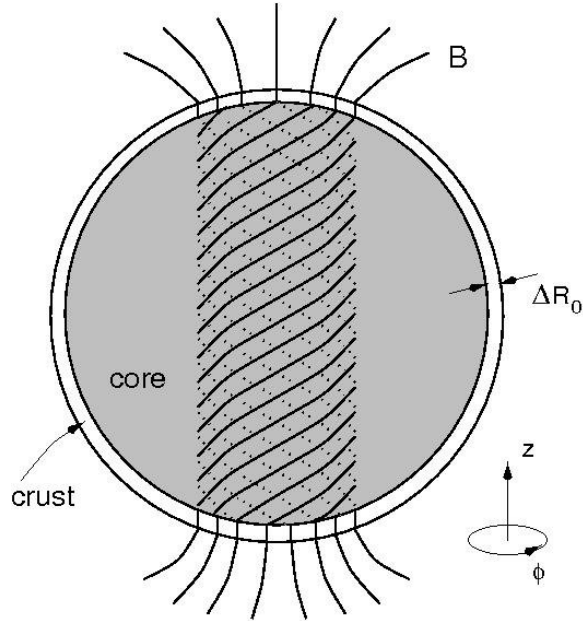


Figure 4 A schematic view of a magnetar internal field (Thompson & Duncan, 2001, ©AAS. Reproduced with permission. A link to the original article via DOI is available in the electronic version).

the star (Thompson, Lyutikov & Kulkarni, 2002). Because the conductivity is much higher in the star’s interior, the currents supporting the non-potential B -field will close in a thin surface layer. The Lorentz force acting on the current, and hence on the layer, is $\vec{F}_L = \vec{j} \times \vec{B}/c = j \times (\vec{B}_p + \vec{B}_t)/c$, where \vec{j} is the current density. The part of \vec{F}_L due to the toroidal field \vec{B}_t tries to produce a vertical displacement, which is unlikely to occur due to the strong stratification (Reisenegger & Goldreich, 1992), while the part associated with the poloidal component \vec{B}_p results in a slippage in the horizontal direction (see Fig. 4).

A direct effect of the magnetically-induced rotation of a surface platelet is the twisting of the external field. Since the external magnetic field lines are anchored to the crust, a torsional displacement of the surface layers produces a transfer of magnetic helicity from the interior to the exterior. If the external field is initially dipolar, it will acquire a non-zero toroidal component, a twist, confined to the field lines whose footpoints are on the displaced layer. In a twisted magnetosphere, currents necessarily flow also along the closed field lines to support the non-potential field. This is at variance with what is usually assumed to occur in “normal” radio-pulsars, where charges (the Goldreich-Julian currents) move only along the open field lines (again because the B -field is non-potential in that region). The presence of large-scale currents in a magnetar magnetosphere has major implications in shaping the emergent spectrum through repeated resonant cyclotron scatterings, as will be discussed in Sec. 3.3. The gradual implant and subsequent decay of a magnetospheric twist has been often invoked to explain the long terms evolutions of some magnetars (Mereghetti et al., 2005b;

Campana et al., 2007), for example the behaviour observed before or after a series of bursts or a giant flare. For instance, before the giant flare emitted by SGR 1806-20, the source properties changed remarkably: a study of the observed long-term variations indicated a clear correlation among the increases in spectral hardening, spin-down rate, and bursting activity (Thompson, Lyutikov & Kulkarni, 2002; Mereghetti et al., 2005b). The proposed scenario assumes the onset of a gradually increasing twist: this, in fact, results in an increasing optical depth for resonant cyclotron scattering, and causes a progressive hardening of the X-ray spectrum. At the same time, the spin-down rate is expected to increase because, for a fixed dipole field, the fraction of field lines that open out across the speed-of-light cylinder grows. Since both the spectral hardening and the spin-down rate increase with the twist, the model predicts that they should be correlated in agreement with the observations.

Although magnetospheric twists are expected to be localized, meaning that they do not affect the entire magnetosphere (Thompson, Lyutikov & Kulkarni, 2002; Beloborodov, 2009), nearly all studies on the properties of the persistent emission from magnetars rely on the “globally twisted magnetosphere” first proposed by Thompson, Lyutikov & Kulkarni (2002). In this model it is assumed that the external magnetic field is initially dipolar and that, as a consequence of crustal displacements, a certain amount of shear is added to the field. If one restricts to magnetostatic equilibria in a low-density plasma, the momentum equation reduces to $\nabla_{\parallel} \vec{j} \times \vec{B} = 0$, which, combined with the Ampère-Maxwell equation $\vec{\nabla} \times \vec{B} = (4\pi/c)\vec{j}$ gives the force-free condition

$$(\vec{\nabla} \times \vec{B}) \times \vec{B} = 0. \quad (1)$$

By expressing the poloidal component through the flux function \mathcal{P} , an axisymmetric field has the most general form

$$\vec{B} = \frac{\vec{\nabla} \mathcal{P}(r, \theta) \times \vec{u}_{\phi}}{r \sin \theta} + B_{\phi}(r, \theta) \vec{u}_{\phi}, \quad (2)$$

where B_{ϕ} is the toroidal component and \vec{u}_{ϕ} the unit vector in the ϕ direction. By exploiting the force-free condition one can explicitly write the magnetic field as

$$\vec{B} = \frac{B_p}{2} \left(\frac{r}{R_{NS}} \right)^{-p-2} \left[-f', \frac{pf}{\sin \theta}, \sqrt{\frac{C p}{p+1}} \frac{f^{1+1/p}}{\sin \theta} \right] \quad (3)$$

where a prime denotes a derivative with respect to $\mu \equiv \cos \theta$, B_p is the polar value of the magnetic field, R_{NS} is the star radius, C is a constant and $0 \leq p \leq 1$ is the radial index. The function $f(\mu)$ satisfies the Grad-Shafranov equation

$$(1 - \mu^2)f'' + p(p+1)f + C f^{1+2/p} = 0 \quad (4)$$

which is a second order ordinary differential equation for the angular part of the flux function. Since equation (4) must be (numerically) solved subject to three boundary conditions (Thompson, Lyutikov & Kulkarni, 2002; Pavan et al., 2009), the constant

¶ SGRs/AXPs are slow rotators and the Coulomb force is negligible in the inner magnetosphere.

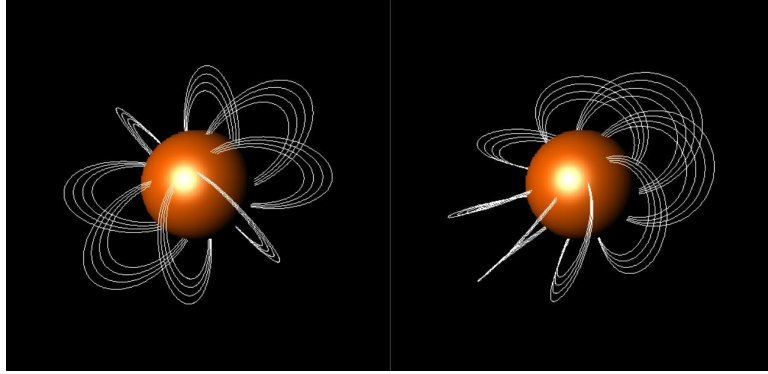


Figure 5 A globally twisted dipolar field (right panel) as compared with a pure dipole magnetic configuration (left panel).

C is an eigenvalue and is completely specified once p is fixed. The solution of equation (4) completely determines the external magnetic field and provides a sequence of magnetostatic, globally-twisted dipole fields by varying the index p . A picture illustrating a globally-twisted dipole is shown in Fig. 5.

Besides controlling the radial decay, the value of p also fixes the amount of shear of the field. In fact, the twist angle, i.e. the angle through which a field line has rotated when it comes back to the stellar surface, is defined as

$$\Delta\phi = \int_{field\ line} \frac{B_\phi}{(1-\mu^2)B_\theta} d\mu = \left[\frac{C}{p(1+p)} \right]^{1/2} \int_0^1 \frac{f^{1/p}}{1-\mu^2} d\mu. \quad (5)$$

The effect of decreasing p is to increase B_ϕ with respect to the other components, and consequently to increase the shear. The limiting values $p = 0, 1$ correspond to a split monopole and an untwisted dipole, respectively.

Primarily to assess the role played by the magnetic geometry on the emergent spectra, the effects on the spectra of other sheared magnetospheric configurations have been investigated. In these models the helicity is not uniformly distributed and, in a sense, they can be thought of as closer to the realistic case in which the twist is localized. Globally-twisted multipolar fields have been considered by Pavan et al. (2009), following essentially the same approach adopted by Thompson, Lyutikov & Kulkarni (2002) for the dipole. More recently, Viganò et al. (2012, see also Viganò, Pons & Miralles 2011) explored more general, non self-similar, force-free configurations for the external B -field in which an arbitrary function is used to control the spatial distribution of the twist. The implications for spectral calculations will be discussed in Sec. 3.3.2

Once implanted by a starquake, the twist must necessarily to decay. In a genuinely static twist ($\partial\vec{B}/\partial t = 0$), in fact, the electric and magnetic fields are orthogonal. This implies that the voltage drop between the footpoints of a field line vanishes since $E_{\parallel} = 0$, so that there is no force that can extract particles from the surface and lift them against gravity thus initiating the current required to sustain the sheared field, $\vec{j}_B = c\vec{\nabla} \times \vec{B}/4\pi$. As discussed by Beloborodov & Thompson (2007, see also Thompson et al. 2000), the

twist decays precisely to provide the potential drop required to accelerate the charges. A non-vanishing E_{\parallel} is maintained by self-induction and the twist evolution is regulated by the balance between the conduction current j and j_B , $\partial E_{\parallel}/\partial t = 4\pi(j_B - j)$. If $j < j_B$ the magnetosphere becomes charge starved and E_{\parallel} grows at the expense of the magnetic field, injecting more charges into the magnetosphere. On the other hand, when $j > j_B$ the field decreases, reducing the current. The magnetosphere is then in a dynamical (quasi-)equilibrium with $j \sim j_B$ over a time-scale $< t_{\text{decay}}$. The potential drop across a field line is maintained close to the pair production threshold, $e\Phi \approx 1 \text{ GeV}$, and the rate of magnetic energy dissipation is $\dot{E}_{\text{mag}} \approx I\Phi$, where $I \approx j_B l^2$ is the current and l the linear size of the twisted region (Beloborodov & Thompson, 2007). The magnetic energy stored in the twist is $E_{\text{mag}} \approx I^2 R_{\text{NS}}/c^2$, and the twist decay time $t_{\text{decay}} \approx E_{\text{mag}}/\dot{E}_{\text{mag}}$ turns out to be $\approx 1 \text{ yr}$ for typical parameter values. The detailed evolution of a twisted magnetosphere has been investigated by Beloborodov (2009).

3.2. Current distribution

A twisted magnetosphere can be regarded as a force-free configuration, threaded by currents that flow along the B -field lines with $\vec{j} \sim \vec{j}_B$. Charges are extracted from the star's surface and accelerated by the electric field parallel to \vec{B} . In the simplest picture (Thompson, Lyutikov & Kulkarni, 2002), the charge flow consists of two counter-streaming currents: electrons and ions moving in opposite directions, so that charge neutrality is ensured. Using a simple, unidimensional circuit analogue, a twisted flux tube is akin to a relativistic double layer (Beloborodov & Thompson, 2007; Carlqvist, 1982), in which electrons/ions leave the anode/cathode and are accelerated by a potential drop, which, in turn, depends on the current. Beloborodov & Thompson (2007) pointed out that such a configuration cannot be realized in the magnetosphere of a magnetar. In order to produce $j \sim j_B$, in fact, the Lorentz factor of the electrons needs to be sufficiently high ($\gamma \approx 10^9$) to make one-photon pair production in the strong magnetic field through resonant cyclotron up-scattering unavoidable well before γ attains such large values. Currents are expected to be carried mostly by pairs, the corona being in a state of self-organized criticality with a voltage drop near the threshold for the ignition of pair cascades.

The analysis by Beloborodov & Thompson (2007) revealed much of the (complex) physics of a twisted magnetosphere. Still, being based on an idealized circuit model, it was not particularly suited for being used in spectral modelling. For this reason most investigations in this direction have resorted to the simpler, albeit less physically sound, picture of electron/ion currents. Under this assumption and having specified the magnetic configuration, the density of magnetospheric particles is automatically fixed once the particle velocity is known. In particular, for a force-free globally twisted dipolar field (Thompson, Lyutikov & Kulkarni, 2002; Fernández & Thompson, 2007; Nobili, Turolla & Zane, 2008a), the charge density can be derived from the condition

$$j = j_B$$

$$n_e(\vec{r}, \beta) = \frac{p+1}{4\pi e} \left(\frac{B_\phi}{B_\theta} \right) \frac{B}{r|\langle\beta\rangle|}, \quad (6)$$

where $\langle\beta\rangle$ is the average charge velocity (in units of c). The previous expression gives the co-rotation charge density of the space charge-limited flow of ions and electrons from the NS surface, that, due to the presence of closed loops in a twisted field, is much larger than the Goldreich-Julian density, n_{GJ} . In a general scenario, positive and negative charges (with densities n_\pm) flow in opposite directions with velocities v_\pm and $j = j_B = e(v_+n_+ - v_-n_-)$, where $v_+v_- < 0$. Electrons are assumed to flow from north to south and conversely for ions. This breaks the symmetry between the star's two hemispheres, and, for instance, implies that the observed spectrum will be different when viewed from the north or the south pole (see Nobili, Turolla & Zane, 2008a). The presence of ions introduces negligible effects on the continuum spectra. Photons may still scatter off ions, which are heavier and concentrated toward the star's surface, but this is likely to give rise at most to a narrow absorption feature at the ion cyclotron energy (Thompson, Lyutikov & Kulkarni, 2002; Fernández & Thompson, 2007; Tiengo et al., 2013, and discussion in Sec. 4.2). For this reason, these models are often referred to as “unidirectional flows”, with reference to electrons only, while the term “bidirectional flows” is used when pairs are accounted for.

In the absence of any detailed modelling of the current flow (e.g. particle acceleration, interaction of charges with radiation traversing the magnetosphere), the velocity distribution is assumed to be spatially independent so that the charge velocity is a free parameter of the model. A major difference between the various models (Fernández & Thompson, 2007; Nobili, Turolla & Zane, 2008a) is in the adopted description of the velocity distribution of the scattering particles. In a strong magnetic field the electron distribution is expected to be largely anisotropic: e^- stream freely along the field lines, while they are confined in a set of cylindrical Landau levels in the plane perpendicular to \vec{B} . For this reason, Nobili, Turolla & Zane (2008a) assumed a collective (bulk) electron motion with velocity v_{bulk} associated with the charge flow in the magnetosphere, superimposed on a 1-D relativistic Maxwellian distribution at a given temperature T_e which simulates the particle velocity spread (and the dissipation due to local turbulence and possible instabilities).

The (invariant) distribution function is then

$$\frac{dn_e}{d(\gamma\beta)} = \frac{n_e \exp(-\gamma'/\Theta_e)}{2 K_1(1/\Theta_e)} = n_e f_e(\vec{r}, \gamma\beta) \quad (7)$$

where $\gamma' = \gamma\gamma_{bulk}(1 - \beta\beta_{bulk})$, $\Theta_e = kT_e/m_e c^2$, K_1 is the modified Bessel Function of the first order and $f_e = \gamma^{-3}n_e^{-1}dn_e/d\beta$ is the momentum distribution function.

In this model electrons are, then, assumed to move isothermally along the field lines, whilst at the same time receiving the same boost from the electric field. This is at least in qualitative agreement with the results of the simplified bidirectional model by Beloborodov & Thompson (2007). A different choice was made by Fernández &

Thompson (2007), who did not include the charge bulk motion in their models (despite this being a necessary ingredient to reproduce the current flow) and assessed the effects of other possible (local) distributions, either thermal or not thermal, in a few representative cases. In particular, they considered:

a) a mildly relativistic, 1-dimensional flow described by a Boltzmann distribution at a temperature $k_B T_0 = (\gamma_0 - 1)m_e c^2$

$$f(\beta\gamma) = \frac{1}{K_1(1/[\gamma_0 - 1])} \exp\left[-\frac{\gamma}{\gamma_0 - 1}\right]; \quad (8)$$

b) a mildly relativistic, one-dimensional gas with the same Boltzmann distribution but extending over positive and negative momenta, in order to simulate an electron-positron flow; and

c) a broad power-law in momentum,

$$f(\beta\gamma) \propto (\beta\gamma)^\alpha, \quad (9)$$

which mimics a warm relativistic plasma.

As we discuss in the next section, charges must flow at mildly relativistic speed ($\gamma \simeq 1$) in the twisted magnetosphere for the model to successfully reproduce the observed X-ray spectra. While this is not a problem for the (over) simplified unidirectional flows discussed earlier on, where the velocity is a tunable parameter, the question of what occurs in a more realistic description which includes pairs is a crucial one. As discussed by Beloborodov & Thompson (2007), in a twisted magnetosphere electrons and ions, lifted from the star's surface and accelerated by the self-induction electric field, must efficiently produce e^\pm , at least if the current circulating in the circuit is $\sim j_B$. According to their analysis, e^\pm flow with highly relativistic speed ($\gamma \approx 10^3$) and a large velocity spread in the inner magnetosphere ($r \sim R_{NS}$). This poses a problem for the mildly-relativistic, counter-streaming model which is only valid in the (unphysical) assumption that pair production is neglected (Beloborodov, 2013a). On the other hand, in the presence of pairs, the electric field along the B -lines, E_{\parallel} , is incapable of counteracting the radiative pull outwards because, at the same time, it acts as an accelerator for the charges of opposite sign. The result is that charges are accelerated outwards at relativistic velocity and no self-consistent solution yielding mildly relativistic flows is possible.

Pair production in a twisted magnetosphere has been investigated in several works. As discussed by Medin & Lai (2007), for an iron crust and magnetic fields as high as $\sim 10^{15}$ G, vacuum gaps may be formed above the polar regions of SGRs/AXPs, with subsequent pair creation. Near the stellar surface, where the magnetic field B exceeds the quantum limit $B_Q \sim 4.4 \times 10^{13}$ G, scattering between fast electrons and ~ 1 keV seed photons generates high-energy gamma rays that immediately convert to electron/positron pairs via one-photon pair production (e.g. Harding & Lai 2006). This idea, originally proposed by Beloborodov & Thompson (2007), has been more recently reconsidered in detail by several teams (Nobili, Turolla & Zane, 2011; Zane et al., 2011b). The main point is that single photon pair production requires photons with

energy higher than the threshold value, ~ 1 MeV. Therefore, in a region dominated by resonant scattering, pair creation occurs in two steps: (i) a seed photon with energy $\epsilon \sim 1$ keV is up-scattered by a relativistic particle with $\gamma = \gamma_{res} \sim (m_e c^2 / \epsilon)(B/B_Q) \sim 1000$, where γ_{res} is the charge Lorentz factor at resonance, gaining a considerable energy $\epsilon' \sim \gamma_{res}^2 \epsilon / (1 + \gamma_{res} \epsilon / m_e c^2)$; (ii) quite immediately, the high-energy photon converts to a e^\pm pair, via single photon pair production. As discussed by Zane et al. (2011b), the pair-dominated region is very thin and located just above the star's surface where $B > 0.05 B_Q$. Here a quasi-equilibrium configuration is reached with a pair multiplicity $\sim L / \lambda_{acc,res}$ of a few, where L is the length of the field line and $\lambda_{acc,res}$ is the distance travelled by a charge before reaching a Lorentz factor γ_{res} . Screening of the electric field limits the potential drop to $e\Phi_0 / m_e c^2 \approx \gamma_{res} \sim 500(B/B_Q)$ and the maximum e^\pm Lorentz factor is γ_{res} . Charges undergo only a few scatterings with thermal photons, but they lose most of their kinetic energy in each collision. In practice, the result is that a steady situation is maintained against Compton losses because electrons and positrons are re-accelerated by the electric field before they can scatter again. The newborn charges are accelerated by the huge electric field that permeates the magnetosphere up to a limit value, so that a cascade of pairs is generated. This runaway process limits the value of γ to the threshold value for pair production, ~ 1000 . Since pairs with $\gamma \sim \gamma_{res}$ are injected from this inner region into the external region, the circuit represented by the field lines behaves quite differently from a double layer, allowing the current to be conducted with only a small potential drop (see also Beloborodov 2011).

A detailed investigation of charge distribution in a twisted magnetosphere, based on analytical considerations and corroborated by numerical tests has been recently presented by Beloborodov (2013a,b). This work confirms the presence of an inner region with intense pair production. This region consists of two parts. The innermost one, where $B \gg B_Q$, is self-organized maintaining the near critical condition of pair production with multiplicity $M \sim 1$, and here the circuit operates as a global discharge (i.e. the accelerating voltage, which is screened by pairs, is distributed smoothly along the field line). Field lines that extend to larger distance from the star's surface enter an outer corona, which extends until $B \sim B_Q$, where both scattering and pair production are much more efficient and $M \sim 100$. Here, due to efficient radiative coupling, plasma and radiation organize themselves into a “locked” outflow with decreasing Lorentz factor. This leads to the formation of an extended equatorial zone in the outer corona, where the flow is slowed down by the combined effect of a large radiation drag and the onset of a two-stream instability with consequent strong Langmuir turbulence. The pair density is near annihilation balance and the charges, decelerated down to mildly relativistic velocities, creates an opaque layer which efficiently up-scatters the soft X-ray photons by distorting the surface thermal spectrum. Outside this equatorial region, and further away in the extended external magnetosphere, charges flow at ultra-relativistic velocity and scattering is relatively inefficient. The charge distribution is illustrated in Fig. 6. Despite this being the most complete study of magnetospheric currents presented so far, it contains some drastic simplifying assumptions. The pair multiplicity, for example,

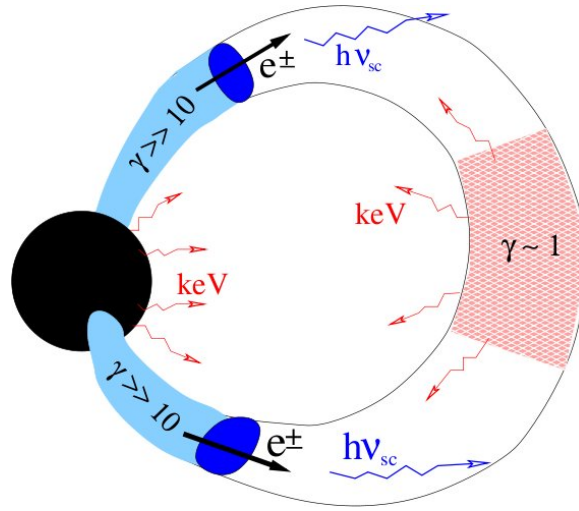


Figure 6 Sketch of an activated magnetic loop as proposed by Beloborodov (2013b). Relativistic particles are injected near the star where $B > B_{QED}$. Large e^\pm multiplicity ($M \sim 100$) develops in the adiabatic zone $B > 10^{13}$ G (shaded in blue). The outer part of the loop is in the radiative zone; here the scattered photons escape and form the hard X-ray spectrum. The outflow decelerates (and annihilates) at the top of the loop, shaded in pink; here it becomes very opaque to the thermal keV photons flowing from the star (from Beloborodov, 2013b, ©AAS. Reproduced with permission. A link to the original article via DOI is available in the electronic version).

is a constant parameter assumed a priori. This clearly affects many of the model results: local screening of the electric field, velocity distribution of the two species, development of the two-stream instability, efficiency of the radiative drag, and ultimately the formation of a zone filled with slowly moving charges. The challenging problem to find a fully consistent solution of current dynamics including the interaction with the radiation field remains so far unsolved.

3.3. Soft and Hard X-ray spectral modelling

3.3.1. Soft X-ray spectral modelling The soft X-ray band (0.3 – 10 keV) is the energy range in which magnetar spectra are best studied, thanks to a large amount of observations that have been collected in more than two decades with X-ray satellites such as *XMM-Newton*, *Chandra*, *Swift*. The observed spectra are generally fitted by a double component model consisting of a thermal component (a blackbody, at about ~ 0.5 keV) and a steep power law (photon index $\sim 3-4$) (Mereghetti, 2008). In a few cases (a notable example being the AXP XTE J1810-197) good spectral fits are also obtained with two blackbodies (Halpern & Gotthelf, 2005). The thermal component, which often dominates in the lowest energy band, most often has an inferred emission region (for the best estimated distances) much smaller than the whole surface of the NS. These spectral fits are of course phenomenological descriptions, but they indicate

that, although the emission is mostly thermal, it is more complex than a blackbody at a single temperature. It is also interesting to note that when one compares the average temperature (from the thermal luminosity) of magnetars with those of other classes of isolated neutron stars, there is a clear correlation between temperature and magnetic field (Aguilera et al., 2008) and the magnetars are systematically more luminous than rotation-powered neutron stars of comparable characteristic age (see a discussion in Mereghetti et al., 2014). The morphology of the soft X-ray pulse profiles of magnetars is varied. A few sources exhibit an (almost symmetric) double-peaked light curve (e.g. 1E 2259+586 and 4U 0142+0162; Patel et al., 2001; Woods et al., 2004; Rea et al., 2007c) with pulsed fraction in the range 10 – 20%. For most other magnetars, instead, the pulsed component is single peaked and often the pulsed fraction is high (see e.g. 1E 1048.1-5937, XTE J1810-197, 1E 1547.0-5408, SGR 0418+5729, and SGR J1822.3-1606 Tam et al., 2008; Bernardini et al., 2009, 2011a; Halpern & Gotthelf, 2011; Dib et al., 2012; Rea et al., 2013a, 2012a). As originally suggested by Marsden & White (2001), as a general rule sources with larger spin-down rate have smaller photon index in the soft X-ray band. This fact has been confirmed with more recent data and it appears to be valid for both persistent and transient sources in outburst, but only for rotational frequencies derivatives $\dot{\nu} \gtrsim 10^{-14} \text{ s}^{-2}$, and with some exceptions (including the transients in outbursts and the recently discovered low-B magnetars, see Sec. 4.2 and Mereghetti et al., 2014). The long term evolution of the power law component and timing properties of SGR 1806-20 indicates that the same correlation between spectral hardness and average spin-down rate also holds for a single source (Mereghetti et al., 2005b). On the wake of this, other correlations between the spectral hardness and the timing properties have been investigated. In particular, that with the dipole strength $B_{dip} \propto (P\dot{P})^{1/2}$ appears the most robust (Kaspi & Boydstun, 2010).

It has been widely suggested that the blackbody plus power law spectral shape that is observed below ~ 10 keV in magnetars' spectra may be accounted for if the soft, thermal spectrum emitted by the star's surface is distorted by resonant cyclotron scattering (RCS) onto the magnetospheric charges. Since electrons permeate a spatially extended region of the magnetosphere, where the magnetic field varies, resonant scattering is not expected to give rise to narrow spectral lines (corresponding to the successive cyclotron harmonics), but instead to lead to the formation of a hard tail superimposed on the seed thermal bump. This model is also in general agreement with the hardness- \dot{P} or hardness-magnetic field correlation mentioned above: stronger and more twisted fields yield a larger spin down rate as well a higher magnetospheric charge density that in turn produces a harder spectral tail. In recent years, several teams have tested the resonant cyclotron scattering model quantitatively against real data in the soft X-ray range, using different approaches and under different approximations. The first, seminal attempts in this direction were presented by Lyutikov & Gavriil (2006) who developed a very simplified one dimensional model. They assumed that seed photons are emitted by the NS surface with a blackbody spectrum, and propagate backward and forward in the radial direction. A thin, plane parallel magnetospheric slab, permeated

by a static, non-relativistic, warm medium at constant electron density is assumed to exist above the star’s surface. Magnetic Thomson scattering occurs between photons and the charges in the slab, and the process is computed by neglecting all effects of electron recoil, as are those related to the current’s bulk motion. Despite being clearly over-simplified, this model has the main advantage of being semi-analytical and, when systematically applied to X-ray data, has proved successful in capturing at least the gross characteristics of the observed soft X-ray spectrum (Rea et al., 2007a,b, 2008).

The same model has been extended by Güver et al. (2007), who relaxed the blackbody approximation for the seed surface radiation and made an attempt to include atmospheric effects, treating the star’s surface emission like that of a passive cooler, i.e. using an atmospheric code akin to those originally developed for sources with purely thermal emission (e.g. Zavlin et al., 1996; Zane et al., 2001; Özel, 2003; Potekhin, 2014, and references therein). This is a quite drastic and somewhat unphysical simplification for sources like magnetars, which are characterized by strong magnetospheric activity leading to particle back-bombardment, heat deposition and other similar effects. Despite this, the model has been applied to real data in an attempt to estimate the surface magnetic field through data fitting of the soft X-ray continuum (Güver et al., 2008, 2011; Özel, 2013). At present the problem appears to be still open: while it is commonly recognized that thermal radiation from the star’s surface is likely to be different from a simple blackbody, either because of local reprocessing by some sort of (non passive) atmosphere or because the surface itself may be in a condensed state, a self consistent inclusion of these effects in numerical models has not yet been carried out.

In order to perform a more physical, 3-D treatment of the RCS problem, the most suitable approach is to make use of a Monte Carlo technique, which is quite easy to code, and, when dealing with purely scattering media at moderate optical depths, relatively fast. The Monte Carlo scheme allows one to follow individually a large sample of photons, treating probabilistically their interactions with charged particles. These simulations have been developed by only a few teams (Fernández & Thompson, 2007; Nobili, Turolla & Zane, 2008a). The numerical codes that have been developed are completely general, inasmuch that in principle they can handle different 3-D geometries (so highly anisotropic thermal maps and magnetic fields) and different radiative models of surface emission. On the other hand, since our understanding of these ingredients is still limited, in order to minimize the number of degrees of freedom, simulations were computed by assuming, for simplicity, that i) the whole surface emits isotropically as a blackbody at a single temperature, ii) the magnetic field is a force-free, self-similar, twisted dipole and iii) the electron velocity distribution is assumed a priori (see Sec. 3.2). Besides, resonant scattering was treated in the magnetic Thomson limit, which allows one to account for polarization (under the two stream approximation) but it neglects electron recoil, limiting the applicability of the results to energies up to a few tens of keVs ($h\nu < mc^2/\gamma$ keV, $B/B_Q < 10$). By comparing the results from the different teams, one may conclude that, while the general effects induced by magnetospheric RCS on primary thermal photons (i.e. the formation of a “thermal-plus-power-law” spectrum) are not

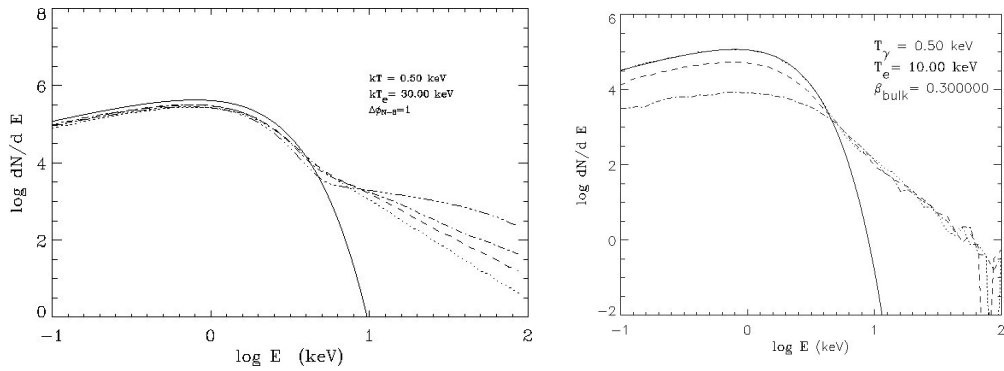
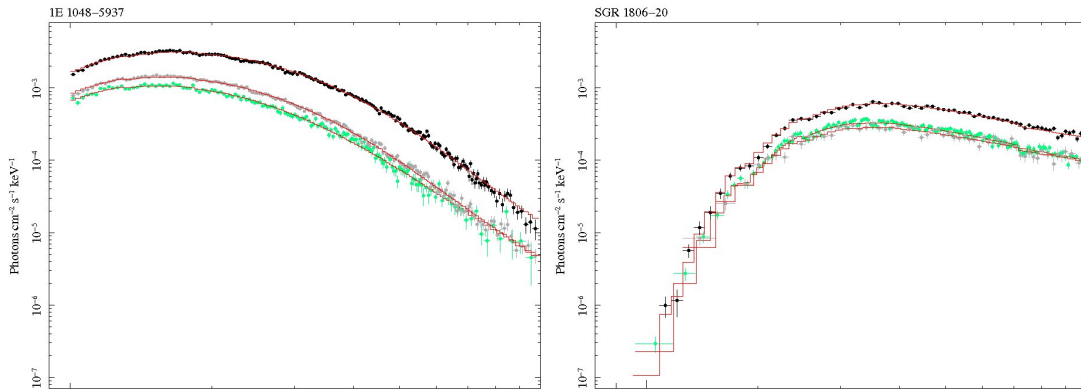


Figure 7 Left: Computed spectra from Monte Carlo simulations for $B = 10^{14}$ G, $kT = 0.5$ keV, $kT_e = 30$ keV, $\Delta\phi = 1$ and different values of β_{bulk} : 0.3 (dotted), 0.5 (short dashed), 0.7 (dash-dotted) and 0.9 (dash-triple dotted). The solid line represents the seed blackbody and spectra are computed at a magnetic colatitude: $\Theta_s = 64^\circ$. Right: Spectrum from a single emitting patch on the star surface. The line of sight is at $\Theta_s = 90^\circ$ and $\Phi_s = 20^\circ$ (dotted line), 140° (dashed line) and 220° (dash-dotted line). These three values correspond to having the emitting patch in full view (seen nearly face on), partially in view and screened by the star. The solid line represents the seed blackbody (readapted from Nobili, Turolla & Zane, 2008a, with OUP permission).



very sensitive to the assumed particle velocity distribution, the details of the spectral shape do, and, as we will discuss later on, this is particularly critical for the model predictions in the hard X-ray band. Nevertheless, in the soft X-ray band, for several combinations of the parameters, the general shape of the continuum is that of a thermal bump and a high-energy tail (see Fig. 7), which is in agreement with what is observed in the *XMM-Newton* and *Chandra* spectra (below ~ 10 keV). The spectral index of the high energy tail changes with the parameters and, in particular, harder spectra are found for increasing twist angle. This was invoked as a possible mechanism to explain the correlated flux-hardening long term variations in some sources (e.g. Thompson, Lyutikov & Kulkarni, 2002; Mereghetti et al., 2005b; Rea et al., 2005; Campana et al., 2007; Nobili, Turolla & Zane, 2008a).

The numerical spectra computed by Nobili, Turolla & Zane (2008a) have been

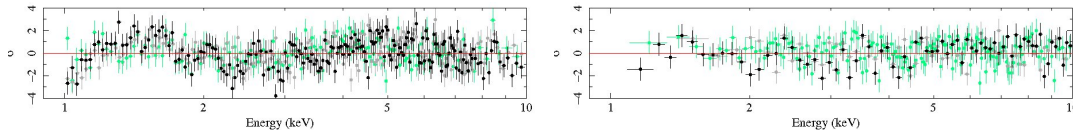


Figure 8 Fit of the *XMM-Newton* spectra of the AXP 1E1048-5937 and SGR 1806-20 with the NTZ model. The panels show a joint fit of spectra taken at three different epochs and the fitting has been restricted to the 1 – 10 keV range (adapted from Zane et al., 2009, with permission).

implemented in XSPEC and successfully fit the *XMM-Newton* spectra of most of the magnetar sources in quiescence (NTZ model, Zane et al., 2009, see also Fig. 8). This allows one to derive of the gross characteristics of the magnetosphere in such sources and to obtain a better estimate of the thermal component.

Interestingly, in the case of two sources, 1E2259+586 and 4U 0142+614, it was not possible to find a satisfactory fit with the NTZ XSPEC model although these spectra were fitted by the simplified 1-D model (Rea et al., 2007a). As suggested in Zane et al. (2009), a plausible cause is that the BB peak appears to be less prominent to the observer because the region that emits the soft seed photons is not completely in view. By modelling the RCS spectra under the assumption that photons are emitted by a single surface patch it is immediately clear that the effects of the different viewing angle on the spectrum are dramatic. When the emitting patch is in full view both the primary, soft photons and those which undergo repeated resonant scattering reach the observer, and the spectrum is qualitatively similar to those presented earlier on, with a thermal component and an extended power-law-like tail. If on the other hand the emitting region is not directly visible, no contribution from the primary blackbody photons is present (see Fig. 7, right panel). The spectrum, which is made up only by those photons which after scattering propagate “backwards”, is depressed and has a much more distinct non-thermal shape, much more similar to the one observed in 1E2259+586 and 4U 0142+614.

Unfortunately, in a realistic situation the thermal surface map is expected to be complex and it cannot always be reconstructed by fitting the X-ray spectrum alone. As discussed in Albano et al. (2010, see also Bernardini et al. 2011a), a better strategy consists of performing a simultaneous fitting of the energy-resolved X-ray lightcurves, since they carry a much more defined imprint of the surface thermal distribution (see Sec. 4 and Fig. 18 therein). While this is not possible for all sources, transient AXPs, for which a set of observations spread over few years and at different flux levels are available, provide a spectacular laboratory for this exercise. Albano et al. (2010) were the first (and so far the only) team to present a comprehensive study of the outburst decay of the two transient AXPs (TAXPs) XTE J1810-197 and CXOU J164710.2-455216, reproducing both the spectral and pulse profile evolution based on fits with three-dimensional Monte Carlo simulations. This allowed them to prove the presence of distinct temperatures zones (up to three) at the star’s surface, some of them possibly heated by the energy

released during the outburst, to model their evolution during the outburst decay, and to constrain the viewing geometry of the sources, i.e., the inclination of the line of sight and the magnetic axis with respect to the rotation axis.

A similar conclusion concerning the need to investigate the pulse profile behaviour when trying to reconstruct inhomogeneous surface thermal maps was reached by Perna et al. (2013). These authors considered the case in which the temperature anisotropy is observed also in quiescence, as is expected if complex magnetic field components in the NS crust and interior make heat transport from the core outward highly anisotropic. They used state-of-the art numerical codes (Viganò et al., 2012, 2013) for the coupled magneto-thermal evolution of neutron stars and computed the expected pulse profiles and spectra (under the assumption of blackbody emission) for a range of magnetic configurations. Particularly compelling is the finding that, while in presence of purely dipolar fields the pulse profile is always double-peaked and with a relatively low pulsed fraction, when strong toroidal components are present the pulse fraction can exceed 50–60% and the pulse profile can be single peaked (as often observed in AXPs and SGRs). Moreover, if the simulated spectra are fitted with a highly absorbed BB model, only relatively concentrated hot peaks are visible, so that the inferred BB radius turns out to be much smaller than the NS radius (even as low as 1-2 km, see Fig. 9). Strong toroidal crustal B-field components, coupled with large absorption column densities ($> 10^{22} \text{ cm}^{-2}$, see e.g. Esposito et al. 2008), can therefore explain the small caps very often required by the spectral fits of AXPs and SGRs. Even smaller (sub-km) hot spots are measured in certain sources (e.g. CXO J164710.2-455216, see e.g. Israel et al. 2007), but they look more likely to be produced by particle bombardment and heat deposition from currents highly concentrated in twisted magnetic polar bundles (Beloborodov, 2009; Turolla et al., 2011) which emerge from the crust, rather than anisotropic internal heat transfer. In this respect it is worth mentioning the work by (Bucciantini et al., 2015), who presented a comprehensive and detailed parameter study, in general relativity, of the role that the current distribution investigating several equilibrium global field configurations derived using a Grad-Shafranov approach (Pili et al., 2015). These authors found that the structure and strength of the magnetic field at the surface is strongly influenced by the location and distribution of currents inside the star, with the result that the surface field can easily be dominated by higher multipoles than the dipole. This means that in some cases the magnetic field at the equator can be even much higher or much smaller than the value of the field at the pole and implies that signatures observed in features originating at or near the surface might differ from the expectations of a dipole dominated model, while observations of processes related to the large scale field, as spin-down, will not (see also the discussion in Sec. 4.2).

3.3.2. Hard X-ray spectral modelling Hard X-ray observations with the *INTEGRAL*, *RXTE* and *Suzaku* satellites have shown that in some magnetar candidates (namely 4U 0142+614, 1RXS J1708-4009, 1E 1841-045, 1E 2259+586, SGR 1806-20, SGR 1900+14; Kuiper et al., 2004, 2006; Mereghetti et al., 2005a; Molkov et al., 2005; Götz et al., 2006;

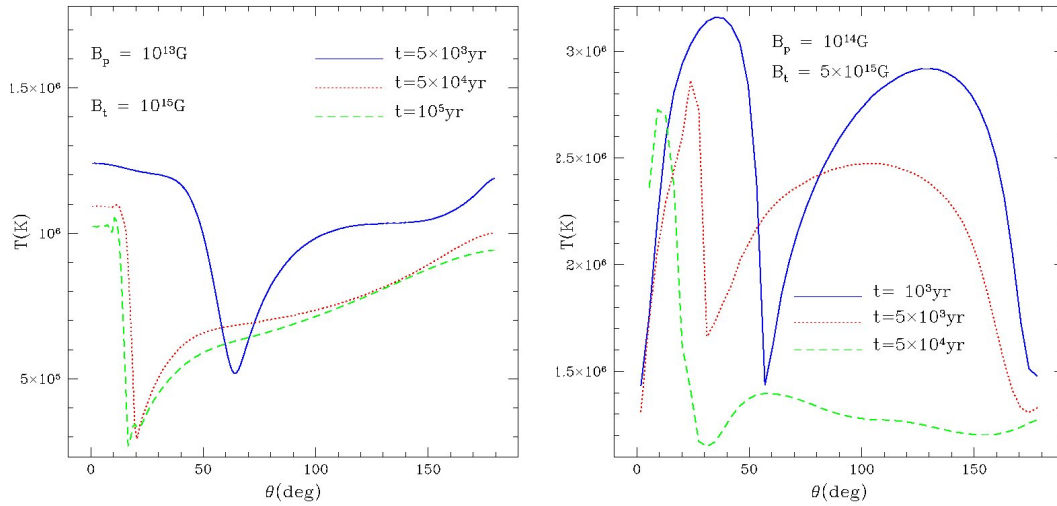


Figure 9 Temperature surface distribution for sources with a magnetic field at birth which has both a poloidal and a toroidal component. For ages typical of magnetars ($10^4 - 10^5$ yrs) the expected thermal map consists of a hot polar spot and an extended colder region; the latter may be undetected if the source is highly absorbed (from Perna et al., 2013, with OUP permission).

Enoto et al., 2011) a large fraction of the total quiescent flux is emitted at energies well above ~ 20 keV. These “hard” tails have a non-thermal (PL) character, and extend up to a few hundreds of keV. Pulsed phase spectroscopy has been performed for a few sources, although with limited statistics due to the low number of counts, revealing that the emission is likely characterized by different components that emerge at different, and sometimes only in limited, phase intervals (den Hartog et al., 2008a,b).

This discovery came quite unexpectedly and suggests that a new magnetar characteristics may be that a considerable fraction of their bolometric luminosity is emitted in the hard, rather than in the soft X-rays. In fact, limits on the non-detected sources are not deep enough to exclude the presence of a similar hard tail. The first observations of emission at > 20 keV revealed a difference between the (at that time separated) AXPs and SGRs (Götz et al., 2006): in the *Integral* and *RXTE* data the AXPs’ hard power law is considerably harder than that observed below 10 keV, while SGRs’ hard spectra are considerably steeper. More recent observations with *NuStar* indicate that the division is not as sharp and magnetar sources show a varied behaviour, which is consistent with the fact that SGRs and AXPs are now considered a single class (An et al., 2014b). *NuStar*, which has a sensitivity roughly two orders of magnitude better than previous missions in this energy band and a high angular resolution, is currently observing a selected sample of magnetars as part of its priority A targets (see An et al., 2014b, for a review and references therein). One of the major goal is to study the spectral location of the soft/hard X-ray turnover, which is expected to correlate with B_{dip} (Kaspi & Boydston, 2010). Interestingly, while for some sources the new *NuStar*

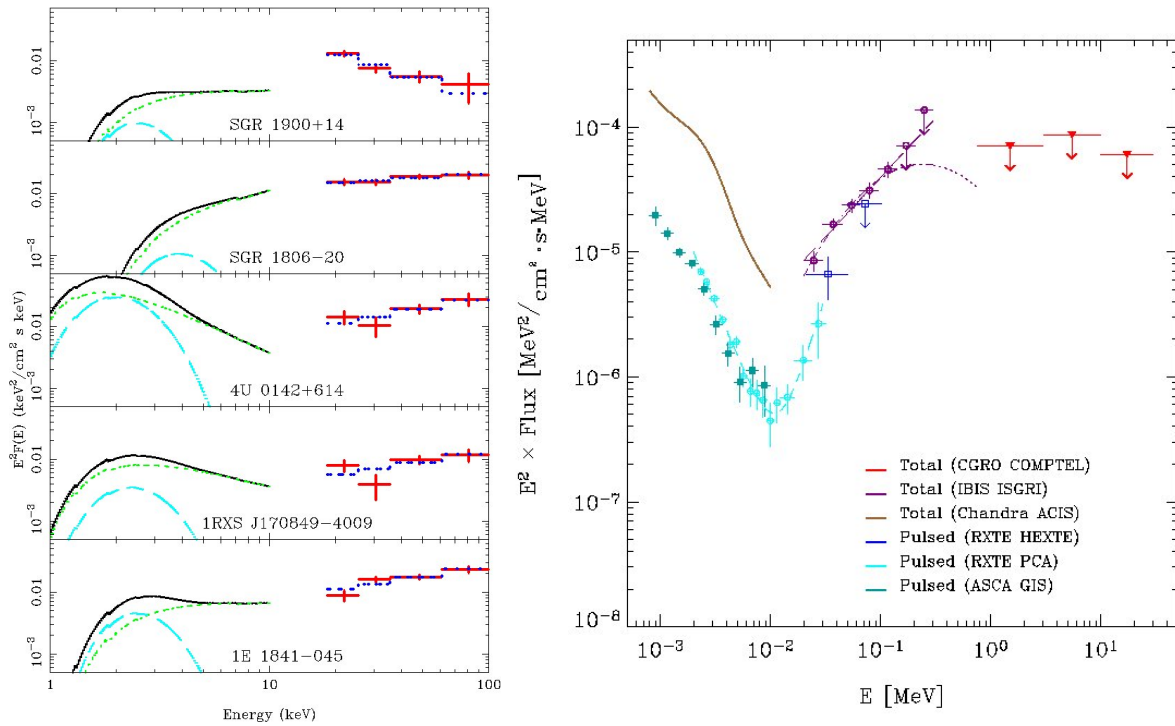


Figure 10 Left: XMM-Newton and INTEGRAL spectra of magnetars (from Götz et al., 2006, reproduced with permission ©ESO). Note the different behavior of SGRs (two top panels) and AXPs: in the latter sources the spectra turn upward above 10 keV, while in the SGRs the spectra steepen. Right: Broad band spectral energy distribution of 4U 0142+614 (from Kuiper et al., 2006, ©AAS. Reproduced with permission. A link to the original article via DOI is available in the electronic version). Both the total and the pulsed emission are indicated. Both figures are readapted from Mereghetti (2008), with kind permission from Springer Science and Business Media.

results are in agreement with the *Integral* and *RXTE* ones, in some other cases (e.g. 1E 2259+586) it appears evident that the hard band spectrum for the total emission is not as hard as the pulsed one. Despite that, the analysis of 1E 2259+586 data confirmed that an additional component, such as a power law, is needed to describe the emission in the hard X-ray band (Vogel et al., 2014). This suggests that at least in some sources the non thermal mechanisms responsible for the emission in the soft and hard X-rays are distinct, or that the charge properties in the two emission regions are different.

Observations at higher energy with Comptel and Fermi LAT failed to detect magnetar emission, implying the presence of a spectral break above a few hundred keV (Kuiper et al., 2006; den Hartog et al., 2006; Sasmaz Mus & Göğüş, 2010). The only exception reported so far is a possible Fermi Large Area Telescope (LAT) detection of γ -ray pulsations above 200 MeV from the AXP 1E 2259+586 (Wu et al., 2013) which however still needs a robust confirmation. Some example of few magnetar spectral energy distributions in the soft/hard X-rays are shown in Fig. 10.

The mechanism responsible for the high energy emission is still poorly understood,

at least in its quantitative details. High energy emission from currents moving in the highly magnetized magnetosphere is expected for a number of reasons. Thompson & Beloborodov (2005) originally suggested that hard X-rays may be produced either by thermal bremsstrahlung in the surface layers heated by returning currents, or by synchrotron emission from pairs created higher up (~ 100 km) in the magnetosphere. A further possibility, according to which the soft γ -rays may originate from resonant up-scattering of seed photons on a population of highly relativistic electrons, has been proposed by Baring & Harding (2005, 2008). As mentioned earlier, most of the RCS models computed with Monte Carlo simulations are based on the assumption that scattering can be treated in the Thomson approximation, which limits their validity up to a few tens of keV. Instead, a proper investigation of the effects of electron recoil and of multiple scatterings from high energy photons demand the use of the full QED cross section. Relatively simple expressions of the QED cross section at resonance, in a form that is simple to include in Monte Carlo simulations, have been computed by Nobili, Turolla & Zane (2008b) and a few examples of the emerging spectra, computed under the assumption of self-similarly distributed twist and constant electron velocity, have been discussed in Zane et al. (2011a). These simulations show that, if magnetospheric electrons are mildly relativistic, when considering self-consistently electron recoil and QED effects the spectrum exhibits a break at a few hundred of keV. This is due to the fact that, in order to populate the hard energy tail, soft seed photons need to experience a series of successive scatterings, each characterized by a limited energy gain because the Lorentz factor of electrons is only $\gamma \sim$ a few. In parallel, the efficiency of the QED cross section decreases with increasing energy (or, since the process is resonant, with increasing magnetic field) and the combination of these two effects leads to the appearance of the spectral break. The energy of the break depends on the effect of the cumulative scatterings and is sensitive to the details of the magnetic field topology and of the currents' distribution and therefore cannot be predicted a priori nor estimated using a simple expression. On the other hand, in the case in which magnetospheric electrons are ultra-relativistic, the energy gain per scattering is so large that the hard tail becomes efficiently populated after just a few scatterings. In this case, now independently of the details of the cross section and magnetic topology, the spectral tail is predicted to be quite flat and unbroken, even up to > 1000 keV (see Fig. 11).

Although these studies are extremely useful in shedding light on the basic behaviour of the QED scattering process, the assumptions of constant charge velocity and self-similar magnetic twists are clearly two major oversimplifications. This is crucial when trying to mimic the hard X-ray emission, since the responsible emitting region is likely to constitute quite a large portion of the whole magnetosphere. We already mentioned that deep INTEGRAL observations of two AXPs 1RXS J1708-4009 and 4U 0142+61 have revealed several different pulse components (at least three) in the hard X-rays, with genuinely different spectra (den Hartog et al., 2008a,b) and a quite spectacular phase-dependence. The hard X-ray spectrum gradually changes with phase from a soft to a hard power law, the latter being significantly detected over a phase interval covering

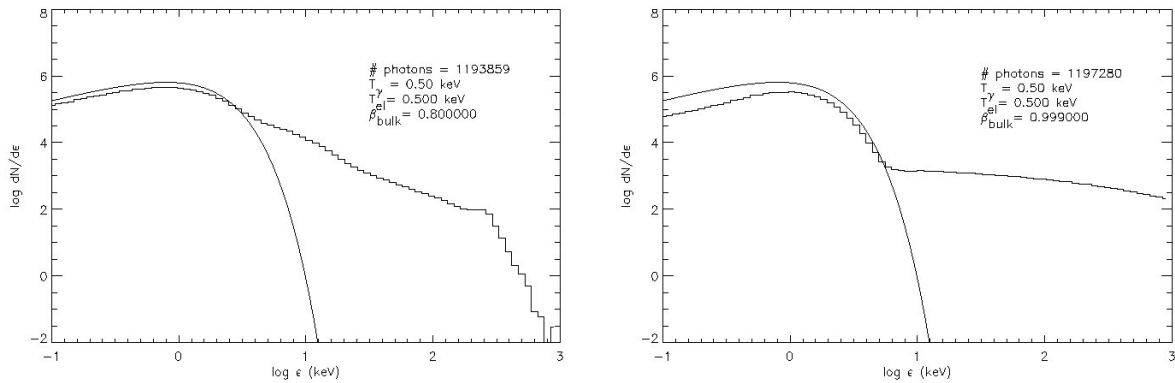


Figure 11 Monte Carlo spectra for $B = 10^{14} G$ and $\Delta\phi = 1$ computed by using the full QED expression of resonant scattering. Left: mildly relativistic electrons ($\gamma = 1.7$). Right: highly relativistic electrons ($\gamma = 22$) (reprinted from Zane et al., 2011a, Copyright 2011, with permission from Elsevier).

$\sim 1/3$, or more, of the spin period. This richness in the phenomenology requires more complex magnetospheric topologies to be explained. Unfortunately, despite many efforts having been devoted to the development of techniques for solving the force-free equation, $\nabla \times B = \alpha(x)B$, no general, affordable method has been presented so far. Pavan et al. (2009) developed a general method to generate twisted, higher-order multipoles solving the Grad-Shafranov equation, and analyzed in detail quadrupolar and octupolar fields. The case of an octupolar field has a special interest because it can be used to mimic a twist localized in a region close to the magnetic pole(s), and hence to investigate the consequence in the expected spectra. Model (Monte Carlo) spectra and lightcurves have been presented for the cases in which the twist is confined to one or both polar regions (each region has semi-aperture of ~ 60 deg), by assuming that only the polar lobes have a non-vanishing shear while the equatorial belt is potential. Interestingly, a configuration with a twist confined to a single lobe has been found to be capable of qualitatively reproducing the main features of the high-energy emission observed with INTEGRAL from the AXPs 1RXS J1708-4009 and 4U 0142+61, in particular the large variation in the pulsed fraction at different energy bands, and a hard tail which is quite pronounced at the peak of the pulse but depressed by almost an order of magnitude at pulse phases close to the minimum of the hard X-ray lightcurve.

More recently, an alternative to the (mathematically simple) self-similar models, has been presented by Viganò et al. (2012), who discussed the effects of more realistic magnetic field geometries on the synthetic Monte Carlo spectra. They presented a numerical method to build general force-free field magnetic configurations, starting from an arbitrary, non-force-free poloidal plus toroidal field and employing artificial dissipation to remove the non-parallel currents. In particular, they considered configurations in which the currents are concentrated in a bundle along the polar axis, as expected for a spatially-limited twist. In this case the pulse fraction is larger with

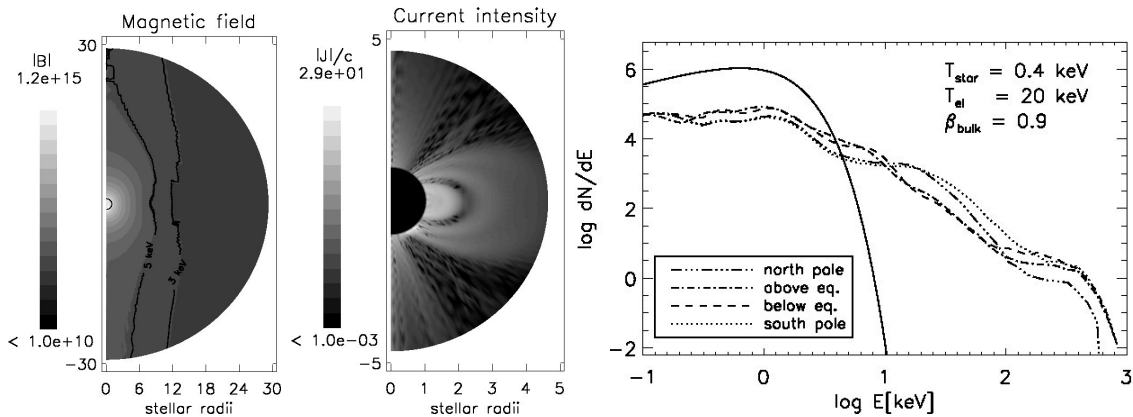


Figure 12 Left and center panel: magnetic field and current distribution for a high helicity model with current and twist concentrated in a closed bundle near the equatorial region and a j-bundle near the southern semi-axis. This configuration is likely more realistic than the self-similar models, since currents are more concentrated near the axis. The two panels show $|\vec{B}|$ (grey logarithmic scale) with superimposed the scattering surfaces for photons of 1, 3 and 5 keV and the current intensity $|\vec{J}|/c$ (gray linear scale) in units of $10^{14} \text{ G}/r_{NS}$. Right: Corresponding synthetic spectra computed with a Monte Carlo simulation. Different curves correspond to four different viewing angles; the seed blackbody is shown for comparison as a solid line. (readapted from Viganò et al., 2012, with permission; a link via DOI to the original version is available in the electronic version of this paper).

respect to that of self-similar models, and the spectrum observed at different angles varies in a much more irregular way (see Fig. 12). Instead of a simple PL, it shows different spectral bumps the relative importance of which can vary by one order of magnitude or more at different colatitudes. The different spectral components inferred from the data may therefore be due to these bumps. Even if a real fit has not been attempted, we may speculate that this is qualitatively in line with the observations of the AXPs 1RXS J1708-4009 and 4U 0142+61.

As mentioned earlier, a further poorly known ingredient of all these simulations is the charge velocity distribution and probably the most detailed solutions published have been presented by Beloborodov (2013a,b). In this scenario, the electron-positron flow decelerates as it propagates away from the neutron star surface (due to Compton drag in the resonant scattering region), then it reaches the top of the magnetic loop where it annihilates. While computed with a Monte Carlo simulation, the corresponding spectra show a distinct peak at $E > 1 \text{ MeV}$ (so far unobserved), the position of which is however strongly dependent on the viewing angle (or, equivalently, on the magnetic colatitude at which the spectrum is emitted, see Fig. 13).

A well defined change in the power law slope from soft to hard X-rays is seen, which makes these spectral models incapable of explaining observations of sources that have a similar slope below and above $\sim 10 \text{ keV}$ (historically these were referred as SGR-like

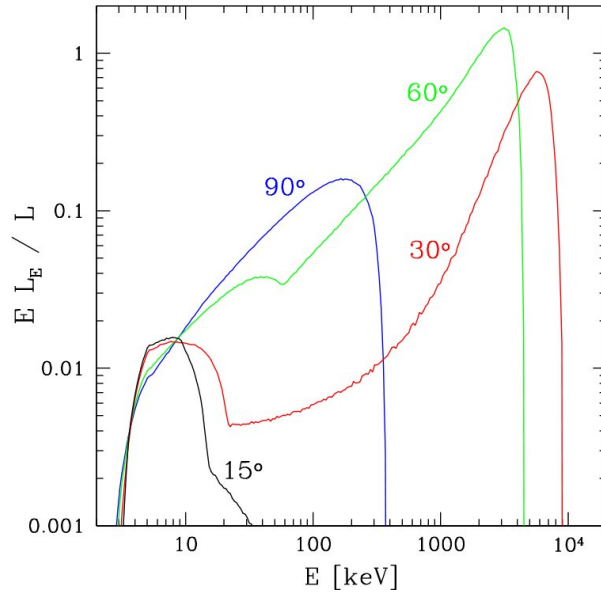


Figure 13 Left: Spectrum emergent from scattering onto charges populating an axisymmetric j-bundle. Different lines represent the spectrum as observed at four different angles with respect to the magnetic axis: 15° , 30° , 60° , and 90° . The spectrum is normalized to the total luminosity of the j-bundle. (from Beloborodov, 2013b, ©AAS. Reproduced with permission. A link to the original article via DOI is available in the electronic version).

spectra), but instead in good qualitative agreement with the observed spectra in which a marked turnover is present (historically, AXP-like spectra). In an attempt to perform a quantitative comparison without to resort to the time-consuming computation of a complete table of Monte Carlo models, Hascoët et al. (2014) developed a simplified model by assuming the same charge velocity distribution but by computing the spectra through a simple calculation of the angle-dependent emissivity alone. The magnetosphere is assumed to be axisymmetric and dipolar, apart from the presence of a current-carrying region (the j-bundle), which is filled with the electron-positron flow. These spectra have been then applied to multi-year hard X-ray observations of 4U 0142+61, 1RXS J1708-4009 and 1E 1841-045, finding that they successfully reproduce the emission observed above ~ 10 keV in both the phase-average and phase-resolved spectra. Unfortunately, the authors found that the model predictions cannot be self consistently applied to explain also the data below 10 keV (probably because of the lack of the particle back-bombardment effects in the simulation). These predictions have therefore been ignored in the fits and instead a blackbody component(s) was used to account for the soft X-ray part of the spectrum. A concern regarding these fits is the fact that the spectra used by Hascoët et al. (2014) do not include photon splitting, which is the main factor responsible for the bump visible in the Monte Carlo spectra at ~ 1 MeV (Beloborodov, 2013b). Although the simplified and complete calculations are in good agreement below ~ 400 keV, they are expected to be markedly different at higher energies. Actually,

there is no guarantee that, should the spectra be computed self-consistently with the Monte Carlo code, the high energy CGRO-Comptel upper limits are not violated (either always or for the derived geometry). This casts some doubts on the robustness of the study and on the constraints on the viewing geometry reported by Hascoët et al. (2014) fitting only the hard X-ray part of the spectrum.

It is interesting to note that spectra presented by Wadiasingh et al. (2013), using a new Sokolov and Ternov formulation of the QED Compton scattering cross section in strong magnetic fields and accounting for spin-dependent effects at resonance, also show a spectral cut-off whose energy is critically dependent on the observer viewing angles and electron velocity, with substantial emission expected up to 1 MeV except for very selected viewing angles.

At the present, unfortunately, what causes the high energy emission and its richness in phenomenology is still an open issue: models have been computed, but they depend dramatically on a large number of degrees of freedom for the magnetospheric setting at large scale. New and future missions such as *Astro-H*, *NuSTAR*, and possibly *LOFT* would provide the possibility of collecting simultaneous soft and hard spectra, to study the correlation between the variability in the two bands, to perform high resolution pulsed phase spectroscopy and to reveal the detail of the slope turn-over (when present) in the soft-to-hard emission. In turn, this will provide a powerful tool to break the model degeneracy and an unprecedented insight into the details of the field and current distributions.

3.4. X-ray polarization

As discussed in Sec. 3.3.1, comparison of RCS models with the soft X-ray spectral data of magnetar candidates has proved quite successful. However, spectroscopy alone cannot provide complete information on the physical properties of the magnetosphere, due to the inherent degeneracy in the RCS model parameters. Moreover, computed spectra are rather insensitive to the source geometry, although in principle they do depend on the angles that the line of sight and the magnetic axis make with the star’s rotation axis (Nobili, Turolla & Zane, 2008a; Zane et al., 2009). Although a simultaneous fit of both the (phase-averaged) spectrum and the pulse profile is effective in this respect, at least for TAXPs (Perna & Gotthelf, 2008; Albano et al., 2010; Bernardini et al., 2011a), polarization measurements at X-ray energies would provide an entirely new approach to the determination of the physical parameters in magnetar magnetospheres.

X-ray radiation from a magnetar is expected to be polarized for essentially three reasons: i) primary, thermal photons, coming from the star’s surface, can be intrinsically polarized, because emission favors one of the modes with respect to the other; ii) scattering can switch the photon polarization state; and iii) once the scattering depth drops, the polarization vector changes as the photons travel in the magnetosphere (the so called “vacuum polarization”, Heyl & Shaviv, 2000, 2002, see also Harding & Lai 2006).

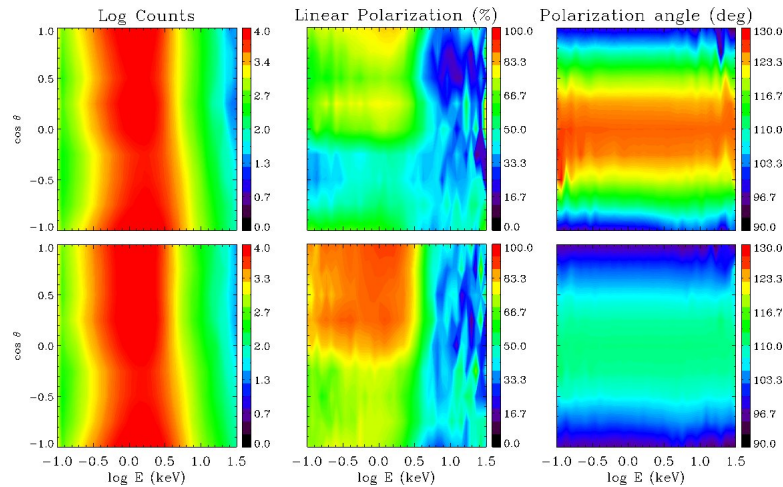


Figure 14 Contour plots for number of counts (in arbitrary units; left column), polarization fraction (middle column) and polarization angle (right column) as functions of the photon energy and $\cos\theta$ for different values of the twist angle and the electron bulk velocity: $\Delta\phi = 1.3$ rad, $\beta = 0.3$ (top row) and $\Delta\phi = 0.7$ rad, $\beta = 0.4$ (bottom row). In both cases it is $B_p = 5 \times 10^{14}$ G (from Taverna et al., 2014, with OUP permission).

Although a preliminary analysis was already contained in Fernández & Thompson (2007) and Nobili, Turolla & Zane (2008a), a detailed study of the polarization properties of magnetar radiation in the X-ray band has been presented by Fernández & Davis (2011) and, more recently, by Taverna et al. (2014), by means of Monte Carlo simulations. Phase-averaged as well as phase-resolved results indicate that the linear polarization fraction Π_L and the polarization angle χ_{pol} , are very sensitive to the magnetospheric twist angle $\Delta\phi$ and the charge velocity β , and also to the geometric angles χ and ξ . This allows one to remove the $\Delta\phi$ - β degeneracy which spectral measures alone cannot disambiguate. An example is shown in Fig. 14 where the photon spectrum, polarization fraction and polarization angle are plotted as functions of viewing angle and energy for two choices of the model parameters. While the photon spectrum is practically the same, the pattern of Π_L and especially χ_{pol} is markedly different in the two cases. According to the simulations by Taverna et al. (2014), polarimetric measurements in bright magnetar candidates, like the AXP 1RXS J1708-4009, are within reach of recently proposed polarimeters which should hopefully fly in future missions.

3.5. IR/optical emission

As mentioned in Sec. 1, variable IR counterparts have now been identified, or in some cases proposed, for a number of magnetars (Mereghetti, 2011; Israel & Rea, 2014). In addition, three magnetars have been detected in the optical band, the two AXPs 4U 0142+61 (Hulleman et al., 2000) and 1E 1048.1-5937 (Durant & van Kerkwijk, 2005), and the SGR 0501+4516 (Fatkhullin et al., 2008; Dhillon et al., 2011). The origin of this emission is still under debate, and the main dispute is whether it is due to the presence

of a fossil disk (Perna et al., 2000) or if it has a magnetospheric origin (Eichler, Gedalin & Lyubarsky, 2002; Beloborodov & Thompson, 2007).

AXP 4U 0142+61 is the only persistent magnetar for which the optical/near IR (NIR) spectrum was measured, although the faintness of the source required extensive observational data (Hulleman et al., 2000). In the case of this source, an IR “excess“ (or “flattening“) was clearly detected with respect to the extrapolation of the additional black body used to account for the optical emission (Israel et al., 2004, 2005a). This may suggest that the IR emission is due to a distinct spectral component, a conclusion that might well hold also for other AXPs, considering the similarity of their IR magnitudes and F_X/F_{IR} ratios (Durant et al., 2011).

The optical/NIR spectrum of 4U 0142+614 was found to be well fitted by a multi-temperature (700-1,200 K) thermal model, leading to the suggestion it originates in an extended disk or shell (Wang et al., 2006). If this detection of a fallback disk is real, it would be the the first direct evidence for supernova fallback in any context. On the other hand, disks may then be ubiquitous while, despite intense campaigns, no similar direct evidence has been found for other sources (see also Posselt et al., 2014, for a report on recent deep limits on fallback disks). The only indirect evidence is one source, in which there is a detected correlation between the NIR and X-ray fluxes (Tam et al., 2004), which, as pointed by Wang et al. (2006), may indicate that the IR emission arises in an X-ray-heated debris disk.

On the other hand, very deep optical and NIR observations of the field of the low-B magnetar SGR 0418+5729, which is the nearest and least extincted magnetar known, failed to detect the source counterpart (Durant et al., 2011). Shallower observation of the field of SGR 0418+5729 with the new Gran Telescopio Canarias 10.4-m telescope and with the William Herschel Telescope where also taken closer to the onset of the outburst (Esposito et al., 2010; Rea et al., 2013a) and only gave upper limits on the counterpart. This negative result is in better agreement with a magnetospheric origin interpretation, in which case the IR/optical flux is expected to be fainter for lower field strengths. Moreover, a magnetospheric scenario is more likely to explain the fact that, when detected, the observed optical emission is pulsed at the pulsar period, with pulsed fractions $> 50\%$, i.e., higher than in soft X-rays (Kern & Martin, 2002; Dhillon et al., 2009, 2011).

Magnetospheric emission in the IR/optical is expected from the inner region of the magnetosphere (Beloborodov & Thompson, 2007; Zane et al., 2011b). As discussed in Sec. 3.2, this region is expected to be pair-dominated, and the Lorentz factor of the electrons and positrons is likely to be frozen at the threshold for pair production ($\gamma \sim 500 - 1000$). In order to estimate the amount of curvature radiation, Zane et al. (2011b) developed a simple geometrical model accounting for misalignment between the observer line of sight and the magnetic axis. Although the model is too simple to allow for a proper spectral fitting, it is detailed enough to make a prediction about the energetics and the computation indicates that curvature radiation is sufficient to explain the amount of observed IR/optical flux, at least if a particle bunching mechanism is

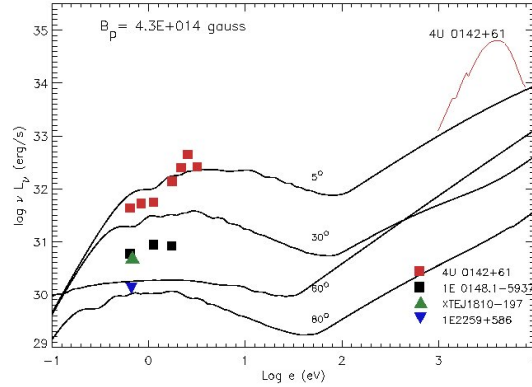


Figure 15 Model spectra for different values of the viewing angle and $B = 4.3 \times 10^{14}$ G. The *XMM-Newton* X-ray spectrum of 1RXS J1708-4009 is from Rea et al. (2008, red solid line). The AXP's IR/optical data are from Durant & van Kerkwijk (2005, 4U 0142+614 and 1E 1048-5937) and Mignani et al. (2007, XTE J1810-197 and 1E 2259+586). The adopted distances for de-reddening are 5 kpc (4U 0142+614, 1RXS J1708-4009), 3 kpc (1E 1048-5937, 1E 2259+586), 4 kpc (XTE J1810-197), 8.5 kpc (1E 1841-045). Curvature emission spectra have been computed accounting for particle bunching (Fig. 2 from Zane et al., 2011b, With kind permission from Springer Science and Business Media) .

efficient (see also Beloborodov & Thompson 2007 and see Fig 15). This is not unlikely, since many models have been suggested to explain the origin of the interactions which push particles together and can lead to the formation of bunches of charged particles localized in phase-space. The most promising explanation seems to be connected with plasma instabilities, like the two-stream (electron-positron/electron-ion) instability. We notice that this mechanism does not affect the emission in other bands. In fact, in order the process to be effective, it has to have $N = n_e l_B^3 > 1$, where l_B is the size of the bunch and n_e is the electron density, which in turns means that only emission at frequencies $\nu < \nu_{co} = n_e^{1/3} c$ is efficiently amplified. Also, a low-energy cut-off is present because of the strong absorption below the electron plasma frequency.

Israel et al. (2005b) proposed a link between the IR and hard X-ray spectrum of AXPs, and correspondingly between AXPs/SGRs and radio-pulsars, based on the analysis and comparison of their broad band energy spectra. These authors pointed out that, similar to the case of a number of young radio pulsars such as the Vela, it is possible to bridge the IR to γ -ray emission of AXPs with a power-law with index of about 0.5-0.6 (see Fig. 16). This peculiar similarity, for classes of neutron stars with otherwise quite different emission properties, may naturally explain the IR excess or flattening in the spectra of AXPs and points toward a similar origin for the less energetic bands and the hard X-ray emission. This scenario may be unambiguously proven through simultaneous studies of the correlated variability in the two bands, which have unfortunately so far been hampered by the lack of gamma-ray observatories sensitive enough to these faint sources.

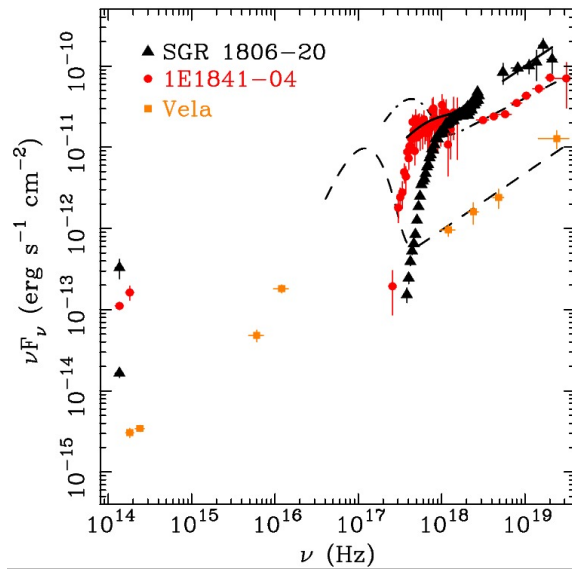


Figure 16 Broad band energy spectrum of SGR 1806-20 (triangles), the AXP 1E 1841+045 (circles) and the radio pulsar Vela (squares). In the case of SGR 1806-20 and 1E 1841+045 high energy data are taken from Mereghetti et al. (2005a,b). Absorbed and unabsorbed IR fluxes ($A_V = 29 \pm 2$, 5th October 2004 NACO observation) are shown in the case of SGR 1806-20, unabsorbed ($A_V = 13 \pm 1$) IR fluxes are instead reported for the likely candidate of 1E 1841+045 (circles; Testa et al., 2008). All the data for Vela are taken from Kaspi (2006). Solid curves (continuous, stepped and dot-stepped) are the unabsorbed fluxes, for the blackbody plus power-law model used to fit the high energy part of the spectra (courtesy G.L. Israel, from Israel et al., 2005b, reproduced with permission ©ESO).

4. Transient Magnetars

The persistent X-ray emission of a number of SGRs/AXPs has been known to be variable all along, with typical flux variations of a factor of a few over a timescale of days to months, often in coincidence with periods of enhanced bursting activity (see Sec. 1; Rea & Esposito, 2011). The first evidence that the luminosity of SGRs/AXPs can change much more dramatically came from observations of SGR 1627-41 (Woods et al., 1999b) and AX J1845.0-0300 (Torii et al., 1998; Vasisht et al., 2000, although the latter source is only a candidate magnetar with no detection of \dot{P}).

It was not until 2002, however, that the existence of a new class of magnetar sources with much more extreme variability was realized, thanks to the discovery of the first transient AXP, XTE J1810-197 (Ibrahim et al., 2004). At present eleven transients are known and, remarkably, they almost make up all of the new magnetars observed in the last 10 yrs (the exception being CXOU J171405.7-381031, Halpern & Gotthelf, 2010). The main properties of transient magnetars are listed in table 1⁺.

⁺ Only sources for which the peak luminosity is > 10 times the quiescent one have been included.

Table 1 Transient magnetar sources⁺

Source	P (s)	\dot{P} (10^{-11} s/s)	B (10^{14} G)	D (kpc)
CXOU J1647-4552	10.61	< 0.04	< 0.7	3.9
XTE J1810-197	5.54	0.77	2.1	3.5
SGR 0501+4516	5.76	0.59	1.9	52.0
SGR 0418+5729	9.08	0.0004	0.06	2.0
SGR 1833-0832	7.56	0.35	1.6	–
PSR 1622-4950	4.33	1.7	2.2	9.0
1E 1547-5408	2.07	4.77	3.2	4.5
Swift J1822.3-1606	8.4	0.02	0.14	1.6
SGR 1627-41	2.59	1.9	2.2	11.0
Swift J1834.9-0846	2.48	0.80	1.4	4.2
SGR J1745-2900	3.76	1.38	2.3	8.3

These sources are characterized by a sudden (\approx hrs) increase of the X-ray flux, by a factor ≈ 10 – 1000 over the quiescent level, accompanied by the emission of short bursts. This active phase, commonly referred to as an outburst, typically lasts ≈ 1 yr, during which the flux declines, the spectrum softens and the pulse profile simplifies. Fig. 17 shows the decay of the X-ray flux for several transient magnetars. Some objects have undergone repeated outbursts (SGR 1627-41, 1E 1547-5408) and the decay pattern is often different from source to source (and even between outbursts from the same source). Outbursts, besides revealing new magnetars which in quiescence are too faint to be detectable, or which passed unnoticed among the host of unclassified, weak X-ray sources, have also occurred in persistent sources like 1E 2259+586 or 1E 1048.1-5937, although drawing a precise line between outbursts and less extreme variability is somewhat haphazard. The group of transient sources also harbours the two peculiar “low-field“ magnetars, SGR 0418+572 and Swift J1822.3-1606 (see Sec. 4.2), and the recently discovered source in the Galactic Centre (see Sec. 4.3).

4.1. Outburst Models

A common feature of all observed outbursts is the presence in the X-ray spectrum of one (or two) thermal component(s) at higher temperature (~ 0.3 – 0.9 keV) with respect to that associated with the cooling star surface during quiescence (~ 0.1 – 0.2 keV). The (radiation) radius of these hotter regions is fairly small ($\lesssim 1$ km) and usually decreases in time as the outburst subsides, when the temperature also declines (e.g. Albano et al. 2010, Rodriguez et al. 2014 for XTE J1810-197, CXOU J1647-4552; Rea et al. 2009, Camero et al. 2014 for SGR 0501+4516; Rea et al. 2013a for SGR 0418+572; Rea et al. 2012a for Swift J1822.3-1606; Israel et al. 2010 for 1E1547.0-5408, and references therein). The variation in time of the spectrum, pulse profile and size of the emitting

⁺ Data from the McGill magnetar catalogue (Olausen & Kaspi, 2014).

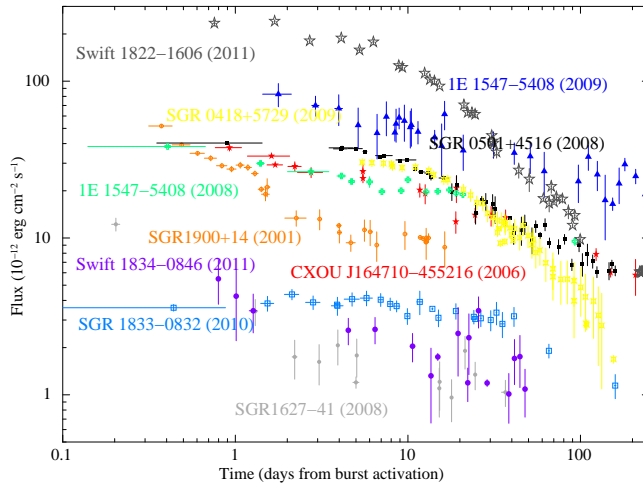


Figure 17 Flux evolution over the first ~ 200 days of all magnetar outbursts (only if observed with imaging instruments, and for which this period span is well monitored). Fluxes are reported in the 1-10 keV energy range, and the reported times are calculated in days from the detection of the first burst in each source. See Rea & Esposito (2011) for the reference of each reported outburst. (From Rea, 2014c, Copyright ? 2014 WILEY-VCH Verlag GmbH & Co. KGaA, Weinheim. Reproduced with permission.)

regions for the AXP XTE J1810-197 during the the outburst decay is shown in Fig. 18.

This has been interpreted as due to some form of heat deposition in a limited region of the star surface which then cools and shrinks. Until now, however, the heating mechanism has not been unambiguously identified. One possibility is that energy is injected deep in the crust, e.g. because of magnetic dissipation, and then flows to the surface, as first suggested by Lyubarsky, Eichler & Thompson (2002).

Pons & Rea (2012) developed a quantitative model for the outburst evolution by simulating the thermal relaxation of the neutron star in response to an impulsive energy injection in the star crust. They found that most of the energy is released in the form of neutrinos, unless injection occurs in the outer crust ($\rho \lesssim 3 \times 10^{11} \text{ g cm}^{-3}$). The successive evolution depends mostly on the energy input in the outer crust, E_{OC} . However it has to be $E_{OC} \gtrsim 10^{40} \text{ erg s}^{-1}$ to produce any visible effect on the surface and, at the same time, E_{OC} is bounded from above at $\sim 10^{43} \text{ erg s}^{-1}$ because any excess energy is efficiently radiated away by neutrinos produced in the heated crust. This limits the surface temperature to $\sim 0.5 \text{ keV}$. Because heat transport occurs mostly along the field, which is predominantly radial in the outer layers, the size of the hot spot on the star surface remains nearly constant in time (which may be problematic in explaining the observed shrinking of the heated region).

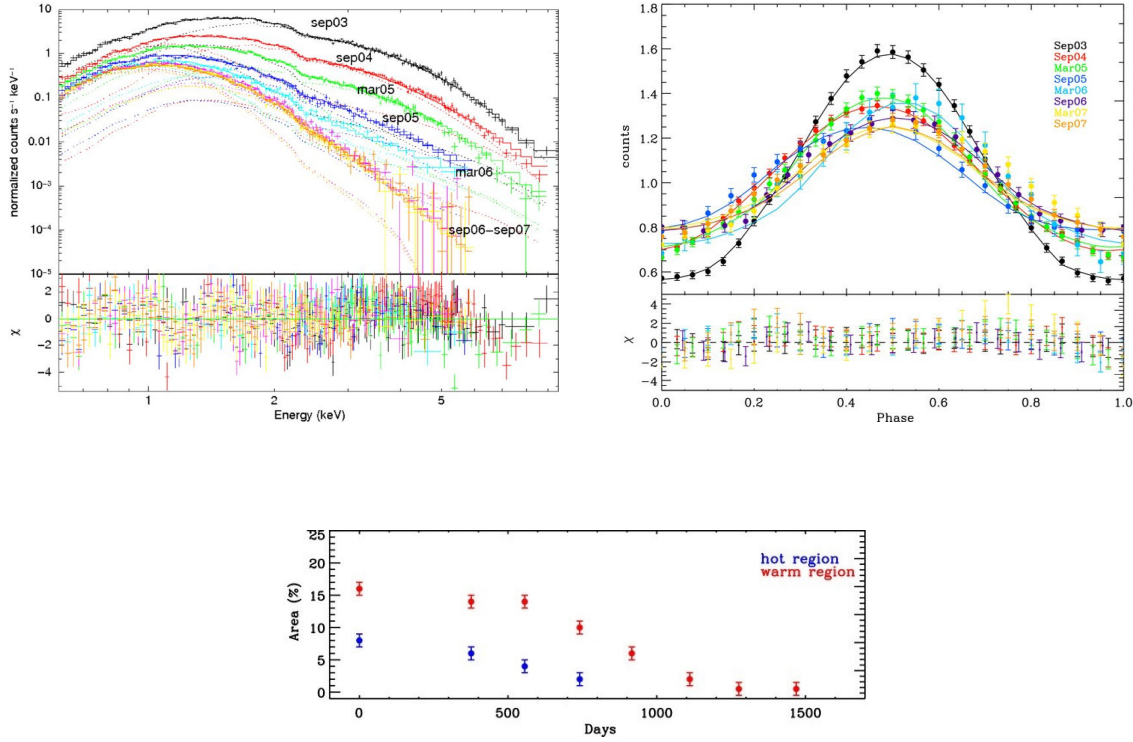


Figure 18 The evolution of the spectrum, pulse profile (top panels) and size of the emitting regions (expressed as fraction of the entire surface, bottom panel) during the outburst of XTE J1810-179. Results are for the three temperature model (hot cap, warm corona and cool surface) of Albano et al. (2010); the cold temperature is fixed at 0.15 keV. The adopted spectral model is the superposition of two NTZ’s (see Sec. 3.3.1) at the hot and warm temperature (adapted from Albano et al., 2010, ©AAS. Reproduced with permission. A link to the original article via DOI is available in the electronic version).

Results were successfully applied by Rea et al. (2012a) to fit the outburst decay in Swift J1822.3-1606 over the entire period covered by their observations, ~ 250 d after the first burst that led to the discovery of the source. The case of SGR 0418+5729, for which a much longer time coverage is available (~ 1200 d), is, however, much less conclusive in this respect (Rea et al., 2013a). The calculated flux in the 0.5–10 keV band systematically overestimates the observed one at later times ($\gtrsim 400$ d), when the luminosity suddenly drops and the hotter blackbody (initially at $kT \sim 0.9$ keV) disappears leaving only a cooler component at ~ 0.3 keV. A similar effect has been recently reported in the decay curve of CXOU J1647-4552 around 1000 d (Rodriguez et al., 2014) and in Swift J1834.9-0846 (Esposito et al., 2013).

Alternatively, heating of the surface layers may be produced by currents flowing in a twisted magnetosphere as they hit the star. As discussed in §3.1, once implanted by

crustal displacements, a twist must necessarily decay in order to supply the potential drop required to accelerate the conduction current (Beloborodov & Thompson, 2007). The evolution of an untwisting magnetosphere proceeds through the expansion of a potential region, where $\vec{\nabla} \times \vec{B} = 0$, which progressively confines the twist to a limited bundle of current-carrying field lines (the j-bundle), until the twist is completely erased (Beloborodov, 2009). Fractures, or plastic deformations, most likely affect only a limited area of the star crust, so the twist is expected to involve only the bundle of field lines whose footpoints are anchored in the displaced region. As the magnetosphere untwists, the area covered by the j-bundle shrinks and the luminosity decreases. The rate of Ohmic dissipation, which depends on the initial twist configuration and on how the twist angle $\Delta\phi$ evolves in time ($\Delta\phi(t)$, is not necessary monotonic, the twist may first decrease and then increase to a maximum value ≈ 1 rad). The simplest model gives

$$L \approx 10^{36} \left(\frac{B}{10^{14} \text{ G}} \right) \left(\frac{\mathcal{V}}{10^9 \text{ V}} \right) \left(\frac{R}{10^6 \text{ cm}} \right)^2 \Delta\phi \sin^4 \theta_{j-b} \text{ erg/s} \quad (10)$$

where \mathcal{V} is the discharge voltage and θ_{j-b} is the angular extension of the j-bundle on the star's surface (this is valid for a small polar bundle with maximal twist, see Beloborodov, 2009). Since heat is unlikely to leak outside the cap at the base of the j-bundle, the area of the X-ray emitting region is $\sim \pi R^2 \sin^2 \theta_{j-b}$. A quite definite prediction of the model is, then, that the luminosity is proportional to the square of the emitting area throughout outburst evolution (this still holds, at least approximately, also for more elaborate versions). A spatially-limited twist can also explain the nearly thermal spectra observed in most transients. If currents fill only a tiny fraction of the magnetosphere, thermal photons produced in the hot surface regions have only a small chance of undergoing resonant scattering to populate a high-energy tail.

Beloborodov (2009) found that the model can satisfactorily reproduce the observed properties of the outburst of XTE J1810-197 for a small twisted region ($\sin^2 \theta_{j-b} \sim 0.03$) and large twist angle ($\Delta\phi \sim 1$ rad). The application to other transient sources is, however, not without difficulties. The main problem is that the small size of the thermally emitting spot, and hence the limited spatial extent of the twist, can make the luminosity released by Ohmic dissipation too low (especially if the magnetic field is $\lesssim 10^{14}$ G) to explain the observed flux, like in SGR 0501+4516 (Rea et al., 2009) or SGR 0418+5729, (Rea et al., 2013a). Moreover, the relation $L \propto A^2$ does not seem to be met in other sources (Rodriguez et al., 2014). Different geometries of the j-bundle, not necessarily involving the polar region, may however ease the energetic requirement.

4.2. Low-field Magnetars

Recently, the commonly accepted picture in according to which the activity in SGRs and AXPs is necessarily related to a super strong-field (the ‘supercritical B ’ paradigm) has been challenged by the discovery of two fully-fledged magnetars, SGR 0418+5729 and Swift J1822.3-1606, (Rea et al., 2010; Turolla et al., 2011; Rea et al., 2012a; Livingstone et al., 2011b; Rea et al., 2013a; Scholz et al., 2012) with a dipole magnetic

field $\lesssim 10^{13}$ G, well within the range of ordinary radio pulsars. A third candidate, XMM J185246.6+003317, has been reported and awaits further monitoring (Rea et al., 2014a).

SGR 0418+5729 was discovered on 2009 June 5, thanks to the detection of a couple of SGR-like bursts (van der Horst et al., 2010). Follow-up observations revealed a previously unknown bright X-ray source at a flux level of a few times 10^{-11} erg cm $^{-2}$ s $^{-1}$, pulsating at a period of 9.1 s (van der Horst et al., 2010; Esposito et al., 2010). Based on *ROSAT* All-Sky Survey data, the upper limit on the source flux in quiescence is of the order of 10^{-12} erg cm $^{-2}$ s $^{-1}$. Despite the dense monitoring, no spin-down was detected during the first ~ 5 months of observations following the outburst onset. The estimated upper limit on the period derivative, 1.1×10^{-13} s s $^{-1}$, translates into an upper limit on the surface dipole magnetic field strength of 3×10^{13} G (Esposito et al., 2010).

This made SGR 0418+5729 the magnetar with the lowest dipole magnetic field ever discovered (for comparison, the previous record holder, the AXP 1E 2259+586, has a spin-down magnetic field about twice as strong, 6×10^{13} G). It took nearly another 3 years of monitoring to finally pinpoint the source spin-down rate from a coherent timing analysis of all the X-ray data spanning ~ 1200 days: $(4 \pm 1) \times 10^{-15}$ s s $^{-1}$, corresponding to $B \sim 6.1 \times 10^{12}$ G and to a characteristic age $\tau_c = P/(2\dot{P}) \simeq 36$ Myrs (Esposito et al., 2010; Rea et al., 2010, 2013a).

Swift J1822.3-1606 was detected on 2011 July 14, when it emitted several magnetar-like bursts (Livingstone et al., 2011b; Rea et al., 2012a, and references therein). A few days after the outburst onset, a new, persistent X-ray source was discovered at a flux level of $\sim 2 \times 10^{-10}$ erg cm $^{-2}$ s $^{-1}$, pulsating with a period of ~ 8.4 s. Contrary to the case of SGR 0418+5729, the source has been already detected in X-rays at a flux level of $\sim 4 \times 10^{-14}$ erg cm $^{-2}$ s $^{-1}$, although its presence in two *ROSAT* X-ray catalogues passed unnoticed (Rea et al., 2012a; Scholz et al., 2012). Swift J1822.3-1606 was intensely monitored between 2011 July and 2012 August with different X-ray satellites (Livingstone et al., 2011b; Rea et al., 2012a; Scholz et al., 2012). Phase coherent timing analyses yield spin-down rates between $\sim 0.7 \times 10^{-13}$ s s $^{-1}$ and $\sim 3.1 \times 10^{-13}$ s s $^{-1}$, and a dipole magnetic field between 2.4×10^{13} G and 5.1×10^{13} G (Rea et al., 2012a; Scholz et al., 2012). Despite a precise measurement of \dot{P} is not available as yet, any of the values proposed so far makes Swift J1822.3-1606 the magnetar with the second lowest dipole magnetic field after SGR 0418+5729. Given the low value of the period derivative, the characteristic age of Swift J1822.3-1606 is quite long, $\tau_c \sim 0.8$ Myr, although the source appears not as old as SGR 0418+5729.

The large characteristic age, the small number of detected bursts with comparatively low energetics and the low persistent luminosity in quiescence have been taken as suggestive that these are “old magnetars” approaching the end of their active life, in which the magnetic field has experienced substantial decay (Esposito et al., 2010; Rea et al., 2010; Turolla et al., 2011). A key question is if, and to what extent, the present (internal) magnetic field is still strong enough to stress the crust and produce bursts/outbursts. Indeed, Turolla et al. (2011) and Rea et al. (2012a) have shown

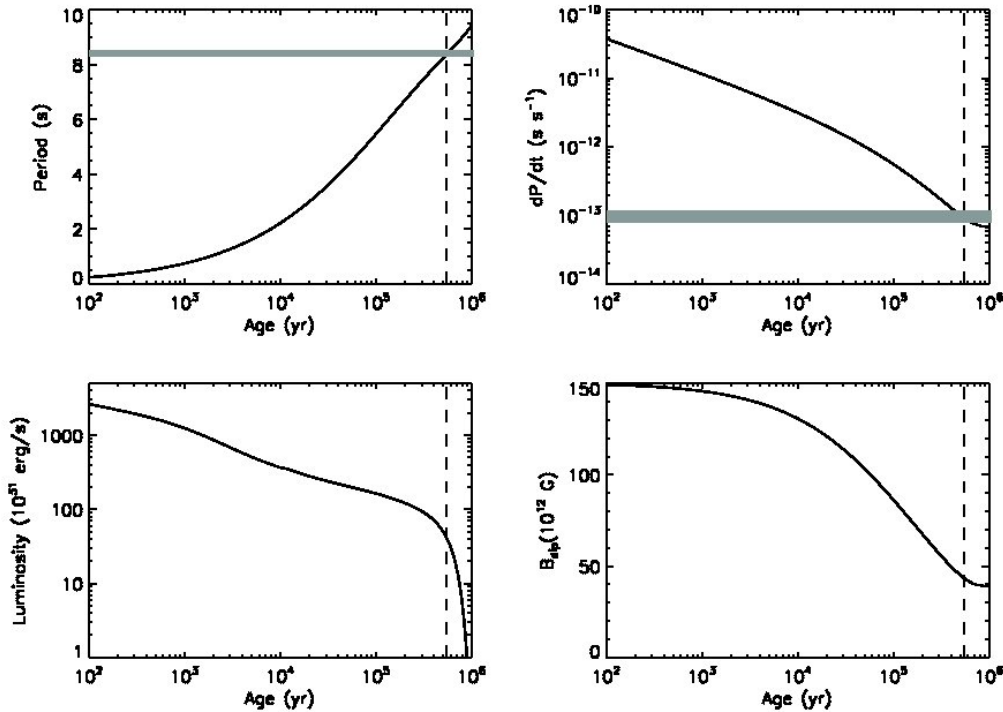


Figure 19 From top left to bottom right: time evolution of P , \dot{P} , L_X and B_p for Swift J1822.03–1606. The dashed vertical line marks the estimated age of the source; the gray strips in the first two panels show the observed values of P and \dot{P} with their uncertainties. The model is for $B_{tor}(t = 0) = 5 \times 10^{15}$ G (from Rea et al., 2012a, ©AAS. Reproduced with permission. A link to the original article via DOI is available in the electronic version).

that the magneto-thermal evolution (Pons et al., 2009; Viganò et al., 2013, see §2) of an initially ultra-magnetized neutron star, $B_p(t = 0) \sim 2 \times 10^{14}$ G, can reproduce the observed P , \dot{P} , B_p and L_X in SGR 0418+5729 and Swift J1822.3–1606, for an age ~ 1 Myr and ~ 0.5 Myr, respectively, provided that the initial internal toroidal field $B_{tor}(t = 0)$ is high enough*. The evolution of the period, period derivative, dipole B -field and luminosity for Swift J1822.03–1606 is shown in Fig. 19. The fact that the characteristic age (assuming a constant B) in these two sources is largely in excess of that derived from magneto-thermal evolution reflects a quite general property of magnetar sources, for which characteristic ages are longer than those derived using other estimators.

* More recent calculations of magneto-thermal evolution including the Hall drift actually show that a strong toroidal component develops regardless of the initial topology the the magnetic field (Viganò et al., 2013).

According to the calculations by Perna & Pons (2011), who modeled the evolution of the internal magnetic stresses in a magnetar, the occurrence of crustal fractures (and hence of bursts/outbursts) can extend to late phases ($\approx 10^5$ – 10^6 yr). Both the energetics and the recurrence time of the events evolve as the star ages and depend on the initial field. The models which successfully reproduce the properties of the two low-field sources imply that the two low- B magnetars could become burst-active despite their age, with an expected (current) event rate of ≈ 0.01 – 0.1 yr $^{-1}$.

Quite recently, Tiengo et al. (2013) reported the discovery of a phase-variable absorption feature in the X-ray spectrum of SGR 0418+5729. The feature is best detected in a 67 ks XMM observation performed on 2009 August 12, when the source flux was still high (5×10^{-12} erg cm $^{-2}$ s $^{-1}$ in the 2–10 keV band) but is also visible in the RXTE and Swift data collected in the first two months after the outburst onset. The line energy is in the range ~ 1 –5 keV, in XMM data, and changes sharply with rotational phase, by a factor of ~ 5 in one-tenth of a cycle (see Fig. 20). These seem to favour an interpretation in terms of a cyclotron line. If protons, e.g. contained in a rising flux tube close to the surface, are responsible for the line, the local value of the magnetic field within the baryon-loaded structure is close to 10^{15} G. SGR 0418+5729 would then be, at the same time, the magnetar with the lowest dipole field and the neutron star with the largest (small-scale) field ever measured.

4.3. Transient Radio Emission

For a long time SGRs and AXPs were thought to be with no exceptions radio quiet, to the point that the lack of (pulsed) radio emission was often quoted as one of their defining properties. In fact, an expanding radio nebula was detected in the aftermath of the Giant Flares from SGR 1806-20 (Gaensler et al., 2005b; Cameron et al., 2005) and SGR 1900+14 (Frail, Kulkarni & Bloom, 1999), but this originated in the shocked material around the neutron star and not from the star magnetosphere.

The first detection of pulsed radio emission from a magnetar came, rather unexpectedly, from the archetypal transient XTE J1810-197 (Camilo et al., 2006), opening a new window in the study of magnetars. For many months, XTE J1810-197 was the brightest radio pulsar in the Galaxy at frequencies above 20 GHz, exhibiting a strong variability in both the radio flux and the pulse shape on different timescales. The radio emission likely began about a year after the onset of the X-ray outburst and lasted a few years (Camilo et al., 2006, 2007a; Lazaridis et al., 2008; Serylak et al., 2009). Pulsed radio emission was then discovered from the AXP 1E 1547-5408 (Camilo et al., 2007b). This source has shown three X-ray outbursts in the past 5 years. Radio emission was observed in the interval between the last two events, during which it declined, to rise again in coincidence with the last outburst, although there was a delay of a few days between the onset of the X-ray outburst and the radio activity (Camilo et al., 2009; Burgay et al., 2009). Another possibility is that the radio emission was blinking, in a way uncorrelated with the start of the X-ray outburst. PSR 1622-4950 (Levin et

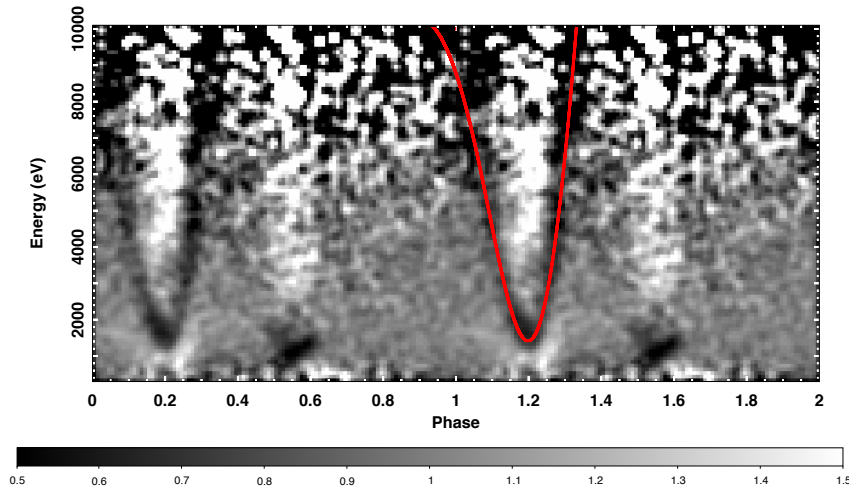


Figure 20 The phase-dependent spectral feature in the EPIC data of SGR 0418+5729. Normalized energy versus phase image obtained by binning the EPIC source counts into 100 phase bins and 100-eV-wide energy channels and dividing these values first by the average number of counts in the same energy bin (corresponding to the phase-averaged energy spectrum) and then by the relative 0.310 keV count rate in the same phase interval (corresponding to the pulse profile normalized to the average count rate). The red line shows (for only one of the two displayed cycles) the results of a simple proton cyclotron model consisting of a baryon-loaded plasma loop emerging from the surface of a magnetar and intercepting the X-ray radiation from a small hot spot (from Tiengo et al., 2013, the authors acknowledge Nature Publishing Group for reproduction).

al., 2010) was the first (and so far the only one) magnetar which was discovered thanks to observations in the radio band. New and archival X-ray observations have shown that the source is likely a transient magnetar which underwent an outburst in 2007 (before the first available Chandra observation). The X-ray flux is still declining as the source approaches quiescence (Anderson et al., 2012). Finally, pulsed radio emission has been detected from the recently discovered magnetar in the Galactic Centre, SGR J1745-2900 (Rea et al., 2013b; Eatough et al., 2013; Shannon & Johnston, 2013; Kaspi et al., 2014). The source entered an outburst phase with the emission of a single burst on April 24 2013. The radio activity switched on 4-5 days after the outburst onset with similar properties to those of the other two magnetars detected at radio wavelengths. Despite intensive searches, pulsed radio emission was not found in other magnetar sources (Burgay et al., 2006; Crawford et al., 2007; Lazarus et al., 2011).

Although the sample is quite limited, a number of common features in the radio

emission from magnetars have started to emerge: i) association with X-ray outbursts, ii) the radio flux decays together with the X-ray flux but its onset is delayed, iii) marked variability in the radio band, and iv) flat radio spectrum. All these properties are much at variance with those of ordinary radio pulsars (including the high-B PSRs). Rea et al. (2012b) have shown that radio-loud magnetars are characterized by $L_X < \dot{E}$ in quiescence, much as ordinary radio pulsars, while the X-ray luminosity always exceeds the rotational energy loss rate in radio-silent magnetars. In fact, as indicated by Ho (2013), this property seems to be characteristic also of other classes of neutron stars, although the inverse is not true: not all sources with $L_X < \dot{E}$ emits in radio. SGR J1745-2900, which was not included in the original sample considered by Rea et al. (2012b), further confirms this picture, having $\dot{E} \sim 5 \times 10^{33} \text{ erg s}^{-1}$ and $L_X \lesssim 10^{32} \text{ erg s}^{-1}$ in quiescence (Rea et al., 2013b). This seems to point to a common origin for the radio emission in PSRs and in transient magnetars. In magnetars with $L_X/\dot{E} < 1$ particle acceleration and the subsequent ignition of the cascade process could proceed as in normal pulsars, and their radio emission might basically follow the same rules, with rotational energy driving pair creation through a cascade. The largely different radio properties between the two groups might result from the presence of a substantial toroidal component in the magnetosphere of the magnetars, contrary to the nearly dipolar field of PSRs. The influence of the large charge density required to support the non-potential field may also act in quenching the radio emission in the brightest magnetars with $L_X/\dot{E} > 1$ (Thompson, 2008a,b), although this latter interpretation is hard to be reconciled with the fact that, in at least few sources (SGR J1745-2900, XTE J1810-197 and possibly also in 1E 1547-5408 during the 2009 outburst), radio emission was seen while the source was bright with $L_X > \dot{E}$.

5. Magnetar bursts

5.1. Burst phenomenology

One of the hallmarks of magnetars is the emission of repeated soft gamma-ray bursts, and this feature played a key role in their discovery (for a nice review of the history of the field, see Woods & Thompson, 2006). Bursts have now been observed from 18 sources whose spin has also been measured (confirming that they are indeed neutron stars) ‡. Magnetars emit bursts in the few keV to few hundred keV energy band (hard X-ray/soft gamma-ray). As mentioned in the Introduction, magnetar bursts are typically grouped into three classes defined primarily by energy released and their duration: short bursts (with energies up to 10^{41} erg), intermediate flares (energies in the range $10^{41} - 10^{43}$ erg), and giant flares (energies in the range $10^{44} - 10^{46}$ erg, see Fig. 21 for example lightcurves from the different types of burst).

Bursting activity is highly variable. Sources can experience long periods of apparent quiescence (when bursting, if it occurs, is in the form of low luminosity bursts below

‡ See the Amsterdam Magnetar Burst Library, <http://staff.fnwi.uva.nl/a.l.watts/magnetar/mb.html>

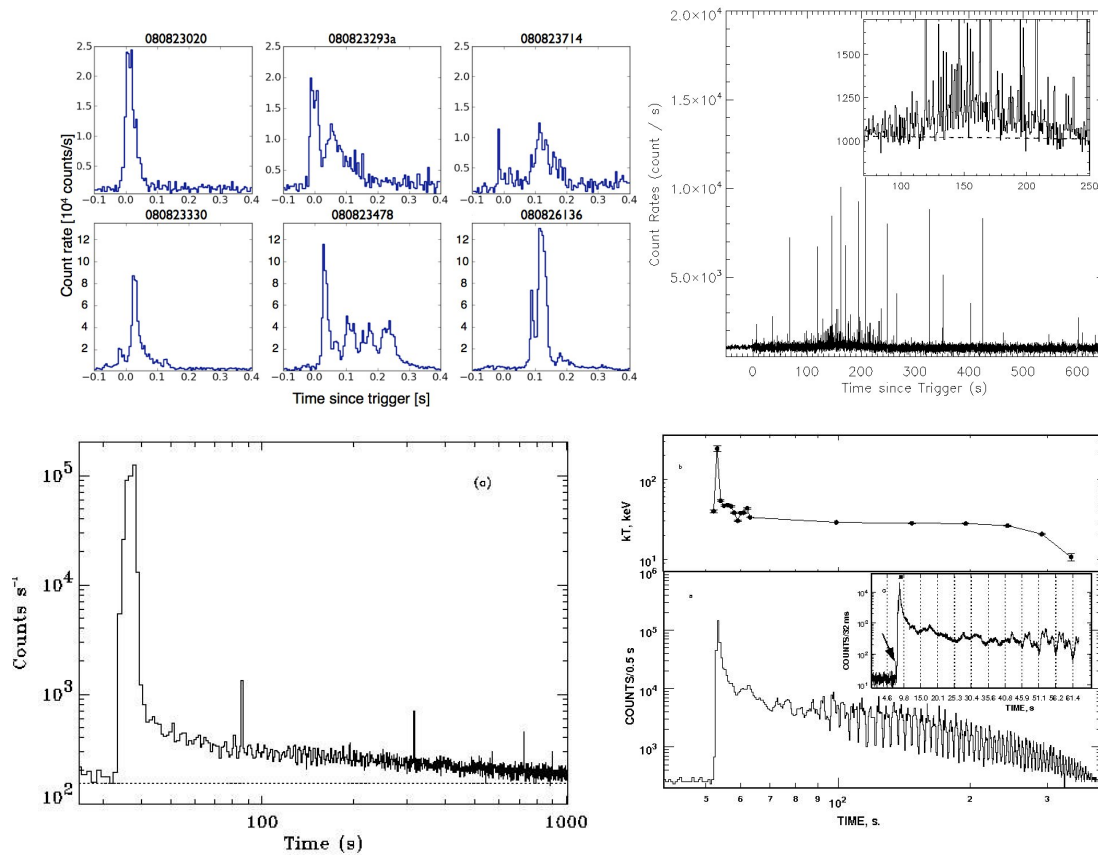


Figure 21 Examples of different types of magnetar bursts. Top left: Short bursts from SGR 0501+4516 recorded by Fermi/GBM (from Huppenkothen et al., 2013). Top right: Burst storm from 1E 1547.0-5408 recorded by Fermi/GBM, with inset showing the overall enhancement in emission during this event (from Kaneko et al., 2010). Lower left: Intermediate burst from SGR 1900+14 recorded by RXTE (from Ibrahim et al., 2001). Lower right: Giant flare from SGR 1900+14 recorded by Ulysses, upper panel showing OTTB spectral temperature (from Hurley et al., 1999b). The first three panels are ©AAS, reproduced with permission. A link to the original articles via DOI is available in the electronic version. The last panel is reprinted by permission from Macmillan Publishers Ltd: Nature, ©1999. The authors acknowledge Nature Publishing Group for allowing reproduction.

the detection threshold of our current generation of space telescopes - note also that there have been gaps in gamma-ray telescope coverage since the discovery of magnetars, due to the lack of suitable telescopes, and that sky coverage even now is never 100%), sporadic and highly occasional bursting, or periods of high burst activity. At their most dramatic, these can climax in burst storms (when several hundreds of bursts can be emitted over just a few hours), or rare giant flares (Fig. 21). During such outburst periods there may also be changes in the overall emission (luminosity, pulsed flux and spectrum, see Rea & Esposito 2011 for an observational review, and Pons & Rea 2012

for a recent theoretical study) and the timing behaviour (spin-down rate and glitching, see for example Woods et al. 2001, 2002, 2003, 2007; Dib & Kaspi 2014). There is no clear dependence of short/intermediate bursting activity on the dipolar magnetic field strength of the source. The most energetic giant flares come from three sources whose inferred dipole fields are amongst the highest (a few times 10^{14} G up to $\sim 10^{15}$ G). However bursts have also been seen from sources with fields apparently below the quantum critical limit, such as Swift J1822.3-1606 with a field $\approx 1.35 \times 10^{13}$ G (Scholz, Kaspi & Cumming, 2014) and SGR 0418+5729 with field 6×10^{12} G (Rea et al., 2010)††.

5.1.1. Short bursts Short bursts are the most common, with fluences in the range $10^{-11} - 10^{-5}$ erg/cm²/s, which for the assumed distances implies isotropic energies in the range $10^{36} - 10^{41}$ erg (Gögüş et al., 1999, 2000; Woods et al., 1999b; Gavriil, Kaspi & Woods, 2004; Kumar, Ibrahim & Safi-Harb, 2010; Scholz & Kaspi, 2011; Lin et al., 2013). Peak luminosities are in the range $10^{36} - 10^{42}$ erg/s, extending to well above the standard Eddington luminosity of $\approx 2 \times 10^{38}$ erg/s for a non-magnetic neutron star. The lowest luminosity bursts recorded are at the sensitivity limit of our current generation of detectors. For sources that have shown sufficient numbers of bursts for meaningful statistical analysis (SGR 1806-20, SGR 1900+14, SGR 1627-41, 1E 2259+286, SGR 0501+5416 and 1E 1547.0-5408), burst fluences are distributed as a power law, $dN = E^{-\gamma} dE$ with $\gamma \sim 1.4 - 2.0$ (Cheng et al., 1996; Aptekar et al., 2001; Woods et al., 1999b; Gögüş et al., 1999, 2000, 2001; Gavriil, Kaspi & Woods, 2004; Kumar, Ibrahim & Safi-Harb, 2010; Savchenko et al., 2010; Lin et al., 2011a; Scholz & Kaspi, 2011; Prieskorn & Kaaret, 2012; van der Horst et al., 2012). Burst durations are $\sim 0.01 - 1$ s and are distributed lognormally with a peak at ~ 0.1 s, less than the rotational period of the star. Duration is correlated with fluence. Bursts from the sources that have shown insufficient events for full statistical analysis are consistent with this picture. Lightcurves are extremely variable in shape: the rise is in general faster than the decay (Gögüş et al., 2001; Gavriil, Kaspi & Woods, 2004), but bursts can be multi-peaked, and no simple phenomenological model has yet been found that would fit the morphologies of the different burst lightcurves. Some short bursts (classified according to their fluence) from five sources have extended faint tails of $\sim 100 - 1000$ s in duration, leading to an overall energy release that can exceed that of the original spike (Woods et al., 2005; Gavriil, Kaspi & Woods, 2004, 2002, 2006; Dib, Kaspi & Gavriil, 2009; An et al., 2014a; Gavriil, Dib & Kaspi, 2011; Mereghetti et al., 2009; Savchenko et al., 2010; Scholz & Kaspi, 2011). The tails appear to be pulsed at the rotational frequency.

From the sources with large samples, wait times (for bursts above the detection threshold, in periods of continuous telescope coverage†) form a lognormal distribution

†† Although note that the dipole field strength as estimated from spin down provides only a lower limit on the magnetic field strength, and there are no constraints on the strength of either higher order poloidal components or toroidal components.

† The recent detection of short bursts from 1E 1547.0-5408, in the VLF radio band due to the ionospheric disturbance that occurs as the incident gamma-rays ionize the Earth's atmosphere opens

with a peak at ~ 100 s. During the active period of SGR 1900+14 in 1998, for example, Göğüş et al. (1999) found wait times ranging from less than 1s to more than 1000s‡, and far longer wait times are clearly possible: SGR 1900+14, for example, has also had quiescent periods \sim years in duration. The shortest wait times observed are comparable to the durations of individual bursts, such that the distinction between single bursts and multi-peaked events is not clear. There appears to be no correlation between burst intensity and wait time to the following burst (Laros et al., 1987; Göğüş et al., 2000; Gavriil, Kaspi & Woods, 2004; Savchenko et al., 2010). Of particular note in the discussion of wait times are burst storms, periods of unusually high short burst activity (which may include some intermediate flares), in which tens to hundreds of bursts occur over only a few hours on top of an overall rise in emission that can be strongly pulsed at the rotational phase (see for example Hurley et al., 1999a; Israel et al., 2008; Gavriil, Kaspi & Woods, 2004; Mereghetti et al., 2009; Kaneko et al., 2010; Savchenko et al., 2010, for the cases SGR 1900+14, 1E 2259+286, and 1E 1547.0-5408). There have also been efforts to determine whether the occurrence of bursts correlates with rotational phase: here the evidence is mixed. For 1E 1048.1-5937, 1E 2259+286 and XTE J1810-197 bursts do seem to occur preferentially at rotational pulse maxima (Gavriil, Kaspi & Woods, 2002, 2004; Woods et al., 2005). However for SGR 1806-20, SGR 1900+14, SGR 1627-41, 4U 0142+61 and 1E 1547.0-5408 no such correlation is found (Palmer, 1999, 2002; Woods et al., 1999b; Gavriil, Dib & Kaspi, 2011; Savchenko et al., 2010; Scholz & Kaspi, 2011; Lin et al., 2012a).

5.1.2. Intermediate flares Intermediate flares, with (isotropic) energies in the range $\sim 10^{41} - 10^{43}$ erg, and peak luminosities that exceed the non-magnetic Eddington limit, have been seen from SGR 1627-41, SGR 1900+14, SGR 1806-20, and 1E 1547.0-5408. The primary bursts appear to be brighter and slightly longer (durations ~ 0.5 s up to a few s) versions of the short bursts. Morphologies, however, are varied. Some have a clear decay and an abrupt end (Mazets et al., 1999a,b; Olive et al., 2004; Israel et al., 2008). In others the initial burst is followed by an extended decaying tail that can last for up to several thousand seconds, but contains less than $\sim 2\%$ of the energy released in the initial peak (Ibrahim et al., 2001; Lenters et al., 2003; Esposito et al., 2007b; Göğüş et al., 2011b). The tails are pulsed at the rotational period of the star: in some cases the pulsed amplitude rises dramatically (Ibrahim et al., 2001; Lenters et al., 2003), as seen during some burst storms (Kaneko et al., 2010); whilst in others no change is seen (Göğüş et al., 2011b). The pulsations appear for the most part to be phase-aligned with the pre-burst pulsations, but there are some occasional exceptions (Guidorzi et al., 2004; Göğüş et al., 2011b). There has also been one burst with a decaying pulsed tail, where the sharp initial burst peak appears to be absent, leading to a rather slow rise time ~ 10 s (Kouveliotou et al., 2001; Guidorzi et al., 2004). Intermediate flares sometimes

up the possibility of using the VLF band to obtain a more complete coverage of the waiting time distribution with being dependent on sky coverage of space telescopes (Tanaka et al., 2010).

‡ The longest wait times in this study were set by the length of the observing window.

have short precursors (Ibrahim et al., 2001; Göğüş et al., 2011b), and during some events short bursts are seen during the extended tail (Ibrahim et al., 2001; Lenters et al., 2003; Göğüş et al., 2011b).

5.1.3. Giant flares The most energetic bursts, the giant flares, are extremely rare. Only three have ever been seen, in 1979, 1998 and 2004, each from a different magnetar (SGR 0526-66, SGR 1900+14, and SGR 1806-20). The total energy released, if the emission is isotropic and assuming reliable estimates of distance, is in the range $10^{44} - 10^{47}$ erg (Fenimore et al., 1996; Feroci et al., 2001; Palmer et al., 2005). The overall properties of the three giant flares are, despite the differences in energy, very similar (in marked contrast with the heterogeneity of the intermediate flares). They have a very bright initial peak, followed by an extended decaying tail with a duration of several hundred seconds that is strongly pulsed at the rotational frequency of the star† (see e.g. Mazets et al., 1979a; Hurley et al., 1999b; Hurley et al., 2005).

The initial peaks, which can have rise times as short as ~ 1 ms, last $\sim 0.1 - 1$ s and are very hard. Luminosities reach up to 10^{47} erg/s (Hurley et al., 2005), which causes substantial dead time and pile up effects in space telescopes. This renders reliable spectral modelling very difficult, however the spectrum is very hard, with emission being detected up to 2 MeV (Mazets et al., 1979a; Hurley et al., 1999b). The initial peaks are strongly variable, on timescales as short as a few ms (Barat et al., 1979; Hurley et al., 1999b; Terasawa et al., 2005; Schwartz et al., 2005). Both the SGR 1900+14 and SGR 1806-20 giant flares were observed to have precursors‡. For SGR 1900+14 the precursor resembled a normal short burst, and occurred < 1 s before the giant flare (Mazets et al., 1999c). For SGR 1806-20 the precursor was flat-topped, with an energy release that puts it in the intermediate flare class, and occurred 142 s prior to the giant flare (Hurley et al., 2005). A discussion of whether the apparent precursors are in fact genuinely causally connected to the giant flares was presented by Gill & Heyl (2010).

The energies emitted in the tails of the three giant flares have been similar ($\sim 10^{44}$ erg). This is 1 – 2% of the energy released in the initial peak of the 2004 giant flare: for the two earlier giant flares the energies released in initial peak and tail were comparable. The overall envelope of the tails (averaged over rotational phase) decays smoothly as a power law, coming to an abrupt end after several hundred seconds. The pulsations in the SGR 0526-66 giant flare tail were seen immediately after the initial peak; for the other two giant flares they appeared only a few tens of seconds later. Pulse profiles can evolve during the tails, in the case of SGR 1900+14 simplifying quite dramatically (Feroci et al., 2001), with evolution being much more minimal for SGR 1806-20 (Palmer

† Note that none of the giant flares were caught during pointed observations: they are so rare but so bright that most are seen off-axis. This means that the sensitivity to late time weak emission is much less than for some of the intermediate flares, which were observed during pointed observations. One should bear this in mind when comparing the apparent durations.

‡ A precursor with the properties observed for SGR 1900+14 giant flare would not have been detectable for the SGR 0526-66 giant flare given the instrumentation at the time (Gill & Heyl, 2010).

et al., 2005; Mereghetti et al., 2005c; Boggs et al., 2007; Xing & Yu, 2011). The giant flares are so strong that they have a detectable effect on the Earth’s electromagnetic field (Mandea & Balasis, 2006) and ionosphere (Inan et al., 1999, 2007; Tanaka et al., 2008), with even the rotational pulsations being clearly visible, and this has been used to put lower limits on the strength of low energy (< 10 keV) emission from the burst (unaffected by satellite dead time issues).

Radio afterglows were detected after both the SGR 1900+14 and SGR 1806-20 giant flares (Frail, Kulkarni & Bloom, 1999; Cameron et al., 2005; Gaensler et al., 2005b; Gelfand et al., 2005; Taylor et al., 2005; Fender et al., 2006). The amount of energy in the radio afterglow is much less than that emitted in the gamma-rays. This is different from what is observed in gamma ray bursts, where the ratio between the two types of emission is of order unity, such that the lower energy and longer duration emission is associated with re-processing of the gamma-ray energy by the surrounding material. The radio afterglow from the magnetar giant flares is linearly polarized, implying that it is caused by electron synchrotron emission, and is observed to expand over time. Its generation requires an ejection of relativistic particles and magnetic fields (in the form of a “plasmon”, which expands and cools) by the burst process (see Section 5.3).

5.2. Burst trigger mechanisms

Rapid magnetic field reconfiguration is assumed to be an integral part of the bursts: as we will discuss in Sec. 5.3, the gamma-ray emission is assumed to come from particles accelerated by rapid field change. Thus slow magnetic evolution builds up stresses in the system, some of which are released catastrophically in bursts, which must either be driven by or result in rapid magnetic field reconfiguration. However the precise trigger mechanism, and the role of the magnetic field within it (if any), remains unclear. Three main locations (and associated families of instabilities) have been considered for the trigger mechanism: below we review each in turn.

The first option, as suggested by Thompson & Duncan (1995), is that the magnetic field evolves into an unstable configuration within the liquid core of the star (Markey, 1973; Wright, 1973; Tayler, 1973; Flowers & Ruderman, 1977), which is then susceptible to a large-scale magnetohydrodynamical instability (Lander & Jones, 2011a; Ciolfi et al., 2011; Kiuchi, Yoshida & Shibata, 2011; Ciolfi & Rezzolla, 2012). This would develop on the Alfvén crossing time of the core, which is ~ 0.1 s for a 10^{15} G interior field ($\tau \sim R/v_A$, where the Alfvén speed v_A is given in Equation 16 later in this paper) and hence broadly compatible with the durations of both the normal bursts and the initial peaks of the giant flares.

Whether such an unstable state could develop is open to question, since if the core is superconducting, the high conductivity should facilitate swift reconfiguration and hence prevent the formation of such an unstable state. However the configuration could be stabilized by currents in the crust, or superconductivity may be suppressed if the core field exceeds $\sim 10^{16}$ G. Such rapid internal magnetic reconfiguration would inject

an Alfvén pulse into the magnetosphere that would then generate the observed burst emission. The energy available to power the burst in this scenario, since it originates in the core, is more than sufficient to power even a giant flare. Some internal heat release may also be expected due to dissipation in core and crust as the instability proceeds.

The second option is that the decay of the core field places magnetic stresses on the solid crust of the star (an ionic lattice to which the field in the crust is locked). The crust can deform elastically to accommodate this up to a certain point, then ruptures catastrophically once its breaking strain is exceeded (Thompson & Duncan, 1995; Thompson & Duncan, 2001). The stored energy released in this scenario would come from the crust and possibly also the core: although initially it was thought that the crust alone could not store enough elastic energy to power the giant flares (Thompson & Duncan, 1995), the latest molecular dynamics simulations predict a higher breaking strain, indicating that this may be feasible after all (Horowitz & Kadau, 2009; Hoffman & Heyl, 2012). Studies are now underway that aim to determine how and where stresses would build up in the crust as a result of core field evolution, the goal being to determine how often, and where (location including depth) the crust is most likely to fail (Perna & Pons, 2011; Pons & Perna, 2011; Beloborodov & Levin, 2014; Lander et al., 2015). Recent calculations by Lander et al. (2015) of the strain induced in a crust by a changing magnetic field configuration find a characteristic burst energy

$$\frac{E}{10^{45}\text{erg}} \approx 0.25 \left(\frac{\sigma_{\text{max}}}{0.001} \right) \left(\frac{d}{R_c} \right)^2 \left(\frac{l}{2\pi R} \right) \quad (11)$$

where σ_{max} is the breaking strain of the crust (which could be as high as 0.1; Horowitz & Kadau, 2009), d is the depth at which the crust ruptures, R_c the crust thickness, R is the star radius, and l the rupture length. The characteristic local field strength related to crust breaking (from the same study) is given by

$$B_{\text{break}} = 2.4 \times 10^{14} \text{G} \left(\frac{\sigma_{\text{max}}}{0.001} \right)^{1/2}. \quad (12)$$

When the crust does rupture it must do so by rapid plastic deformation, not via brittle fracture, due to the impossibility of opening up voids under the conditions of extreme pressure that pervade in neutron star crusts (Jones, 2003). The role of the magnetic field during crust rupture however is not clear: Levin & Lyutikov (2012) have argued that under some circumstances the field deformation induced by an incipient rupture may act as a brake on its propagation. Shear wave timescales (which control the timescale on which the crust ruptures, $\tau \sim \pi R/v_s$, where the shear speed v_s is given by Equation 15 later in this paper) are compatible with those observed in bursts and flares (see for example Schwartz et al., 2005), injecting an Alfvén pulse into the magnetosphere. However the transfer of energy into the external magnetosphere may be slowed by a large impedance mismatch at the crust-magnetosphere boundary (Link, 2014). Crustal rupture would most likely lead to local heating as well.

The final possibility is that the core and crust evolve smoothly, and that stress builds up instead in the magnetosphere. Stress release is then envisaged as taking place via

a plasma instability involving spontaneous magnetic reconnection (see Uzdensky, 2011, for a review). A number of studies have looked at how the external magnetosphere might respond to the expulsion of magnetic helicity due to the decaying core field, and have found that the development of unstable configurations with strong magnetic shear, that might be prone to reconnection instabilities, is feasible (Thompson, Lyutikov & Kulkarni, 2002; Beloborodov, 2009; Parfrey, Beloborodov & Hui, 2012; Parfrey et al., 2013). The resulting explosive reconnection event would progress on the Alfvén crossing time in the magnetosphere, which is $\lesssim 0.01$ s (since in the magnetosphere $v_A \sim c$), and the energy that can be released is more than sufficient to power even the giant flares. Specific instabilities that have been considered primarily for the giant flares (driven by earlier concerns about the ability of crust ruptures to release enough energy) are the relativistic tearing mode (Lyutikov, 2003, 2006; Komissarov et al., 2007) and collisionless Hall reconnection mediated by emission from precursor bursts (Gill & Heyl, 2010), the precursors presumably being triggered in this scenario by another mechanism. Similarities between the giant flares and reconnection driven coronal mass and flux tube ejection events in solar physics have also been explored in some depth (Masada et al., 2010; Yu, 2011, 2012; Yu & Huang, 2013; Huang & Yu, 2014a,b; Meng et al., 2014). Instabilities may also arise from the interaction of MHD waves with the vacuum in fields above the quantum critical limit (where QED effects are important, Heyl & Hernquist, 2005). All of these mechanisms would lead directly to particle acceleration and radiation in the magnetosphere, with possible crustal heating via particles impacting the surface.

At present it is by no means clear which of the various mechanisms are in operation, and given the diversity of burst properties (Sec. 5.1) more than one may be in operation. Timescales, as discussed above, appear to be roughly compatible with either burst rise times or durations (assuming that the emission process timescales reflect those of the trigger mechanism). Moreover both starquakes and magnetospheric reconnection could in principle explain the power law distribution of fluences (which is often taken as evidence for Self-Organised Criticality, see for example Aschwanden et al., 2014). Serious efforts are now being made to simulate the build up of stress and the development of instabilities, but in order to allow meaningful tests of the data, consideration must be given to how these various triggers connect to the emission that we see. We discuss this in the next section (Sec. 5.3).

5.3. Burst emission processes

5.3.1. Sources of emission Magnetar bursts are complex, with varied spectra and morphologies. The emission process for all bursts is generally assumed to be started by rapid rearrangement of the magnetic field (resulting from one of the trigger mechanisms discussed in Sec. 5.2), possibly involving either induced or spontaneous magnetic reconnection. This accelerates charged particles with ensuing gamma-ray emission, since the rapid acceleration of electrons in a strong curved field leads to a cascade of pair creation and gamma-rays (Sturrock, Harding & Daugherty, 1989). To obtain the hardest

emission, there must be very low contamination by baryonic material (since scattering would lead to softening). Fully self-consistent models of the emission resulting from the various proposed trigger mechanisms do not yet exist. Despite this, the rise timescale of the gamma-ray emission has frequently been used as a key piece of evidence to argue for a particular trigger mechanism, as discussed in the previous section. However it is not clear that this is warranted: details of the gamma-ray emission process may in fact completely obscure the timescales associated with the original trigger mechanism (see for example Hoshino & Lyubarsky, 2012).

To obtain the radio afterglow seen in the giant flares, it is necessary to postulate the ejection of a plasmoid of magnetic fields and trapped shocked plasma, that gradually cools (Sec. 5.1). Such plasmoid ejection is a natural and expected consequence of a large-scale reconnection event in the magnetosphere (see Sec. 5.2 and for example Lyutikov, 2006).

The initial spike of magnetar flares may also lead to radio emission (explored for example in Lyutikov, 2002). More recently it has been suggested that the interaction between strongly magnetized relativistic ejecta (expelled by the initial spike of giant flares) and the surrounding wind nebula might be responsible for extragalactic Fast Radio Bursts (Popov & Postnov, 2007, 2013; Thornton et al., 2013; Lyubarsky, 2014). At present this remains speculative.

If the local energy generation rate is high enough, as explained above, it will lead to copious production of electron-positron pairs and gamma-rays. If this occurs in a closed field line region, where the charged pairs cannot cross magnetic field lines, they become trapped. As density increases, so does optical thickness, trapping the photons as well and leading to rapid thermalization (Thompson & Duncan, 1995). The field necessary to confine the plasma can be estimated by requiring that magnetic pressure exceed the pressure of the radiation and the pairs at the outer boundary of the fireball, yielding

$$B_{\text{dipole}} > 2 \times 10^{14} \left(\frac{E_{\text{fireball}}}{10^{44} \text{ erg}} \right)^{1/2} \left(\frac{\Delta R}{10 \text{ km}} \right)^{-3/2} \left(\frac{1 + \Delta R/R}{2} \right)^3 \text{ G} \quad (13)$$

(Thompson & Duncan, 2001), where ΔR is the characteristic size of the fireball and R the neutron star radius.

Such a trapped pair plasma fireball would then cool and contract due to radiative diffusion from a thin surface layer, with the bulk of the radiation leakage occurring close to the stellar surface since this is where the field is strongest and scattering the most suppressed. The opacity at the surface will be dominated by the electron-ion plasma ablated from the neutron star surface (especially if the emergent flux is close to the magnetic Eddington limit) which form the photosphere. This trapping would prolong the emission from the burst by acting as a reservoir for the energy. Fireball formation is not exclusively linked to any one trigger mechanism (Thompson & Duncan, 1995; Heyl & Hernquist, 2005).

The fireball model has been very successful at explaining the later decaying tail phase of giant flares (Thompson & Duncan, 2001). A cooling fireball trapped on

closed field lines should have a luminosity L whose time-dependence is described by the following function

$$L(t) = L(0) \left[1 - \frac{t}{\tau_{\text{evap}}} \right]^{a/(1-a)} \quad (14)$$

where the cooling luminosity is assumed to vary as a power of the remaining fireball energy, $L \propto E^a$ (Thompson & Duncan, 2001). This proves to be a good fit to giant flare tail data, with τ_{evap} of order a few hundred seconds, and a value of a that is close to that expected for a spherical fireball of uniform temperature (Feroi et al., 2001). Spectral fitting indicates that the emitting area falls while the temperature of the radiation remains roughly constant at the level expected for the photosphere of a trapped fireball in a magnetic field in excess of the quantum critical field (Thompson & Duncan, 1995; Feroi et al., 2001). The observed photospheric temperature ($\sim 20 - 30$ keV) is lower than the inferred temperature in the core of the fireball, which is ~ 100 keV (Thompson & Duncan, 1995; Thompson & Duncan, 2001). Thompson & Duncan (1995) argue that this is an intrinsic property of the way various processes act to preserve thermal equilibrium in the fireball, and the way that radiation gradually escapes. However other processes such as photon splitting as the emitted radiation propagates through the strong magnetic field may also be important (Baring, 1995). The beaming of radiation as it leaks from the base of the fireball and streams along field lines provides a simple explanation for the strong rotational pulses seen in the giant flare tails (Fig. 22). Whether fireballs form in the smaller bursts is still not clear (energy release may not occur at a fast enough rate (Gögüş et al., 2001), although the similarity of the spectra of the short bursts to the spectra in the tails of the giant flares suggests that there may be a link.

Some of the energy released during the burst is likely to excite vibrations, either of the star (crust/core, see Sec. 5.4) or in the form of Alfvén waves in the magnetosphere. This too can act as a store for energy that is then radiated on longer timescales. If the vibration rate is slow enough, this can act as a source of ongoing excitation that forms an extended pair corona (that obscures and scatters the radiation from the trapped fireball) from which the radiation emerges isotropically (Feroi et al., 2001; Thompson & Duncan, 2001). The presence of such an extended pair corona has been invoked to explain the smooth emission immediately after the peak of the giant flares, which then clears over 30-40 s to reveal the strongly beamed rotational pulse emanating from the trapped fireball beneath (Feroi et al., 2001).

A burst may also have a thermal component of emission that is produced by residual heat of crust rupturing (Lyubarsky, Eichler & Thompson, 2002; Kouveliotou et al., 2003), extreme heating and possible melting of the crust immediately underneath a trapped fireball (Thompson & Duncan, 1995), or bombardment of the stellar surface by magnetospheric particles (Lyutikov, 2006; Beloborodov, 2009). Such thermal components, particularly deep crustal heating, are one possible explanation for the presence of both the additional pulsed components seen after some bursts (short and

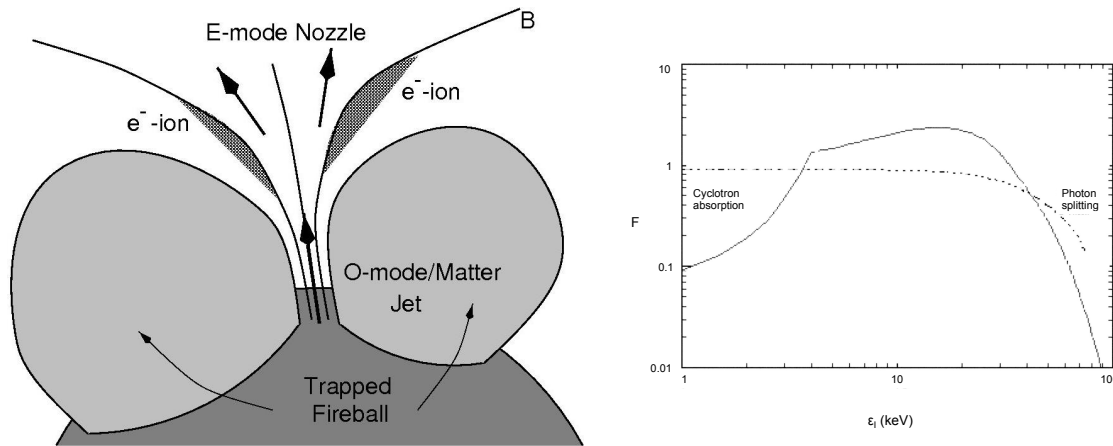


Figure 22 Left: Figure from Thompson & Duncan (2001), to illustrate how radiation escapes from a trapped photon-pair plasma fireball. Scattering opacities are strongly polarization dependent, with most radiation escaping from the fireball in the E-mode. This radiation is then collimated along open magnetic field lines (due to the magnetic field dependence of the scattering opacities), forming a beam that is then modulated by the star's rotation to give rise to a rotational pulse (from Thompson & Duncan, 2001, ©AAS. Reproduced with permission. A link to the original article via DOI is available in the electronic version). Right: Figure from Lyubarsky (2002) showing how the photospheric spectrum from a fireball with temperature 15keV (dashed line) would be modified by various high field radiation processes: cyclotron absorption, for a 6×10^{14} G field, and photon splitting (from Lyubarsky, 2002, with OUP permission).

intermediate) - as a localised hotspot - and the must longer decaying afterglows seen after burst active periods, intermediate flares and giant flares (Kouveliotou et al., 2003; Feroci et al., 2003).

The location of the emitting regions is further complicated by the fact that the luminosity of the bright bursts may exceed the relevant Eddington limit, leading to photospheric expansion and ejection of material as radiation pressure overwhelms the gravitational force (see for example Thompson & Duncan, 1995; Watts et al., 2010). Magnetar bursts can easily exceed the non-magnetic Eddington limit. However strong magnetic fields suppress scattering opacities, increasing the Eddington luminosity even before magnetic confinement effects - which can increase the limit still further - are taken into account (Paczynski, 1992; Thompson & Duncan, 1995; Miller, 1995; van Putten et al., 2013).

5.3.2. Radiative transfer processes Short burst spectra, in an era of improved broadband coverage, are typically well fit as either two blackbodies (2BB, with temperatures ~ 5 keV and ~ 15 keV) or using a Comptonization (power law with a high energy cutoff) model (Feroci et al., 2004; Olive et al., 2004; Nakagawa et al., 2007; Israel et al., 2008; Esposito et al., 2008; Lin et al., 2011a; Scholz & Kaspi, 2011; van

der Horst et al., 2012; Lin et al., 2012a). There is a sharp correlation between radius and temperature of the blackbodies in the 2BB fits, with the softer BB component saturating before the harder one as burst fluence increases. For some sources bursts tend to harden with increasing fluence, whereas for others they soften (Gögüş et al., 2001; Gavriil, Kaspi & Woods, 2004; Götz et al., 2004; Kumar, Ibrahim & Safi-Harb, 2010; Savchenko et al., 2010; Scholz & Kaspi, 2011; van der Horst et al., 2012). Earlier burst papers tend to use an Optically Thin Thermal Bremsstrahlung (OTTB) model (Gögüş et al., 1999; Woods et al., 1999b; Gögüş et al., 2000; Aptekar et al., 2001), which fit the data well above 15 keV although they overpredict the flux of photons at low energies (Fenimore, Laros & Ulmer, 1994; Feroci et al., 2004). Despite this, OTTB fits are often included in more recent analysis, to allow comparison with earlier studies. OTTB temperatures are typically in the range 20-40 keV, and in general no emission is seen from short bursts above 150-200 keV. There have however been a handful of events from SGR 1900+14 with a much harder spectrum, and emission extending up to 500 keV (Woods et al., 1999d). There have also now been studies exploring the softest part of the burst spectrum, using data from *XMM-Newton*, where the burst spectra appear to be well fit with a more physically-motivated model comprising a modified blackbody plus resonant cyclotron scattering Lin et al. (2012b, 2013, and see Sec. 5.3). There have also been strong efforts to search for spectral lines in magnetar bursts. For a long time the only reported detections, from 5 keV to 13-14 keV, in bursts from SGR 1806-20, XTE J1810-197, 4U 0142+61, and 1E1048.1-5937 came from *RXTE* data (Ibrahim et al., 2002; Woods et al., 2005; Gavriil, Kaspi & Woods, 2002, 2006; Gavriil, Dib & Kaspi, 2011). However recently a similar feature has been detected in bursts from 1E1048.1-5937 observed by *NuSTAR* (An et al., 2014a), increasing confidence that they are indeed intrinsic to the bursts. The line energy is close to that expected for the proton cyclotron line given the inferred magnetic field strength. In addition to time-integrated spectra, data quality are now sufficiently good that it is possible to do time-resolved spectroscopy. These studies indicate that although the best fit spectral model remains the same during individual bursts, the parameters can evolve (Israel et al., 2008; Lin et al., 2011a; Younes et al., 2014). However between bursting episodes, the best fit model for individual sources may change (von Kienlin et al., 2012).

The spectra of the initial spikes of intermediate flares are similar to the short bursts (Mazets et al., 1999a,b; Olive et al., 2004; Israel et al., 2008). The spectrum of the extended decaying tails is however different (in contrast with the tails seen after some short bursts, where the peak and tail have similar spectra). Tail spectra for intermediate flares are well fit by a BB, possibly with an additional power law component, and the emission softens during the tail (Ibrahim et al., 2001; Lenters et al., 2003; Esposito et al., 2007b; Gögüş et al., 2011b).

For the giant flares, reliable spectral modelling in the initial spike is complicated enormously by dead time and pile up (Fenimore et al., 1996; Mazets et al., 1999c). However OTTB models or quasi-BB models yield spectral temperatures in the range 200-300 keV, and emission has been detected up to 2 MeV (Mazets et al., 1979a; Hurley

et al., 1999b; Hurley et al., 2005). The spectrum of the emission in the tail is very similar to that of the short bursts, with OTTB temperatures $\sim 10 - 30$ keV (Fenimore et al., 1981; Hurley et al., 1999b) that vary with rotational phase. Other spectral models such as BB or 2BB, possibly with a power law, also provide a good fit to the data. A significant hard (> 1 MeV) component was seen during the tail and subsequent afterglow from the SGR 1806-20 giant flare (Mereghetti et al., 2005c; Frederiks et al., 2007; Boggs et al., 2007).

Although the spectral models described above provide a reasonable fit for the data, they are not based on physical models that take into account all of the scattering and resonant processes known to be important in such strong magnetic fields. Any thermal emission, for example, as might be expected from a trapped fireball (Thompson & Duncan, 1995; Thompson & Duncan, 2001), would be strongly modified, see Fig. 22. Lower energy photons scatter less and can hence escape from deeper, hotter parts of the atmosphere. The radiation at low energies should thus exceed that expected for simple blackbody emission (Ulmer, 1994; Lyubarsky, 2002). Photon splitting and merging will also be important in modifying the spectrum (Miller, 1995; Baring, 1995; Thompson & Duncan, 2001) at energies above around 30 keV, and resonant cyclotron scattering (RCS, see Sec. 3.3.1) will also be important. Efforts to fit burst spectra using more physical models, or to interpret the phenomenological models in terms of physical parameters, are however very rare. Israel et al. (2008) (also Kumar, Ibrahim & Safi-Harb (2010)) suggested that the two blackbodies in the 2BB model fits might be the photospheres associated with the different polarization modes, although theoretical calculations of the properties of the two photospheres do not match those inferred from the fits (van Putten et al., 2013). Lin et al. (2011a) attempted to interpret the parameters of the Comptonization and 2BB model fits in terms of a population of coronal electrons scattering surface emission (for example from a fireball), see also van der Horst et al. (2012) and Younes et al. (2014). More recently, Lin et al. (2012b, 2013) made an effort to fit soft burst emission using the modified blackbody model developed by Lyubarsky (2002), augmented to include effects of RCS. The fact that physical model interpretations are still so scarce, however, emphasizes the huge uncertainty in terms of the location of the emission mechanisms, how they form, and how the released energy is partitioned between them.

5.4. Burst seismology

Asteroseismology is a precision technique for the study of stellar interiors, and it is magnetars that have opened up this field for neutron stars. This began when Quasi-Periodic Oscillations (QPOs) in the hard X-ray emission were found in the tails of the giant flares from the magnetars SGR 1806-20 (Israel et al., 2005; Watts & Strohmayer, 2006; Strohmayer & Watts, 2006) and SGR 1900+14 (Strohmayer & Watts, 2005). In the tail of the SGR 1806-20 giant flare (Fig. 23) there were several QPOs in the range 18-150 Hz, and two isolated higher frequency signals at 625 Hz and 1840 Hz. The QPOs

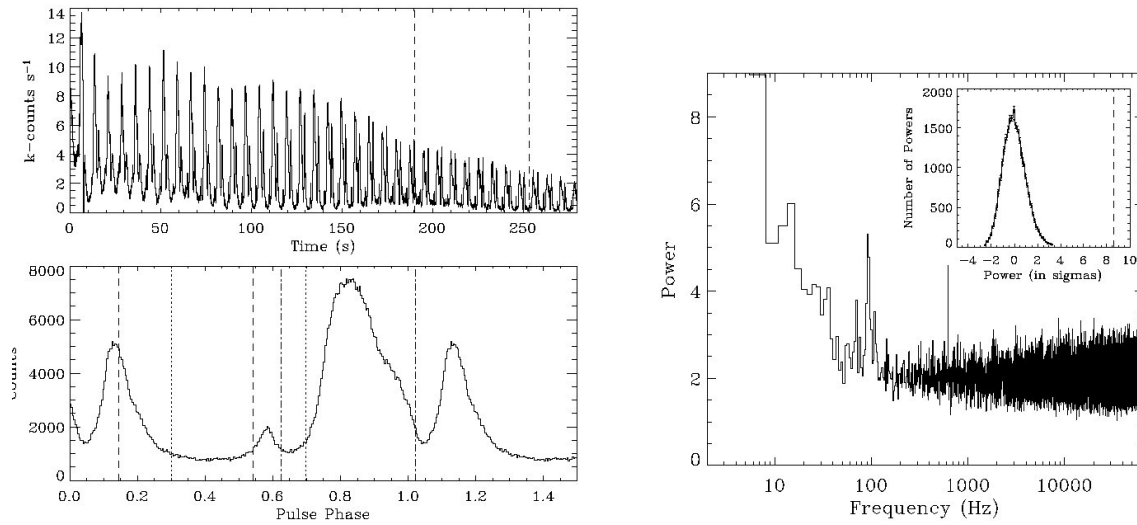


Figure 23 Figure from Strohmayer & Watts (2006) showing the two strongest QPOs detected in the tail of the SGR 1806-20 giant flare. Top left: RXTE lightcurve of the event. Lower left: Rotational pulse during this time: the power spectra shown are computed using the segments enclosed by the dashed lines. Right: Power spectrum made by averaging nine 3 s segments from the time interval marked by dashed lines in the top left panel. The 92 Hz and 625 Hz QPOs are clearly visible, and the inset illustrates the significance of the 625 Hz feature (from Strohmayer & Watts, 2006, ©AAS. Reproduced with permission. A link to the original article via DOI is available in the electronic version)

detected in the tail of the giant flare from SGR 1900+14 had frequencies in the range 28-155 Hz. Widths (FWHM) were in the range 1-20 Hz, with fractional amplitudes up to $\sim 20\%$ rms that are strongly rotational phase-dependent.

The idea that giant flares might excite global seismic vibrations was first predicted by Duncan (1998), and this is the most plausible explanation that has yet been advanced to explain the QPOs (Israel et al., 2005). If this interpretation is correct, such vibrations offer an unprecedented opportunity to constrain the interior field strength and geometry (something that is very hard to measure directly), and also perhaps the dense matter equation of state (Samuelsson & Andersson, 2007; Watts & Reddy, 2007). In order to do this, however, the modes must be correctly identified.

The QPOs were initially tentatively identified with torsional shear modes of the neutron star crust and torsional Alfvén modes of the highly magnetized fluid core. These identifications were based on the expected mode frequencies, which are set by both the size of the resonant volume and the relevant wave speed. For crustal shear modes, the appropriate speed is the shear speed $v_s = (\mu_s/\rho)^{1/2}$ where μ_s is the shear modulus and ρ the density. The shear modulus is of the order of the Coulomb potential energy $\sim Z^2 e^2/r$ per unit volume r^3 , where $r \sim (\rho/Am_p)^{-1/3}$ is the inter-ion spacing, while Z and A are the effective atomic number and mass number, respectively, of the

ions in the crust. Using the shear modulus computed by Strohmayer et al. (1991) and scaling by typical values for the inner crust (Douchin & Haensel, 2001), the shear velocity as shown by Piro (2005) is:

$$v_s = 1.1 \times 10^8 \text{cm/s} \left(\frac{\rho}{10^{14} \text{g/cm}^3} \right)^{1/6} \left(\frac{Z}{38} \right) \left(\frac{302}{A} \right)^{2/3} \left(\frac{1 - X_n}{0.25} \right)^{2/3} \quad (15)$$

where X_n is the fraction of neutrons. This yields a rough estimate for the frequency for the fundamental crustal shear mode of $\nu \sim v_s/2\pi R = 18$ (10 km/ R) Hz. Full mode calculations find similar values, but with additional dependencies on the mass and radius of the star due to relativistic effects (see for example Samuelsson & Andersson 2007), and it is this dependence that makes the modes potentially powerful diagnostics of the dense matter equation of state (Lattimer & Prakash, 2007). Many of the lower QPO frequencies could be explained as angular harmonics with no radial nodes, whilst the two highest frequencies in the SGR 1806-20 giant flare were identified as radial overtones of these crustal modes.

For torsional Alfvén modes of the core, the appropriate wave speed is the Alfvén speed $v_A = B/\sqrt{4\pi\rho}$ where B is the magnetic field strength, giving

$$v_A = 10^8 \text{cm/s} \left(\frac{B}{10^{16} \text{G}} \right) \left(\frac{10^{15} \text{g/cm}^3}{\rho} \right)^{1/2}. \quad (16)$$

This yields a very rough estimate for the frequency of the fundamental torsional Alfvén mode of $\nu \sim v_A/4R = 25$ (10 km/ R) Hz (Thompson & Duncan, 2001). Note however that the value of the field strength B in magnetar cores is highly uncertain, as is the appropriate value of the density ρ . In principle only the charged component (~ 5 -10% of the core mass) should participate in Alfvén oscillations, reducing ρ , however there are mechanisms associated with superfluidity and superconductivity that can couple the charged and neutral components, leading to additional mass-loading. As above, full mode calculations that take into account relativistic effects lead to additional dependencies on neutron star mass and radius (see for example Sotani et al. 2008). It should also be noted that the Alfvén modes constitute continua rather than a set of discrete frequencies, since the field lines within the core have a continuum of lengths. The observed QPOs would then be associated with turning points of the Alfvén continuum, since these tend to dominate the oscillatory properties when one computes the time evolution of systems with continua (Levin, 2007; Sotani et al., 2008).

In fact, for a star with a magnetar strength field, crustal vibrations and core vibrations should couple together on very short timescales (Levin, 2006, 2007). Considering them in isolation, as described above, is therefore not appropriate. The current viewpoint, based on more detailed modelling that takes into account the magnetic coupling between crust and core, is that the QPOs are in fact associated with global magneto-elastic axial (torsional) oscillations of the star (Glampedakis et al., 2006; Lee, 2008; Andersson et al., 2009; Steiner & Watts, 2009; van Hoven & Levin, 2011, 2012; Colaiuda & Kokkotas, 2011, 2012; Gabler et al., 2012, 2013; Passamonti

& Lander, 2013, 2014; Asai & Lee, 2014; Glampedakis & Jones, 2014). However since magneto-elastic oscillations depend on the same physics described above, albeit now in a coupled system, they have frequencies in the same broad range as the simple estimates given above. Current magneto-elastic torsional oscillation models can thus in principle explain the presence of oscillations at frequencies of 155 Hz and below.

Until very recently, however, it appeared that there was a significant problem with the higher frequency QPOs. This is because although there are crust shear modes in this frequency range, they should overlap with the various Alfvén continua (there are no gaps between the harmonics of the continua as the frequency increases). As a result, the coupled oscillation should damp very rapidly, on timescales of less than a second (van Hoven & Levin, 2012; Gabler et al., 2012). The data analysis, however, indicated that the oscillations persisted for up to ~ 100 s (Watts & Strohmayer, 2006; Strohmayer & Watts, 2006). Various solutions to this problem have been explored, including coupling to polar modes (Lander et al., 2010; Lander & Jones, 2011a; Colaiuda & Kokkotas, 2012), and resonances between crust and core that might develop as a result of superfluid effects (Gabler et al., 2013; Passamonti & Lander, 2014). It is clear from these studies that superfluidity in particular can have a large effect on the characteristics of the mode spectrum: and since superfluidity is certainly present in neutron stars, mode models must start to take this into account before we can make firm mode identifications (Fig. 24).

However the debate over this issue also exposed the fact that the initial data analysis did not actually test whether the signal could also be there in much shorter data segments, more consistent with the theoretical predictions. Huppenkothen, Watts & Levin (2014) have since re-analysed data for the 625 Hz QPO in the SGR 1806-20 giant flare and found that the data are in fact consistent with a short-duration signal that damps and is re-excited several times (rather than a long-lasting low-amplitude QPO). What might cause late time excitation and re-excitation remains an open question, and is relevant to the lower frequency QPOs as well since several seem to appear only late in the tails of the giant flares. Aftershocks may play an important role in exciting and re-exciting the QPOs that we see, and there may also be intrinsic delays in the process whereby vibrations are excited by the flare due to impedance mismatching between the different components of the star (Link, 2014).

Since giant flares are very rare, there have also been efforts to search for seismic vibrations in the much more frequent lower energy bursts[‡]. As discussed above, it is not yet entirely clear whether these bursts are caused by the same mechanism as the giant flares. However if they are, it is quite possible that they might excite seismic vibrations at frequencies similar to those seen in the giant flares, particularly if we

[‡] There have also been a number of searches for gravitational waves associated with magnetar flares and any associated starquakes or global seismic oscillations (Abbott et al., 2007, 2008, 2009; Abadie et al., 2011). So far only upper limits have been reported, but new analysis techniques are being developed for the next generation of detectors (Murphy et al., 2013).

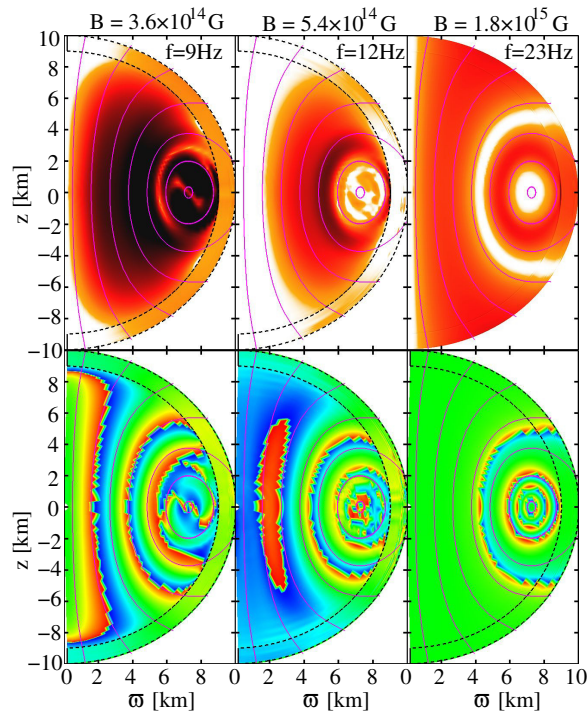


Figure 24 Simulations of QPOs of a magnetized neutron star with a solid crust and superfluid core, in General Relativity, from Gabler et al. (2013). The upper panels show the Fourier amplitude and the lower panels the phase. Both frequency and mode structure change as the field strength varies. The color scale ranges from white-blue (minimum) to orange-red (maximum) in the top panel, and from $\theta = \pi/2$ (blue) to $\theta = -\pi/2$ (orange-red), respectively. The crust is indicated by the dashed black line, and magnetic field lines by the solid magenta lines (from Gabler et al., 2013, ©2013 American Physical Society, reproduced with permission).

are genuinely seeing global modes of vibration of the star \S . Searching for QPOs in the smaller bursts is however complicated by the short, transient nature of the burst lightcurves themselves, and this has required the development of specially tailored statistical methods (Huppenkothen et al., 2013; Huppenkothen et al., 2014b).

So far these techniques have been applied to several data sets. A sample of 27 bursts from the magnetar SGR 0501+4516, using Fermi GBM data, made one candidate detection, but its significance was weak (Huppenkothen et al., 2013). A search of a larger sample of 286 Fermi GBM bursts from SGR J1550-5418, however, found significant QPOs at 93 Hz and 127 Hz after averaging together multiple bursts from highly active episodes (Huppenkothen et al., 2014). Similar analysis using RXTE data from the most burst-active magnetars SGR 1806-20 and SGR 1900+14 (the two sources for which

\S The search for global seismic vibrations in small and intermediate magnetar flares is a core science driver for future hard X-ray and gamma-ray missions such as the proposed *Large Observatory for X-ray Timing* (Feroci et al., 2014).

QPOs have been observed in the giant flares||) led to the detection of a QPO at 57 Hz after averaging together multiple bursts from SGR 1806-20 Huppenkothen et al. (2014b). These frequencies are in the range found in the giant flares, and the QPO widths are also comparable. It therefore seems plausible that they are instances of the same phenomenon. If these frequencies do indeed represent global magneto-elastic oscillations the implication is that such vibrations are excited not only by giant flares, but also by trains of shorter bursts. This is important information when we start to consider how modes are excited by the trigger mechanism.

The analysis of SGR J1550-5418, however, also revealed a QPO in a single burst, at a much higher frequency of 260 Hz. In addition to being in a different frequency band, this QPO was much broader than those seen in the giant flares and had very high fractional amplitude. If this is a magneto-elastic oscillation mode, then it is of interest since models predict that modes in this frequency range should die out on timescales comparable to the duration of short bursts. This could explain the observed low coherence, since broad width is a natural consequence of a rapidly exponentially decaying signal. This signal could, however be something quite different, such as a plasma instability associated with magnetic reconnection (Kliem, Karlický & Benz, 2000) or a local oscillation in a smaller, temporarily decoupled, cavity (Huppenkothen et al., 2014). In this case it may be a fingerprint of the burst trigger process. Variability in the impulsive phase of the giant flares has previously been suggested, but dead time and saturation effects strongly distort timing analysis for the very brightest events (Barat et al., 1983; Terasawa et al., 2006).

Another open question is how magneto-elastic oscillations couple to the magnetosphere and hence modulate the emission from the star. An important concern is that the fractional amplitude of the QPOs is in some cases quite high, and certainly much higher than the likely amplitude of any oscillations of the neutron star's crust. Emission in the tails of the giant flares is dominated by radiation leaking from the trapped pair-plasma fireball. This emission is strongly beamed (giving rise to the strong rotational pulse), and thus in principle could act to amplify small surface vibrations, however analysis of the beams from the giant flares indicates that although the effect is real it is unlikely to be strong enough to explain the highest observed fractional amplitudes (D'Angelo & Watts, 2012). This suggests that there is some additional effect modulating the intensity of the emission: something that takes on added importance in the light of QPOs detected in the smaller bursts, where it is not clear that fireballs even form. A likely mechanism is a modulation of the optical depth to Resonant Cyclotron Scattering (see Sec. 3.3.1), via changes in particle number density (Timokhin, Eichler & Lyubarsky, 2008) and/or magnetic field geometry (Gabler et al., 2014). However the details of this process, and the interaction with the fireball, remain to be worked out fully.

|| Very few bursts from these sources have been observed in the period since Fermi GBM has been flying, and no giant flares have yet been observed in the Fermi era.

6. Summary and Conclusions

There is now a general agreement that the key observational phenomena that make soft gamma repeaters and anomalous X-ray pulsars so unique are well explained by the presence of a magnetar, a neutron star with ultra-strong magnetic field. In the absence of accretion from a binary companions and of large enough rotational energy losses, magnetic energy appears the only reasonable option to power both the persistent and bursting emission at the observed levels. Recently, thanks to the discovery of the so-called “low-B” sources, it has become increasingly evident that to make an “active” magnetar what matters is not (or not only) a large ($\gtrsim 10^{14}$ G) dipole field, but a strong, residual poloidal component of the internal magnetic field. In this section we summarize the status of theoretical modelling, within the magnetar scenario, in the attempt to highlight what are, in our opinion, the issues which are basically settled and those which are still open.

A clear picture has now emerged of where magnetars stand in relation to the population of isolated neutron stars, at least in terms of their observational properties. However, borders among the different classes are somehow blurry and the possible (evolutionary ?) links remain still to be fully understood. The existence of “low-B” and transient magnetars, implying that the number of highly magnetized neutron stars may be much larger than previously thought, makes it apparent that there may be a “birthrate” problem, unless there is an overlap between classes, meaning that objects that we see as observationally diverse are just neutron stars at different evolutionary stages, or magnetars can form through channels different from standard supernova events.

A better understanding of magnetar’s formation path may help to bring clarity here. One of the biggest open questions is how magnetars acquire their super-strong magnetic field, as compared to those of the, apparently much more abundant, radio pulsars. Despite much effort, no definite conclusion has been reached as yet. Nonetheless, the very recent discovery that the magnetar in the Westerlund 1 cluster may have originated in a binary system points quite strongly towards a particular formation route involving massive binaries. Much theoretical attention has also been given to the idea that newborn magnetars are the central engines for gamma-ray bursts and newly developed models have had a great deal of success in explaining the “plateau” phase of the observed lightcurve. A conclusive proof for this seems now to rest with the observers, and may come in the next few years if a GRB is definitely linked to the gravitational wave detection of a compact binary interaction.

A topic of the greatest relevance is the magnetic field configuration in newborn magnetars. In particular how the field structure varies across core, crust, and magnetosphere; the balance between toroidal and poloidal components; and the small-scale structure of the external field. The state of the magnetic field at birth, and its subsequent evolution, are critical input for many aspects of magnetar physics. This is an active area of study that has also been given new impetus by the discovery of

magnetars with low surface dipole field strengths. There has been a good deal of progress in this area in recent years, although the various physical processes likely to affect the evolution of the magnetic field in the crust, where coupling of magnetic and thermal effects becomes important, remain challenging to model.

There has been great progress in understanding the emission processes of magnetars. The existence of a twisted magnetosphere seems now to be generally accepted. Resonant cyclotron scattering onto pairs flowing in a twisted magnetosphere provides spectra which are in good quantitative agreement with the soft X-ray data, and also a natural explanation for the emission in the other wavebands (hard X-ray, optical/IR). However, a complete solution of the non-linear charge acceleration problem, including the various QED effects leading to photon splitting, positronium dissociation, and the fact that the twisted magnetosphere is expected to be strongly dynamic, has not yet been found. Another of the major open issues is the lack of a credible model of the interplay between crustal, atmospheric and magnetospheric emission, capable of explaining the broadband spectral energy distribution of magnetar sources.

For the bursts, some aspects do seem clear. It is widely accepted, in the absence of a better model, that reconnection is likely to be required to explain the observed gamma-ray emission. For the giant flares, plasma ejection must take place to explain the radio afterglows, and a magnetically trapped pair plasma fireball seems the only viable hypothesis for the pulsed tails of the giant flares. The trigger mechanism for all bursts, however, remains unknown, as do the emission processes in the smaller and intermediate bursts. It will also be important to ensure that the bursts and persistent emission are considered as a whole: constraints on the magnetospheric structure and radiative transfer environment obtained from study of the persistent emission should be applied consistently, for example, when considering the radiation propagating in the aftermath of a burst. The detection of quasi-periodic oscillations in bursts has also provided new insight. The idea that these are caused by global seismic vibrations, excited by the burst process, is certainly the most plausible model put forward to date, although details of how the stars oscillate remain to be worked out. Far more work is required, however, is to examine self-consistently the conditions for excitation, decay, and modulation of the emission.

Some theoretical predictions must await more advanced observational capabilities in order to be tested fully. *NuStar* (and possibly in the future *ASTRO-H*) is now offering the first opportunity to provide simultaneous data on the hard X-rays/soft X-rays turn over (at few tens of keV). *ATHENA* (the second large mission that will be developed by ESA, with launch in 2028) is the most important X-ray mission on the horizon and will have an unprecedented capability for compact objects and collapsar physics. A large area X-ray timing mission, such as the Large Observatory for X-ray Timing (*LOFT*, studied as a candidate for an ESA M3 mission), would also enable a large increase in capability to detect seismic vibrations in magnetar bursts and resolve both any mode splitting and their evolution on short timescales, two things that would both help to distinguish theoretical models. This may open the possibility

of performing, systematically, asteroseismology studies in neutron stars. The role of gravitational wave observatories in pinning down the mechanism behind short gamma-ray bursts, and the possible role of millisecond magnetars in that process, has already been described above. In fact, magnetars are wonderful candidates for detection by ground-based, long-baseline, interferometric gravitational wave detectors such as LIGO and Virgo. Magnetars are also powerful probes of the Galactic structure and the interstellar medium: pulsar timing arrays are also starting to be used to hunt background stochastic gravitational waves.

Magnetar radiation is expected to be strongly polarized, and the polarization observables may also probe the so-called “vacuum polarization” effect, which is predicted by nonlinear QED, but has not yet been verified experimentally. Future X-ray polarimetry experiments, currently under consideration for several small and medium missions (e.g. *IXPE*, a NASA SMEX candidate, and *XIPE*, an ESA M4 candidate) may therefore open a completely new window on our understanding of the radiation processes around magnetars and on the physics of matter and radiation in superstrong fields.

Acknowledgments

This work benefitted from discussions with a number of colleagues. In particular, we would like to thank Paolo Esposito, Sandro Mereghetti, Yuri Lyubarsky, Sergei Popov, Luigi Stella for a careful reading of the manuscript and for their useful comments. ALW would also to thank Thijs van Putten, Chris Elenbaas, and Daniela Huppenkothen for comments on an early draft of Sec. 5. The work of RT is partially supported by INAF through a PRIN grant. ALW acknowledges support for her work on magnetars from an NWO Vidi Grant, and from the Nederlandse Onderzoekschool voor Astronomie NOVA’s Network 3 programme.

References

- Abadie J. et al., 2011, ApJL, 734, L35
- Abbott B. et al., 2007, Phys Rev. D, 76, 062003
- Abbott B. et al., 2008, Phys. Rev. Lett., 101, 211102
- Abbott B. et al., 2009, ApJL, 701, L68
- Albano A., Turolla R., Israel G.L., Zane S., Nobili L., Stella L. 2010, ApJ, 722, 788
- Aguilera, D.N., Pons, J.A., & Miralles, J.A. 2008, A&A, 486, 255
- Aguilera, D.N., Cirigliano, V., Pons, J.A., Reddy, S., Sharma, R. 2009, PRL, 102, 091101
- Akgün, T., Reisenegger, A., Mastrano, A., Marchant, P. 2013, MNRAS, 433, 2445
- An, H., Hascoët, R., Kaspi, V.M., et al., 2013, ApJ, 779, 163
- An H. et al. 2014a, ApJ, 790, 60

- An H. et al. 2014b, AN, 335, 280
- Anderson, G., Gaensler, B.M., Slane, P.O. et al. 2012, ApJ, 751, 53
- Andersson, N., Glampedakis, K., & Samuelsson, L. 2009, MNRAS, 396, 894
- Aptekar R.L. et al. 2001, ApJS, 137, 227
- Aptekar R.L. et al. 2009, ApJL, 698, L82
- Asai H., Lee U., 2014, MNRAS, 790, 66
- Aschwanden M.J. et al. 2014, Space Science Reviews, arXiv:1403.6528
- Atteia J.-L. et al. 1987, ApJ, 320, L105
- Barat C. et al. 1979, A&A, 79, L24
- Barat C., Hayles R.I., Hurley K., et al. 1983, A&A, 126, 400
- Baring M.G., 1995, ApJL, 440, L69
- Baring, M.G., Harding, A.K., 2005, ApJ, 630, 430
- Baring, M.G., Harding, A.K., 2008, AIPC, 968, 93
- Beloborodov A.M. and Thompson, C. 2007, ApJ, 657, 967
- Beloborodov A.M. 2009, ApJ, 703, 1044
- Beloborodov A.M. 2011, High-Energy Emission from Pulsars and their Systems, Astrophysics and Space Science Proceedings. Springer-Verlag Berlin Heidelberg, p. 299
- Beloborodov A.M., 2013a, ApJ, 777, 114
- Beloborodov A.M., 2013b, ApJ, 762, 13
- Beloborodov A.M., Levin Y., 2014, ApJL, 794, L24
- Bernardini, F., Israel, G.L., Dall’Osso, S., Stella, L. et al. 2009, A&A, 498, 197-207
- Bernardini, F., Perna, R., Gotthelf, E.V., Israel, G.L., Rea, N., Stella, L. 2011a, MNRAS, 418, 638
- Bernardini, M.G., Margutti, R., Chincarini, G., Guidorzi, C., Mao, J. 2011b, A&A, 526, A27
- Bernardini, M.G., Margutti, R., Mao, J., Zaninoni, E., Chincarini, G. 2012, A&A, 539, A3
- Bibby, J.L., Crowther, P.A., Furness, J.P., Clark, J.S. 2008, MNRAS, 386, L23
- Boggs, S. E. et al. 2007, ApJ, 661, 458
- Bogomazov, A.I., & Popov, S.B. 2009, MNRAS, 53, 325–333
- Braithwaite, J. and Nordlund, Å. 2006, A&A, 450, 1077
- Braithwaite, J. and Spruit, H. C. 2006, A&A, 450, 1097
- Braithwaite, J. 2008, MNRAS, 386, 1947
- Braithwaite, J. 2009, MNRAS, 397, 763
- Bucciantini, N., Quataert, E., Arons, J., Metzger, B.D., Thompson, T.A. 2007, MNRAS, 380, 1541

- Bucciantini, N., Pili A.G., Del Zanna L. 2015, MNRAS, 447, 3278–3290
- Burgay, M., Rea, N., Israel, G.L. et al. 2006, MNRAS, 372, 410
- Burgay, M., Israel, G.L., Possenti, A. et al. 2009, ATel, 1913
- Burke-Spolaor, S. 2012, in Neutron Stars and Pulsars: Challenges and Opportunities after 80 years, Proceedings IAU Symposium No. 291, 2012, J. van Leeuwen, ed.
- Burrows, A., Dessart, L., Livne, E., Ott, C.D., Murphy, J. 2007, ApJ, 664, 416-434
- Camero, A., Papitto, A., Rea, N. et al. 2014, MNRAS, 438, 3291
- Cameron, P.B., Chandra, P., Ray, A. et al. 2005, Nature, 434, 1112
- Camilo, F., Ransom, S.M., Halpern, J.P. et al. 2006, Nature, 442, 892
- Camilo, F., Cognard, I., Ransom, S.M., et al. 2007a, ApJ, 663, 497
- Camilo, F., Ransom, S.M., Halpern, J.P., Reynolds, J. 2007b, ApJ, 666, L93
- Camilo, F., Halpern, J.P., Ransom, S.M. 2009, ATel, 1907
- Campana S., Rea N., Israel G. L., Turolla R., Zane S. 2007, A&A, 463, 1047
- Carlqvist, P. 1982, Ap&SS, 87, 21
- Cheng B., Epstein R.I., Guyer R.A., Young A.C. 1996, Nature, 382, 518
- Ciolfi, R., Lander, S.K., Manca, G.M., Rezzolla, L. 2011, ApJ, 736, L6
- Ciolfi R., Rezzolla L., 2012, ApJ, 760, 1
- Ciolfi R., Rezzolla L., 2013, MNRAS, 435, L43
- Ciolfi, R. 2014, AN, 335, 624?629
- Clark, J.S., Negueruela, I., Crowther, P.A., Goodwin, S.P. 2005, A&A, 434, 949
- Clark, J.S., Muno, M.P., Negueruela, I. et al. 2008, A&A, 347, 147
- Clark, J.S., Ritchie, B.W., Najarro, F., Langer, N., Negueruela, I. 2014, A&A, 565, A90
- Cline T.L. et al. 1980, ApJL, 237, L1
- Colaiuda, A., & Kokkotas, K. D. 2011, MNRAS, 414, 3014
- Colaiuda, A., & Kokkotas, K. D. 2012, MNRAS, 423, 811
- Corbel S., Chapuis C., Dame T.M., Durouchoux P. 1999, ApJ, 526, L29
- Crawford, F., Hessels, J.W.T., Kaspi, V.M. 2007, ApJ, 662, 1183
- Crowther, P.A., Bibby, J.L., Furness, J.P., Simon, C.J. 2011, Advances in Space Research, 47, 1341-1345
- Curran, P.A., Starling, R.L.C., O'Brien, P.T., Godet, O., Van Der Horst, A.J., Wijers, R.A.M.J. 2008, A&A, 487, 533
- Dall'Osso, S., Shore, S.N., Stella, L. 2009, MNRAS, 398, 1869
- Dall'Osso, S., Stratta, G., Guetta, D., et al. 2011, A&A, 526, 121
- Dall'Osso, S., Granot, J., Piran, T. 2012, MNRAS, 422, 2878
- D'Angelo C.R., Watts A.L., 2012, ApJL, 751, L41
- Davies, B., Figer, D.F., Kudritzki, R.-P. et al. 2009, ApJ, 707, 844

- De Luca, A. 2008, in 40 Years of Pulsars, C.G. Bassa et al. eds., AIP Conf. Proc., 983, 311
- den Hartog, P.R., Hermsen, W., Kuiper, L., et al., 2006, A&A, 451, 587
- den Hartog, P.R., Kuiper, L., Hermsen, W., 2008a, A&A, 489, 263
- den Hartog, P.R., Kuiper, L., Hermsen, W., et al., 2008b, A&A, 489, 245
- Dhillon, V.S., et al. 2009, MNRAS, 394, L112
- Dhillon, V.S., et al. 2011, MNRAS, 416, L16
- Dib R., Kaspi V.M., Gavriil F.P., 2008, ApJ, 673, 1044
- Dib R., Kaspi V.M., Gavriil F.P. 2009, ApJ, 702, 614
- Dib, R., Kaspi, V.M., Scholz, P., Gavriil, F.P. 2012, ApJ, 748, 13
- Dib R., Kaspi V.M., 2014, ApJ, 784, 37
- Douchin, F., & Haensel, P. 2001, A&A, 380, 151
- Duncan R. C. 1998, ApJL, 498, L45
- Duncan, R.C. & Thompson, C. 1992, ApJ, 392, L9
- Durant, M. & van Kerkwijk, M.H. 2005, ApJ, 627, 376
- Durant, M. & van Kerkwijk, M.H. 2006, ApJ, 650, 1082
- Durant, M., Kargaltsev, O., Pavlov, G.G. 2011, 742, 77
- Eatough R.P., Falcke H., Karuppusamy R., et al. 2013, Nature, 501, 391
- Eichler, D., Gedalin, M., & Lyubarsky, Yu. 2002, ApJ, 578, L121
- Eikenberry S.S., Garske M.A., Hu D., Jackson M.A., Patel S.G., Barry D.J., Colonna M.R., Houck J.R. 2001, ApJ 563, L133
- Enoto T. et al. 2011, PASJ, 63, 387
- Esposito P. et al. 2007a, A&A, 461, 605
- Esposito, P. et al. 2007b, A&A, 476, 321
- Esposito P. et al. 2008, MNRAS, 390, L34
- Esposito, P., Israel, G.L., Turolla, R. et al. 2010, MNRAS, 405, 1787
- Esposito P. et al. 2011, MNRAS, 416, 205
- Esposito P. et al. 2013, MNRAS, 429, 3123
- Fan, Y.-Z., Xu, D., 2006, MNRAS, 372, L19
- Fatkhullin, T., et al. 2008, GCN 8160
- Fender R.P. et al. 2006, MNRAS, 367, L6
- Fenimore E.E., Evans W.D., Klebesadel R.W., Laros J.G., Terrell J., 1981, Nature, 289, 442
- Fenimore E.E., Laros J.G., Ulmer A. 1994, ApJ, 432, 742
- Fenimore E.E., Klebesadel R.W., Laros J.G. 1996, ApJ, 460, 964
- Fernández R., Thompson C. 2007, ApJ, 660, 615

- Fernández R., Davis S.W. 2011, *ApJ*, 730, 131
- Feroci M. et al. 1999, *ApJ*, 515, L9
- Feroci M., Hurley K., Duncan R.C., Thompson C., 2001, *ApJ*, 549, 1021
- Feroci M. et al. 2003, *ApJ*, 596, 470
- Feroci M., Caliendo G.A., Massaro E., Mereghetti S., Woods P.M. 2004, *ApJ*, 612, 408
- Feroci M. et al., 2014, *Proc. SPIE*, 91442T
- Ferrario, L. & Wickramasinghe, D. 2006, *MNRAS*, 367, 1323
- Ferrario, L. & Wickramasinghe, D. 2008, *MNRAS*, 389, L66
- Figer D.F., Najarro F., Geballe T.R., Blum R.D., Kudritzki R.P. 2005, *ApJ*, 622, L49
- Flowers E., Ruderman M.A., 1977, *ApJ*, 215, 302
- Frail D.A., Kulkarni S.R., Bloom J.S. 1999, *Nature*, 398, 127
- Frederiks D.D. et al. 2007, *Astronomy Letters* 33, 1
- Gabler, M., Cerdá Durán, P., Font, J. A., Müller, E., & Stergioulas, N. 2011, *MNRAS*, 410, L37
- Gabler, M., Cerdá-Durán, P., Stergioulas, N., Font, J. A., & Müller, E. 2012, *MNRAS*, 421, 2054
- Gabler, M., Cerdá-Durán, P., Font, J. A., Müller, E., & Stergioulas, N. 2013, *MNRAS*, 430, 1811
- Gabler M., Cerdá-Durán P., Stergioulas N., Font J.A., Müller E., *Phys Rev Lett*, 111, 211102
- Gabler M., Cerdá-Durán P., Stergioulas N., Font J.A., Müller E. 2014, *MNRAS*, 443, 1416
- Gaensler, B.M., McClure-Griffiths, N.M., Oey, M.S., et al. 2005, *ApJ*, 620, L95
- Gaensler, B.M., Kouveliotou, C., Gelfand, J.D. et al. 2005, *Nature*, 434, 1104
- Gavriil F.P., Kaspi V.M., Woods P.M. 2002, *Nature*, 419, 142
- Gavriil F.P., Kaspi V.M., Woods P.M., 2004, *ApJ*, 607, 959
- Gavriil F.P., Kaspi V.M., Woods P.M., 2006, *ApJ*, 641, 418
- Gavriil F.P. et al. 2008, *Science*, 319, 1802
- Gavriil F.P., Dib R., Kaspi V.M. 2011, *ApJ*, 736, 138
- Gelfand J.D. et al. 2005, *ApJ*, 634, L89
- Gelfand J.D., Gaensler, B.M. 2007, *ApJ*, 667, 1111
- Geppert, U., Küker, M., & Page, D. 2004, *A&A*, 426, 267
- Geppert, U., Küker, M., & Page, D. 2006, *A&A*, 457, 937
- Giacomazzo B. & Perna R. 2013, *ApJ*, 771, L26
- Gill R., Heyl J., 2010, *MNRAS*, 407, 1926
- Glampedakis, K., Samuelsson, L., & Andersson, N. 2006, *MNRAS*, 371, L74

- Glampedakis, K., Jones, D.I., & Samuelsson, L. 2011, MNRAS, 413, 2021
- Glampedakis, K., & Jones, D. I. 2014, MNRAS, 439, 1522
- Glampedakis, K., Lander S.K., Andersson N. 2014, MNRAS, 447, 2–8
- Goldreich, P., & Reisenegger, A., 1992, ApJ, 395, 250
- Gögüş E. et al. 1999, ApJ, 526, L93
- Gögüş E. et al. 2000, ApJ, 532, L121
- Gögüş E. et al. 2001, ApJ, 558, 228
- Gögüş E. et al. 2010, ApJ, 718, 331
- Gögüş E. et al. 2010b, ApJ, 722, 899
- Gögüş E. et al. 2011a, ApJ, 728, 160
- Gögüş E. et al. 2011b, ApJ, 740, 55
- Götz D., Mereghetti S., Tiengo A., Esposito P. 2006, A&A, 449, L31
- Golenetskii S.V., Mazets E.P., Ilinskii V.N., Guryan Y.A. 1979, Soviet Astronomy Letters, 5, 340
- Golenetskii S.V., Ilinskii V.N., Mazets E.P., 1984, Nature, 307, 41
- Golenetskii, S. V., Aptekar, R. L., Guryan, Y. A., Ilinskii, V. N., & Mazets, E. P. 1987, Soviet Astronomy Letters, 13, 166
- Gonzalez M.E. et al. 2010, ApJ, 716, 1345
- Götz D., Mereghetti S., Mirabel I.F., Hurley K. 2004, A&A, 417, L45
- Granot J. et al. 2006, ApJ, 638, 391
- Guidorzi, C., Frontera, F., Montanari, E., Feroci, M., Amati, L., Costa, E., & Orlandini, M. 2004, A&A, 416, 297
- Gullón, M., Miralles, J.A., Viganò, D., Pons, J.A. 2014, MNRAS, 443, 1891
- Güver T., Özel F., Gögüş E., Kouveliotou, C. 2007, ApJ, 667, L73
- Gotthelf, E.V., Halpern, J.P. & Alford, J. 2013 ApJ 765, 16
- Güver T., Özel F., Gögüş E. 2008, ApJ, 675, 1499
- Güver T., Gögüş E., Özel F. 2011, MNRAS, 418, 2773
- Halpern, J.P. & Gotthelf, E.V. 2005, ApJ, 618, 874-882
- Halpern, J.P. & Gotthelf, E.V. 2010, ApJ, 725, 1384-1391
- Halpern, J.P. & Gotthelf, E.V. 2011, ApJ, 733, L28-L31
- Harding, A.K. 2013, Front. Phys., 8(6), 679
- Harding A.K., Lai D. 2006, Rep. Prog. Phys. 69, 2631
- Hascoët, R., Beloborodov, A.M., den Hartog, P.R., 2014, ApJL, 786, L1
- Heyl J.S., Hernquist L., 2005, ApJ, 618, 463
- Heyl J.S., Shaviv N.J. 2000, MNRAS, 311, 555
- Heyl J.S., Shaviv N.J. 2002, Phys. Rev. D, 66, 023

- Ho, W.C.G. 2012, in Neutron Stars and Pulsars: Challenges and Opportunities after 80 years, Proceedings IAU Symposium No. 291, 2012, J. van Leeuwen, ed.
- Ho W.C.G. 2013, MNRAS, 429, 113
- Hoffman K., Heyl J. 2012, MNRAS, 426, 2404–2412
- Horowitz C.J., Kadau K., 2009, Phys. Rev. Lett., 102, 191102
- Hoshino J., Lyubarsky Y., 2012, Space Science Reviews, 173, 521
- Huang L., Yu, C. 2014, ApJ, 784, 168
- Huang L., Yu C., 2014, ApJ, 796, 3
- Hulleman, F., van Kerkwijk, M.H., Kulkarni, S.R. 2000, Nature, 408, 689
- Hulleman F., van Kerkwijk M.H., Kulkarni S.R. 2004, A&A, 416, 1037
- Huppenkothen, D., Watts, A. L., Uttley, P., et al. 2013, ApJ, 768, 87
- Huppenkothen, D., D’Angelo C., Watts A.L., Heil L., van der Klis M., van der Horst A., Kouveliotou C., Baring M., Göğüş E., Granot J., Kaneko Y., Lin L., van Kienlin A., Younes G. 2014, ApJ, 787, 128
- Huppenkothen D., Watts A.L., Levin Y., 2014, ApJ, 793, 129
- Huppenkothen D., Heil, L.M., Watts A.L., Göğüş E., 2014, ApJ, 795, 114
- Hurley K. et al. 1999a, ApJ, 510, L107
- Hurley, K. et al. 1999b, Nature, 397, 41
- Hurley K., Li P., Kouveliotou C., Murakami T., Ando M., Strohmayer T., van Paradijs J., Vrba F., Luginbuhl C., Yoshida A., Smith I. 1999, ApJ, 510, L111
- Hurley K., et al. 2005, Nature, 434, 1098-1103
- Hurley, K. 2011a, AdSpR, 47, 1337
- Hurley, K. 2011b, AdSpR, 47, 1326
- Ibrahim A.I. et al. 2001, ApJ, 558, 237
- Ibrahim A.I. et al. 2002, ApJ, 574, L51
- Ibrahim, A.I., Markwardt, C.B., Swank, J.H. et al. 2004, ApJ 609, L21
- Igoshev, A.P., Popov, S.B., Turolla, R. 2014, AN, 335, 262
- Inan U.S. et al. 1999, Geophysical Research Letters, 26, 3357
- Inan U.S. et al. 2007, Geophysical Research Letters, 34, L08103
- Israel, G.L. et al. 2002, ApJ, 580, L143
- Israel, G.L., et al. 2004, proceedings of the IAU Symposium no. 218. Edited by Fernando Camilo and Bryan M. Gaensler. San Francisco, CA: Astronomical Society of the Pacific, p.247
- Israel, G. L., Belloni, T., Stella, L., et al. 2005, ApJL, 628, L53
- Israel, G.L., et al. 2005a, Proceedings of the Frontier Objects in Astrophysics and Particle Physics, Vulcano Workshop 2008, F. Giovannelli and G. Mannocchi eds., p.349

- Israel, G.L., et al. 2005b, *A&A*, 438, L1
- Israel, G.L., Campana, S., Dall’Osso, S., Munro, M.P., Cummings, J., Perna, R., Stella, L., 2007, *ApJ*, 664, 448
- Israel G.L. et al. 2008, *ApJ*, 685, 1114
- Israel, G.L., Esposito, P., Rea, N. et al. 2010, *MNRAS*, 408, 1387
- Israel, G.L., Rea, N. 2014, XXXX submitted
- Jones P.B., 2003, *ApJ*, 595, 342
- Kaminker A.D., Yakovlev D.G., Potekhin A.Y., Shibazaki N., Sthernin P.S., Gnedin O.Y. 2006, *MNRAS*, 371, 477
- Kaminker A.D., Yakovlev D.G., Potekhin A.Y., Shibazaki N., Sthernin P.S., Gnedin O.Y. 2007, *Ap&SS*, 308, 423
- Kaminker A.D., Potekhin A.Y., Yakovlev D.G., Chabrier, G. 2009, *MNRAS*, 395, 2257
- Kaneko Y. et al. 2010, *ApJ*, 710, 1335
- Kargaltsev O. et al. 2012, *ApJ*, 748, 26
- Kaspi, V.M., Lackey J.R., Chakrabarty D. 2000, *ApJ*, 537, L31
- Kaspi V.M. et al. 2003, *ApJ*, 588, L93
- Kaspi V.M., Gavriil F.P., Woods P.M., Jensen J.B., Roberts M.S.E., Chakrabarty D. 2003, *ApJ*, 588, L93
- Kaspi V.M. 2006, In: Compact stellar X-ray sources. Edited by Walter Lewin & Michiel van der Klis. Cambridge Astrophysics Series, No. 39. Cambridge, UK: Cambridge University Press, 2006, p. 279–339
- Kaspi V.M. 2007, *Ap&SS*, 308, 1
- Kaspi, V.M. 2010, *PNAS*, 107, 7147-7152
- Kaspi, V.M., & Boydstun, K. 2010, *ApJ*, 710, L115
- Kaspi, V.M. Archibald, R.F., Bhallerao, V. et al. 2014, *ApJ*, 786, 84
- Keane, E.F. & Kramer, M. 2008, *MNRAS*, 391, 2009
- Keane, E.F., Kramer, M., Lyne, A.G., Stappers, B.W., McLaughlin, M.A. 2011, *MNRAS*, 415, 3065
- Kennea J.A. et al. 2013, *ApJL*, 770, L24
- Kern, B., & Martin, C. 2002, *Nature*, 417, 527
- Kiuchi K., Yoshida S., Shibata M., 2011, *A&A*, 532, 30
- Kliem B., Karlický M., Benz A.O. 2000, *A&A*, 360, 715
- Klose S., Henden A.A., Geppert U., Greiner J., Guetter H.H., Hartmann D.H., Kouveliotou C., Luginbuhl C.B. 2004, *ApJ*, 609, L13
- Komissarov S.S., 2002, *MNRAS*, 336, 759
- Komissarov S.S., Barkov M., Lyutikov M., 2007, *MNRAS*, 374, 415
- Kouveliotou C. et al. 1987, *ApJ*, 322, L21

- Kouveliotou C. et al. 1993, *Nature*, 362, 728
- Kouveliotou C. et al. 1994, *Nature*, 368, 125
- Kouveliotou, C. et al. 2001, *ApJL*, 558, L47
- Kouveliotou C. et al. 2003, *ApJ*, 596, L79
- Kuiper, L., Hermsen, W., Mendez, M. 2004, *ApJ*, 613, 1173
- Kuiper, L., Hermsen, W., den Hartog, P.R., Collmar, W. 2006, *ApJ*, 645, 556
- Kulkarni, S.R., Kaplan, D.L., Marshall, H.L., Frail, D.A., Murakami, T., Yonetoku, D. 2003, *ApJ*, 585, 948-954
- Kumar H.S., Ibrahim A.I., Safi-Harb S. 2010, *ApJ*, 716, 97
- Lander, S. K., & Jones, D. I. 2011b, *MNRAS*, 412, 1730
- Lander, S. K., & Jones, D. I. 2011a, *MNRAS*, 412, 1934
- Lander, S. K., Jones, D. I., & Passamonti, A. 2010, *MNRAS*, 405, 318
- Lander, S.K., 2013, *MNRAS*, 437, 424
- Lander S.K., Andersson N., Antonopoulou D., Watts A.L. 2015, *MNRAS*, 449, 2047
- Laros J.G. et al. 1987, *ApJ*, 320, L111
- Lattimer, J. M., & Prakash, M. 2007, *Physics Reports*, 442, 109
- Lazaridis, K., Jessner, A., Kramer, M., et al. 2008, *MNRAS*, 390, 839
- Lazarus, P., Kaspi, V.M., Champion, D.J., Hessels, J.W.T., Dib, R. 2011, *ApJ*, 744, 97
- Lazzati, D., Ghirlanda, G., Ghisellini, G. 2005, *MNRAS*, 362, L8-L12
- Lee U., 2008, *MNRAS*, 385, 2069
- Lenters G.T. et al., 2003, *ApJ*, 587, 761
- Levin, L., Bailes, M., Bates, S. et al. 2010, *ApJ*, 721, L33
- Levin Y., 2006, *MNRAS*, 368, L35
- Levin Y., 2007, *MNRAS*, 377, 159
- Levin Y., Lyutikov M., 2012, *MNRAS*, 427, 1574
- Liang E.P.T. 1981, *Nature*, 292, 319
- Lin L. et al., 2011a, *ApJ*, 739, 87
- Lin L. et al, 2011b, *ApJ*, 749, 15
- Lin L. et al., 2012, *ApJ*, 756, 54
- Lin L. et al. 2012, *ApJ*, 761, 132
- Lin L. et al. 2013, *ApJ*, 778, 105
- Link B., 2014, *MNRAS*, 441, 2676
- Livingstone M.A., Kaspi V.M., Gavriil F.P. 2010, 710, 1710
- Livingstone M.A. et al. 2011a, *ApJ*, 730, 66
- Livingstone, M.A., Scholz, P., Kaspi, V.M., Ng, C.-Y., Gavriil, F.P. 2011, *ApJL*, 743, L38

- Lyons, N., O'Brien, P.T., Zhang, B., Willingale, R., Troja, E., Starling, R.L.C. 2010, MNRAS, 402, 705
- Lyubarsky, Y. E. 2002, MNRAS, 332, 199 s
- Lyubarsky Y., Eichler D., Thompson C. 2002, ApJ, 580, L69
- Lyubarsky Y., 2014, MNRAS, 442, L9
- Lyutikov M., 2002, ApJ, 580, L65
- Lyutikov M., 2003, MNRAS, 346, 540 (L03)
- Lyutikov M., 2006, MNRAS, 367, 1594
- Lyutikov M., 2014, arXiv:1407.5881
- Lyutikov, M. & Gavriil, F.P. 2006, MNRAS, 368, 690
- MacFadyen A.I. & Woosley S.E. 1999, ApJ, 524, 262
- Makishima, K. et al. 2014, PRL, 112, 171102
- Makishima, K. et al. 2015, PASJ, submitted
- Mandea, M., & Balasis, G. 2006, GeoJI, 167, 586–591
- Margutti, R., Guidorzi, C., Chincarini, G., Bernardini, M.G., Genet, F., Mao, J., Pasotti, F. 2010, MNRAS, 406, 2149
- Marsden D., & White N.E. 2001, ApJ, 551, L155
- Markey P., Tayler R.J., 1973, MNRAS, 163, 77
- Masada Y., Nagataki S., Shibata K., Terasawa T. 2010, PASJ, 62, 1093
- Matsumoto J., Masada Y., Asano E., Shibata K. 2011, ApJ, 733, 18
- Mazets E.P., Golenetskij S.V., Guryan Y.A. 1979a, Sov. Astron. Lett. 5, 343
- Mazets E.P., Golenetskij S.V., Ilinskii V.N., Aptekar R.L., Guryan I.A. 1979b, Nature, 282, 587
- Mazets E.P., Golenetskii S.V., 1981, ApSS, 75, 47
- Mazets E.P. et al. 1999a, ApJ, 519, L151
- Mazets E.P. et al. 1999b, AstL, 25, 628
- Mazets E.P. et al. 1999c, AstL, 25, 635
- McLaughlin, M.A., Rea, N., Gaensler, B.M. et al. 2007 ApJ, 670, 1307
- Medin Z., Lai D. 2007, MNRAS, 382, 1833
- Meng Y. et al., 2014, ApJ, 785, 62
- Mereghetti S., Stella, L. 1995, ApJ, 442, L17
- Mereghetti S., Götz D., Mirabel I.F., Hurley K. 2005a, A&A, 433, L9
- Mereghetti S., et al. 2005b, ApJ, 628, 938
- Mereghetti S. et al. 2005, ApJ, 624, L105
- Mereghetti S., 2008, A&ARv, 15, 225
- Mereghetti S. et al. 2009, ApJL, 696, L74

- Mereghetti S., 2011, *AdSR*, 47, 1317
- Mereghetti S., Pons J.A., Melatos, A. 2014, submitted
- Metzger B.D., Quataert E. & Thompson T.A. 2008, *MNRAS*, 385, 1455
- Metzger B.D., Giannios D., Thompson T.A., Bucciantini N., Quataert E. 2011, *MNRAS*, 413, 2031
- Miller, M. C. 1995, *ApJ*, 448, L29
- Mignani, R.P., et al. 2007, 471, 265
- Mignani, R.P., Vande Putte, D., Cropper, M. et al. 2013, *MNRAS*, 429, 3517
- Molkov, S., Hurley, K., Sunyaev, R., Shtykovsky, P., Revnivtsev, M., Kouveliotou, C. 2005, *A&A*, 433, L13–L16
- Muno, M.P., Clark, J.S., Crowther, P.A. et al. 2006, *ApJ*, 636, L41
- Muno M.P. et al. 2007, *MNRAS*, 378, L44
- Murphy D. et al., 2013, *Phys. Rev. D*. 87, 103008
- Nakagawa Y.E. et al., 2007, *PASJ*, 59, 653
- Nakano, T., Murakami, H., Makishima, K., et al. 2015, *PASJ*, 67, 9
- Ng C.-Y. et al. 2011, *ApJ*, 729, 131
- Nobili, L., Turolla, R., Zane, S. 2008a, *MNRAS*, 386, 1527
- Nobili, L., Turolla, R., Zane, S. 2008b, *MNRAS*, 389, 989
- Nobili, L., Turolla, R., Zane, S. 2011, *AdSR*, 47, 1305
- Nousek, J.A., et al. 2006, *ApJ*, 642, 389
- Olausen, S.A. & Kaspi, V.M. 2014, *ApJS*, 212, 60
- Olive J.-F. et al. 2004, *ApJ*, 616, 1148
- Özel F. 2003, *ApJ*, 583, 402
- Özel F. 2013, *Rep. Prog. Phys.*, 76, Issue 1, id. 016901
- Paczynski, B. 1986, *ApJ*, 308, L43
- Paczynski B., 1992, *Acta Astronomica*, 42, 145
- Palmer D.M. 1999, *ApJL*, 512, L113
- Palmer D.M. 2002, *Memorie della Societa Astronomica Italiana*, 73, 578
- Palmer D.M., Barthelmy S., Gehrels N., et al.. 2005, *Nature*, 434, 1107
- Parfrey K., Beloborodov A.M., Hui L., 2012, *ApJL*, 754, L12
- Parfrey K., Beloborodov A.M., Hui L., 2013, *ApJ*, 774, 92
- Passamonti A., Lander, S., 2013, *MNRAS*, 429, 767
- Passamonti A., Lander, S., 2014, *MNRAS*, 438, 156
- Patel, S.K., Kouveliotou, C., Woods, P.M., et al. 2001, *ApJ*, 563, L45–L48
- Pavan, L., Turolla, R., Zane, S., Nobili, L. 2009, *MNRAS*, 395, 753
- Perna, R., Hernquist, H., & Narayan, R. 2000, *ApJ*, 541, 344

- Perna, R., Gotthelf, E.V. 2008, ApJ, 681, 522
- Perna, R., Pons, J.A. 2011, ApJL, 727, L51
- Piro, A. L. 2005, ApJL, 634, L153
- Perna, R., Viganò, D., Pons, J. A., Rea, N., 2013, MNRAS, 424, 2362
- Pili, A.G., Bucciantini, N., Del Zanna L. 2015, MNRAS, 447, 2821–2835
- Pons, J.A., & Geppert, U. 2007, A&A, 470, 303
- Pons, J.A., Miralles, J.A., Geppert, U. 2009, A&A, 496, 207
- Pons J.A., Perna R., 2011, ApJ, 741, 123
- Pons, J.A., Rea, N. 2012, ApJL, 750, L6
- Popov, S.B., Turolla, R., Possenti, A. 2006 MNRAS, 369, L23
- Popov, S.B., Stern, B.E. 2006, MNRAS, 365, 885-890
- Popov, S.B., Prokhorov, M.E. 2006, MNRAS, 367, 732–736
- Popov S.B., Postnov K.A., 2007, arXiv:0710.2006
- Popov, S.B., Pons, J.A., Miralles, J.A., Boldin, P.A., Posselt, B. 2010, MNRAS, 401, 2675
- Popov S.B., Postnov K.A., 2013, arXiv:1307.4924
- Potekhin, A.Y. 2014, Physics-Uspekhi, ??? (arXiv:1403.0074)
- Posselt, B., Pavlov, G.G., Popov, S., Wachter, S. 2014, ApJ Suppl., 215, 3
- Prieskorn Z., Kaaret P., 2012, ApJ, 755, 1
- Rea N., et al. 2005, MNRAS, 361, 710
- Rea N., Zane S., Lyutikov M., Turolla R., 2007a, Ap&SS, 308, 61
- Rea N., Turolla R., Zane S., Tramacere A., Stella L., Israel G.L., Campana R. 2007b, ApJ 661, L65
- Rea, N., Nichelli, E., Israel, G.L., et al. 2007, MNRAS, 381, 293-300
- Rea N., Zane S., Turolla R., Lyutikov M., Götz D. 2008, ApJ, 686, 1245
- Rea N. et al. 2010, Science, 330, 6006
- Rea N., Esposito P., 2011, *Magnetar outbursts: an observational review*, in High energy emission from pulsars and their systems, Proc. Astrophys. Space Science, Springer-Verlag Berlin Heidelberg, p.247
- Rea, N, Esposito, P., Turolla, R. et al. 2009, MNRAS, 396, 2419
- Rea, N, Esposito, P., Turolla, R. et al. 2010, Science, 330, 944
- Rea, N., Esposito, P. 2011, in High-Energy Emission from Pulsars and their Systems, Astrophysics and Space Science Proceedings. Springer-Verlag Berlin, Heidelberg, p. 247
- Rea, N., Israel, G.L., Esposito, P. et al. 2012a, ApJ, 754, 27
- Rea, N., Pons, J.A., Torres, D, Turolla, R. 2012b, ApJL, 748, L12
- Rea, N., Israel, G.L., Pons, J.A. et al. 2013, ApJ, 770, 65

- Rea, N., Esposito, P., Pons, J.A., et al. 2013, *ApJL*, 775, 34
- Rea, N., Viganò, D., Israel, G.L., Pons, J.A., Torres, D.F. 2014a, *ApJL*, 781, L17
- Rea, N. 2014, *Proceedings of the IAU*, Vol. 302, p. 429
- Rea, N. 2014, *AN*, Vol. 335, p. 329–333
- Reisenegger, A. and Goldreich, P. 1992, *ApJ*, 395, 240
- Rodríguez Castillo, G.A., Israel, G.L., Esposito, P. et al. 2014, *MNRAS*, 441, 1305
- Rosswog S., Ramirez-Ruiz E., Davies M.B. 2003, *MNRAS*, 345, 1077
- Rowlinson, A., O’Brien, P.T., Metzger, B.D., Tanvir, N.R., Levan, A.J. 2013, *MNRAS*, 430, 1061-1087
- Ruiz, M., Paschalidis V. & Shapiro S.L. 2014, *Phys. Rev. D*, 89, id. 084045
- Samuelsson, L., & Andersson, N. 2007, *MNRAS*, 374, 256
- Sasmaz Mus, S., Göğüş, E., 2010, *ApJ*, 723, 100
- Savchenko V., Neronov A., Beckmann V., Produit N., Walter R. 2010, *A&A*, 510, 77
- Scholz P., Kaspi V.M., 2011, *ApJ*, 739, 94
- Scholz P. et al. 2012, *ApJ*, 761, 66
- Scholz P., Kaspi V.M., Cumming A. 2014, *ApJ*, 786, 62
- Schwartz S.J. et al. 2005, *ApJ*, 627, L129
- Serylak, M., Stappers, B.W., Weltevrede, P. et al. 2009, *MNRAS*, 394, 295
- Shannon, R.M. and Johnston, S. 2013, *MNRAS*, 435, L29
- Sotani, H., Kokkotas, K. D., & Stergioulas, N. 2007, *MNRAS*, 375, 261
- Sotani, H., Kokkotas, K. D., & Stergioulas, N. 2008, *MNRAS*, 385, L5
- Spruit, H.C. 2008, in 40 years of pulsars:millisecond pulsars, magnetars and more, *AIP Conf. Proc.*, 983, 391
- Steiner, A. W., & Watts, A. L. 2009, *Physical Review Letters*, 103, 181101
- Stella, L., Dall’Osso, S., Israel, G.L., Vecchio, A. 2005, *ApJ*, 634, L165
- Strohmayer, T., van Horn, H. M., Ogata, S., Iyemori, H., & Ichimaru, S. 1991, *ApJ*, 375, 679
- Strohmayer, T. E., & Watts, A. L. 2005, *ApJL*, 632, L111
- Strohmayer, T. E., & Watts, A. L. 2006, *ApJ*, 653, 593
- Sturrock P.A., Harding A.K., Daugherty J.K., 1989, *ApJ*, 346, 950
- Svinkin, D.S., Hurley, K., Aptekar, R.L., Golenetskii, S.V., Frederiks, D.D. 2015, *MNRAS*, 447, 1028–1032
- Takiwaki, T., Kotake, K., Sato, K. 2009, *ApJ*, 691, 1360
- Tam, C.R., Kaspi, V.M., van Kerkwijk, M.H. & Durant, M. 2004, *ApJ*, 617, L53
- Tam, C.R., Gavriil, F.P., Dib, R., Kaspi, V.M., Woods, P.M., Bassa, C. 2008, *ApJ*, 677, 503-514

- Tanaka Y.T. et al. 2007, ApJL, 665, L55
- Tanaka Y.T. et al. 2008, Journal of Geophysical Research: Space Physics, 113, A07307
- Tanaka Y.T. et al. 2010, ApJL, 721, L24
- Tanvir, N.R., Chapman, R., Levan, A.J., Priddey, R.S. 2005, Nature, 438, 991-993
- Taverna, R., Muleri, F., Turolla, R., Soffitta, P., Fabiani, S., Nobili, L. 2014, MNRAS, 438, 1686
- Tayler R.J., 1973, MNRAS, 161, 365
- Taylor G.B. et al. 2005, ApJ, 634, L93
- Terasawa T. et al. 2005, Nature, 434, 1110
- Terasawa T., Tanaka Y.T., Yoshikawa I., Kawai N., 2006, JPhCS, 31, 76
- Terrell J., Evans W.D., Klebasadel R.W., Laros J.G. 1980, Nature, 285, 383
- Testa V. et al. 2008, A&A, 482, 607
- Thompson, C. & Duncan, R.C. 1993, ApJ, 408, 194
- Thompson, C. and Duncan, R. C. 1995, MNRAS, 397, 763
- Thompson, C., Duncan, R. C., Woods, P. M., Kouveliotou, C., Finger, M. H. and Van Paradjis, J. 2000, ApJ, 543, 340
- Thompson, C., & Duncan, R. C 2001, ApJ, 561, 980
- Thompson, C., Lyutikov, M. and Kulkarni, S. R. 2002, ApJ, 574, 332
- Thompson, C., Beloborodov, A., 2005, ApJ, 634, 565
- Thompson, C. 2008a, ApJ, 688, 499
- Thompson, C. 2008b, ApJ, 688, 1258
- Thompson, T.A., Chang, P., Quataert, E. 2004, ApJ, 611, 380
- Thornton D. et al. 2013, Science, 341, 53
- Tiengo, A., Esposito, P., Mereghetti, S., et al. . 2013, Nature, 500, 312
- Timokhin A.N., Eichler D., Lyubarsky Y. 2008, ApJ, 680, 1398
- Torii, K., Kinugasa, K., Katayama, K., Tsunemi, H., Yamauchi, S. 1998, ApJ, 503, 843
- Troja, E., et al. 2007, ApJ, 665, 599
- Turolla, R. 2009, ASSL, 357, 141
- Turolla, R., Zane, S., Pons, J.A., Esposito, P., Rea, N. 2011, ApJ, 740, 105
- Turolla, R., Esposito, P. 2013, IJMPD, 22, 1330024
- Ulmer, A. 1994, ApJ, 437, L111
- Uryu, K.,ourgoulhon, E., Markakis C.M., et al. 2014, Phys. Rev. D 90, 101501
- Usov, V.V. 1992, Nature, 357, 472
- Uzdensky D.A., 2011, Space Science Reviews, 160, 45
- Vasisht, G., Gotthelf, E.V., Torii, K., Gaensler, B.M. 2000, ApJ, 542, L49
- van der Horst A.J. et al. 2010, ApJL, 711, L1

- van der Horst A.J. et al. 2012, ApJ, 749, 122
- van Hoven, M., & Levin, Y. 2008, MNRAS, 391, 283
- van Hoven, M., & Levin, Y. 2011, MNRAS, 410, 1036
- van Hoven, M., & Levin, Y. 2012, MNRAS, 420, 3035
- van Putten T., Watts A.L., D'Angelo C.R., Baring M.G., Kouveliotou C. 2013, MNRAS, 434, 1398
- Vedrenne G. et al. 1979, Soviet Astronomy Letters, 5, 314
- Viganò, D., Pons, J. A., Miralles, J. A. 2011, A&A, 533, 125
- Viganò, D., Pons, J.A., Miralles, J.A. 2011b, Comp. Phys. Comm., 183, 2042
- Viganò, D., Parkins, N., Zane, S., Turolla, R., Pons, J. A., Miralles, J. A. 2012, J. Phys., Conf. Ser., 342, 012013
- Viganò, D., Rea, N., Pons, J. A., Perna, R., Aguilera, D.N., Miralles, J.A., 2013, MNRAS, 434, 123
- Viganò, D., Perna, R., Rea, N., Pons, J. A., 2014, MNRAS accepted
- Vink, J. & Kuiper, L. 2006, MNRAS, 370, L14
- Vink, J. 2008, AdSR, 41, 503
- Vogel, J.K. et al. 2014, ApJ, 789, 75
- von Kienlin A. et al. 2012, ApJ, 755, 150
- Vrba, F.J. et al. 2000, ApJ, 533, L17
- Wadiasingh, Z., Baring, M.G., Gonthier, P.L., 2013, HEAD meeting #13, #126.09
- Wang, Z., Chakrabarty, D., & Kaplan, D.L. 2006, Nature, 440, 772
- Watts, A. L., & Strohmayer, T. E. 2006, ApJL, 637, L117
- Watts A.L., Reddy S., 2007, MNRAS, 379, L63
- Watts A.L. et al. 2010, ApJ, 719, 190
- Woods P.M. et al. 1999a, ApJ, 518, L103
- Woods P.M. et al. 1999b, ApJ, 519, L139
- Woods P.M. et al. 1999c, ApJ, 524, L55
- Woods P.M. et al. 1999d, ApJ, 527, L47
- Woods P.M. et al. 2001, ApJ, 552, 748
- Woods P.M. et al. 2002, ApJ, 576, 381
- Woods P.M. et al. 2003, ApJ, 596, 464
- Woods, P.M., Kaspi, V.M., Thompson, C., et al. 2004, ApJ, 605, 378-399
- Woods P.M. et al. 2005, ApJ, 629, 985
- Woods P.M., Thompson C., 2006, in *Compact Stellar X-ray sources*, eds Lewin W., van der Klis M., Cambridge Astrophysics Series 39, Cambridge University Press, p. 547-586

- Woods P.M. et al. 2007, ApJ, 654, 470
- Woosley S.E. 1993, ApJ, 405, 273
- Wright G.A.E. 1973, MNRAS, 162, 339
- Wu, J.H.K., Hui, C.Y., Huang, R.H.H., et al., 2013, JASS, 30, 83
- Xing Y., Yu W., 2011, ApJ, 729, 1
- Younes G. et al. 2014, ApJ, 785, 52
- Yu, C. 2011, ApJ, 738, 75
- Yu C. 2012, ApJ, 757, 67
- Yu C., Huang L., 2013, ApJL, 771, L46
- Zane S., Turolla R., Stella, L., Treves, A. 2001, ApJ, 560, 384
- Zane S., Rea N., Turolla R., Nobili L. 2009, MNRAS, 398, 1403
- Zane S., Turolla R., Nobili L., Rea, N., 2011a, ADSS, Modeling the broadband persistent emission of magnetars, 47, 1298, Copyright (2011)
- Zane S., Nobili, L., Turolla R. 2011b, High-Energy Emission from Pulsars and their Systems, Astrophysics and Space Science Proceedings. Springer-Verlag Berlin Heidelberg, p. 329
- Zavlin, V.E., Pavlov, G.G., Shibano, Y.A. 1996, A&A, 315, 141
- Zhang, B. & Mészáros P. 2001, ApJ, 552, L35
- Zhang, B., Fan Y.Z., Dyks, J., Kobayashi, S., Mészáros P., Burrows, D.N., Nousek, J.A., Geherls, N. 2006, Apj, 642, 354
- Zhu W. et al. 2008, ApJ, 686, 520